Hypercapnia decreases Na,K-ATPase plasma membrane abundance by impairing endoplasmic reticulum maturation of its β-subunit in alveolar epithelial cells

Inaugural Dissertation

submitted to the

Faculty of Medicine

in partial fulfillment of the requirements

for the PhD-Degree

of the Faculties of Veterinary Medicine and Medicine

of the Justus Liebig University Giessen

by

Kryvenko, Vitalii

of

Zaporizhia, Ukraine

Giessen 2020

From the Department of Internal Medicine II

Director: Prof. Dr. Werner Seeger

of the Faculty of Medicine of the Justus Liebig University Giessen

First Supervisor and Committee Member	Prof. Dr. Werner Seeger
Second Supervisor and Committee Member:	Prof. Dr. Martin Diener
Committee Members:	Prof. Dr. Norbert Weissmann
	Prof. Dr. Wolfgang M. Kübler

Date of Doctoral Defense: 18.03.2021

Declaration

I declare that I have completed this dissertation single-handedly without the unauthorized help of a second party and only with the assistance acknowledged therein. I have appropriately acknowledged and referenced all text passages that are derived literally from or are based on the content of published or unpublished work of others, and all information that relates to verbal communications. I have abided by the principles of good scientific conduct laid down in the charter of the Justus Liebig University of Giessen in carrying out the investigations described in the dissertation.

Kryvenko, Vitalii

Giessen

Table of contents

Abbreviations

2,4-DNPH	2,4-dinitrophenylhydrazine
2-APB	2-Aminoethoxydiphenyl borate
A549	Human adenocarcinoma alveolar epithelial cell
AEC	Alveolar epithelial cell
AFC	Alveolar fluid clearance
ALI	Acute lung injury
AMPK	AMP-activated protein kinase
AQP	Aquaporin
ARDS	Acute respiratory distress syndrome
ASK1	Apoptosis signal-regulating kinase 1
ATF4	Activating transcription factor 4
ATF6	Activating transcription factor 6
ATI	Alveolar epithelial cell type I
ATII	Alveolar epithelial cell type II
ATP	Adenosine triphosphate
BiP, GRP78	Binding immunoglobulin protein
Ca^{2+}	Calcium ion
cAMP	Cyclic adenosine monophosphate
cDNA	Complimentary DNA
CFTR	Cystic fibrosis transmembrane conductance regulator
CHOP	CCAAT/enhancer-binding protein-homologous protein
Cl^-	Chloride ion
CNX	Calnexin
CO_2	Carbon dioxide
Co-IP	Co-immunoprecipitation
COPD	Chronic obstructive pulmonary disease
CPAP	Continuous positive airway pressure
CREB	cAMP response element-binding protein
CRT	Calreticulin
Ctrl	Control
DMEM	Dulbecco's modified Eagle's medium
DMSO	Dimethyl sulfoxide

DNA	Deoxyribonucleic acid
DNP	Dinitrophenylhydrazone
DTT	Dithiothreitol
EDEM1	ER degradation-enhancing alpha-mannosidase-like protein 1
eIF2α	Eukaryotic initiation factor 2α
eIF4E	eukaryotic initiation factor 4E
ER	Endoplasmic reticulum
ERAD	Endoplasmic reticulum associated degradation
ERK	Extracellular signal-regulated kinase
FBS	Fetal bovine serum
FiO_2	Fraction of inspired oxygen
FXYD	FXYD domain-containing ion transport regulator
GADD34	Growth arrest and DNA damage-inducible protein
GAPDH	Glyceraldehyde 3-phosphate dehydrogenase
GCN2	General control nonderepressible 2 kinase
GFP	Green fluorescence protein
Glc	Glucose
GlcNAc	N-acetylglucosamine
GM130	Golgin subfamily A member 2
GPCR	G protein-coupled receptor
GRP94	Heat shock protein 90 beta member 1
h	Hour
H^+	Hydrogen ion
HCO_{3-}	Bicarbonate
HRI	Heme-regulated kinase
HRP	Horseradish peroxidase
IB	Immunoblotting
ICU	Intensive care unit
IgG	Immunoglobulin G
IL	Interleukin
IP	Immunoprecipitation
IP3R	1,4,5-triphosphate receptor
IRE1	Serine/threonine-protein kinase/endoribonuclease inositol-requiring enzyme 1

JNK	c-Jun N-terminal kinase
K^+	Potassium ion
kDa	Kilodaltons
KGF	Keratinocyte growth factor
Man	Mannose
MAN1B1	Mannosyl-oligosaccharide 1,2-alpha-mannosidase
min	Minute
mmHg	Millimeters of mercury
MOPS	3-(N-morpholino)propanesulfonic acid
mRNA	Messenger RNA
n	Number of independent experiments
Na,K-ATPase	Sodium–potassium adenosine triphosphatase
Na^+	Sodium ion
NKA	Na,K-ATPase
NO	Nitric oxide
ORAI	Calcium release-activated calcium channel protein
$PaCO_2$	Partial carbon dioxide pressure
PCLS	Precision cut lung slices
PCR	Polymerase chain reaction
PDI	Protein disulfide-isomerase
PEEP	Positive end-expiratory pressure
PERK	Protein kinase R (PKR)-like endoplasmic reticulum kinase
pH_e	pH extracellular
PKR	Protein kinase RNA-activated
PM	Plasma membrane
qPCR	Quantitative polymerase chain reaction
QRT	Quercetin
RIDD	RNA IRE1-dependent decay
RNA	Ribonucleic acid
ROS	Reactive oxygen species
rpm	Rounds per minute
RyR	Ryanodine receptor
s	Second

sAC	Soluble adenylyl cyclase
SD	Standard deviation
Ser	Serine
SERCA	Sarco/endoplasmic reticulum calcium ATPase
siRNA	Small interfering RNA
STIM	Stromal interaction molecule
TCA	Tricarboxylic acid cycle
TfR	Transferrin receptor
TG	Thapsigargin
TNF	Tumor necrosis factor
TRAF2	TNF receptor-associated factor 2
UPR	Unfolded protein response
WCL	Whole cell lysate
XBP1	X-box-binding protein 1
α-KG	α-ketoglutaric acid

Summary

The main hallmarks of acute respiratory distress syndrome (ARDS) are impaired gas exchange and alveolar edema, which are often associated with elevated levels of CO_2 (hypercapnia) due to the disruption of the alveolar-capillary barrier and in part as a consequence of lung-protective mechanical ventilation by using low tidal volumes. Both decreased alveolar fluid clearance (AFC) and hypercapnia have been shown to be associated with worse outcomes in patients with ARDS. The resolution of alveolar edema directly correlates with AFC, which is driven by a vectorial Na^+ transport, mediated by the coordinated action of the apically-localized epithelial Na^+ channel (ENaC) on the apical and the Na,K-ATPase (NKA) on the basolateral side. The endoplasmic reticulum (ER) is the main organelle that is involved in the proper maturation of glycoproteins. NKA is a heterodimeric glycoprotein that in order to be delivered to the plasma membrane must be assembled in the ER. A disturbance in the ER maturation may result in a decreased plasma membrane abundance of the transporter and an impaired alveolar fluid clearance.

Here, we provide evidence that hypercapnia (pCO_2=120 mmHg; pH_e=7.4) decreases the NKA plasma membrane abundance by affecting the ER folding of the β-subunit of the enzyme in alveolar epithelial cells. We found that the short-term exposure of cells to elevated CO_2 levels (up to 1 hour) results in depletion of the ER Ca^{2+} stores by a leakage through 1,4,5-triphosphate receptors (IP3R). The rapid activation of serine/threonine-protein kinase/endoribonuclease inositol-requiring enzyme 1α (IRE1α) triggers ER-associated degradation (ERAD) of the NKA β-subunit, which subsequently decreases the cell surface expression of the transporter. The inhibition of Ca^{2+} release through IP3R receptors stabilizes the levels of the ER-resident NKA-β and increases the plasma membrane abundance of the enzyme. In contrast, long-term hypercapnia (up to 72 hours) promotes significant retention of the NKA β-subunit in the ER. This is followed by increased protein oxidation in the ER and the disruption of the Na,K-ATPase α/β-complex formation. Furthermore, disturbances in ER homeostasis activate the adaptive unfolded protein response (UPR) by increasing the phosphorylation of eukaryotic initiation factor 2α (eIF2α) by protein kinase R-like endoplasmic reticulum kinase (PERK). Moreover, we demonstrate that administration of α-ketoglutaric acid to hypercapnia-exposed cells prevents ER protein oxidation and restores plasma membrane abundance of the Na,K-ATPase.

Taken together, short- and long-term exposure to elevated CO_2 levels result in misfolding of the Na,K-ATPase β-subunit in the ER and decrease the plasma membrane expression of the Na,K-ATPase α/β-complex, which impairs alveolar fluid clearance. Understanding the mechanisms of hypercapnic respiratory failure may provide new approaches in the treatment of patients with ARDS.

Zusammenfassung

Die Hauptmerkmale des akuten Atemnotsyndroms (ARDS) umfassen ein Lungenödem und einen gestörten Gasaustausch, die häufig mit einem erhöhten CO_2-Gehalt (Hyperkapnie), aufgrund einer Störung der alveolo-kapillären Barriere, und einer lungenschützenden mechanischen Beatmung, mithilfe eines niedrigen Tidalvolumen, verbunden sind. Es zeigte sich, dass das Zusammenspiel von Hyperkapnie und einer verminderten Clearance der Alveolarflüssigkeit (AFC) zu einem schlechteren Krankheitsverlauf bei ARDS-Patienten führt. Das Ausschwämmen des Lungenödems korreliert direkt mit der AFC, welche durch einen zielgerichteten vektoriellen Na^+-Transport, einerseits durch den apikal lokalisierten epithelialen Na^+-Kanals (ENaC) und anderseits durch die basolateral lokalisierten Na,K-ATPase (NKA) bestimmt wird. Das endoplasmatische Retikulum (ER) ist die Hauptorganelle, die an der ordnungsgemäßen Reifung von Glykoproteinen beteiligt ist. NKA ist ein heterodimeres Glykoprotein, dessen Untereinheiten im ER aufgebaut und danach von der Plasmamembran freigegeben wird. Eine Störung im Reifungsprozess des ER kann zu einer verringerten Transporterfreisetzung führen, was eine beeinträchtigte Alveolarflüssigkeitsclearance nach sich ziehen könnte.

Unsere vorliegenden Daten belegen, dass die Hyperkapnie (pCO_2=120 mmHg; pH_e=7.4) den Zusammenbau einer Enzym-β-Untereinheit im ER von Alveolarepithelzellen beeinflusst, was die NKA-Freisetzung an den Plasmamembranen verringert. Es zeigte sich, dass die kurzfristige Erhöhung des CO_2-Spiegels (bis zu 1 Stunde) zu einer Erschöpfung des Ca^{2+}-Speichers führte, was wiederum in einem Verlust der IP3R-Rezeptoren und der raschen Aktivierung von IRE1α im ER resultierte. Anschließend löste dies den ER-assoziierten Abbau (ERAD) der NKA-β-Untereinheit aus und verringerte die Transporterexpression an der Zellöberflache. Eine Hemmung der Ca^{2+}-Freisetzung durch die IP3R-Rezeptoren stabilisierte die Anzahl von ER-residenten NKA-β und erhöhte die Emission des Enzyms an der Plasmamembran. Dagegen führte eine langfristige Hyperkapnie (bis zu 72 Stunden) signifikant zu einer verminderten Freisetzung der NKA-β-Untereinheit im ER, gefolgt von einer erhöhten Oxidation des ER-Proteins und einer Bildungsstörung des Transporter-α:β-Komplexes. Darüber hinaus kam es zu einer adaptiv entwickelten Proteinreaktion durch eine aktivierte Störung der ER-Homöostase, indem die Phosphorylierung durch PERK von eIF2α erhöht wurde. Zusätzlich konnten wir zeigen, dass durch die Zugabe von α-Ketoglutarsäure zu den Hyperkanie-exponierten Zellen die Proteinoxidation im ER und die Freisetzung der Na, K-ATPase wiederhergestellt werden konnte.

Zusammenfassend führt eine kurz- und langfristige Exposition mit erhöhten CO_2-Spiegeln zu einer Fehlbildung der β-Untereinheit im ER und einer verminderten Expression der Na, K-ATPase an der Plasmamembran, was zu einer verschlechterten Clearance der Alveolarflüssigkeit führen kann. Diese neu erworbenen Kenntnisse über die Mechanismen der durch Hyperkapnie induzierten respiratorischen Insuffizienz, könnten neue Ansätze in der Pathophysiologie und in der Behandlung von Patienten mit ARDS liefern.

1. Introduction

1.1 Acute respiratory distress syndrome

The acute respiratory distress syndrome (ARDS) remains one of the main mortality causes in patients in the intensive care unit (ICU). Although it has been described around 50 years ago, there is still no specific treatment for this syndrome and the mortality remains very high. In the recently published international LUNG SAFE study involving almost 30,000 patients, the overall mortality in the ARDS cohorts varies from 34.9% up to 46.1% depending on the syndrome severity (1). Recent evidence suggests that ARDS is observed in a wide range, from 10 to 86 cases per 100,000 patients with the highest rates diagnosed in Australia and the United States (2). According to the current Berlin clinical definition, ARDS is characterized by onset within 7 days after known clinical insult with bilateral opacities, a PaO_2:FiO_2 ratio ≤ 300 mmHg and the need of mechanical ventilation with a minimum positive end-expiratory pressure (PEEP) of 5 cmH_2O (3).

The lung injury represents the main hallmark of ARDS, which in its pathogenesis may have direct or indirect causes. The direct causes include pneumonia in the presence or absence of pulmonary sepsis (which covers over 85% of all admissions with ARDS), aspiration of gastric contents, pulmonary contusion, inhalation injury, and drowning. In addition, sepsis (of nonpulmonary origin), nonthoracic trauma, hemorrhagic shock, pancreatitis, major burn injury, drug overdose, transfusion of blood products, cardiopulmonary bypass, reperfusion edema after lung transplantation or embolectomy are assigned as indirect causes of the lung injury (4).

The evolution of ARDS is characterized by three states: an exudative, a proliferative and a fibrotic phase. The first, exudative phase, is characterized by a massive injury of endothelial and epithelial cells, destruction of the alveolar-capillary barrier and accumulation of a protein-rich alveolar edema fluid, prominent neutrophil, monocyte/macrophage recruitment and activation of effector T-cells (2). The second, proliferative phase is indicated by alveolar repair processes, which involve the restoration of epithelial and endothelial barrier integrity, progenitor cells proliferation and reabsorption of alveolar edema. Due to prolonged mechanical ventilation, formation of collagen deposits and excessive proliferation of fibroblasts may be observed in some patients, which could lead to increased mortality (4). Various inflammatory, noninflammatory, gaseous and mechanical determinants contribute to the alveolar-capillary barrier damage during ARDS (Figure 1.1).

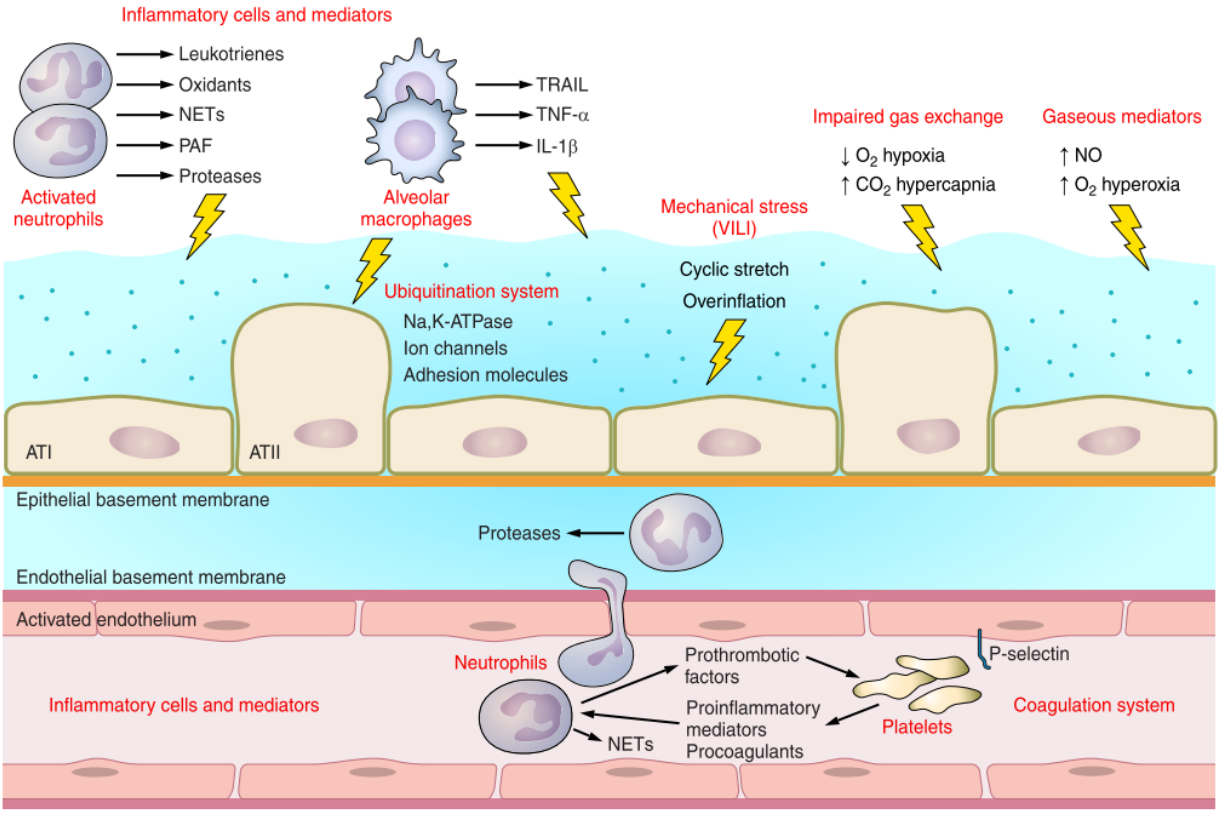

Figure 1.1 Schematic presentation of inflammatory, noninflammatory and mechanical stimuli that contribute to the pathogenesis of ARDS (ALI). TRAIL, tumor necrosis factor-related apoptosis-inducing ligand; VILI, ventilator-induced lung injury; NETs, neutrophil extracellular traps; PAF, platelet-activating factor; ATI and ATII, alveolar type I and II cells, respectively. Adapted from Herold *et al*, Am J Physiol Lung Cell Mol Physiol, 2013 (5).

As shown in Figure 1.1, an unbalanced inflammatory systemic response mediated by macrophages, neutrophils and platelets leads to increased production of IL-1β, TNF-α, IL-6 and IL-8, thus aggravating lung injury (6). Upregulation of the cytokines release is a consequence of enhanced activation of danger- or pathogen-associated molecular patterns (DAMP/PAMP), toll-like (TLR), NOD-like (NLR), RIG-I-like (RLR), lectin C-type and absence in melanoma 2-like (AIM2) receptors (5). In addition to the cellular activation and cytokine release, disruption of the alveolar-capillary barrier results in impaired gas exchange and therefor reduces blood oxygen levels while levels of carbon dioxide (CO_2) rise (7). As a consequence of the above-mentioned mechanisms, most of the ARDS patients require apparated ventilation, which additionally produces mechanical stress by cyclic stretch and lung overinflation, which may further exacerbate lung injury (8).

One of the main goals of current ARDS research is identification of biomarkers that will predict and improve therapeutic tactics. In recent decades, several candidates have been proposed as potential predictors of outcome in ARDS, such as angiotensin-converting enzyme, IL-8, IL-10, TNF-α, vascular endothelial growth factor (VEGF), extracellular superoxide dismutase (SOD3), myosin light chain kinase (MYLK) and pulmonary surfactant-associated protein B (SFTPB) (2). However, expression levels of these markers strongly vary during the evolution of ARDS and thus, trials measuring their significance as a diagnostic tool are still ongoing (9).

More recent attention has been focused on the fact that ARDS patients may be divided into subphenotypes, based on the mechanisms of lung injury, as well as clinical and laboratory measurements (10). An independent latent class model analysis, involving clinical and laboratory biomarker profiles shows that a two-class model is helpful in characterizing the ARDS populations (10). While comparing phenotypes of both classes, it has been shown that the first (inflammatory) phenotype had higher plasma levels of inflammatory markers (IL-6, IL-8, sTNFr-1 and PAI-1), higher heart rate and a higher total minute ventilation, lower systolic blood pressure, bicarbonate and protein C as compared to a non-inflammatory type (10). In addition, recent clinical trials show that phenotype-based ARDS patient sub-classes respond differently to treatment modalities, such as fluid management and statins response (11,12).

Despite the progress in understanding ARDS pathophysiology and phenotyping, the therapeutic options for these patients remain entirely supportive. Although, animal studies show beneficial effects of β_2-adrenergic stimulation, treatment with keratinocyte growth factor (KGF) or nitric oxide (NO) (13-15), their use in clinical trials have failed to reduce short- and long-term mortality (4,16).

Up to date, mechanical ventilation, prone positioning, fluid management and extra-corporeal membrane oxygenation (ECMO) are the only supportive therapeutic options that increase oxygenation and survival in ARDS patients (2,4,17,18). Mechanical ventilation in critical care patients depends on two main parameters: PEEP and tidal volume (V_t). Based on previous publications, PEEP has been found to be beneficial in the prevention of alveolar collapse in mechanically ventilated ARDS patients (19). Furthermore, low V_t (~6 ml/kg) compared to high V_t, resulted in decreased lung stretching, inflammatory response and significantly reduced mortality (20). However, while ventilation with low V_t is clearly beneficial, it may result in carbon dioxide retention (CO_2) additionally increasing CO_2 levels that are often elevated as a consequence of impaired alveolar-capillary barrier in the setting of ARDS (21).

1.2 Alveolar epithelial barrier, fluid transport and lung edema

The primary function of the lung is gas exchange, which involves oxygen absorption and carbon dioxide excretion. The central gas exchange lung units – the alveoli, consist of alveolar epithelial and endothelial cells. Together with the basement membrane these anatomic structures form the alveolar-epithelial barrier (22). The main alveolar cell types are the alveolar epithelial type I (ATI) and type II (ATII) cells, which form a very tight and polarized cellular monolayer. This monolayer is primarily impermeable to proteins and large solutes (22). ATI cells are flat and cover more than 95% of the alveolar surface. ATII cells are smaller, cuboidal and their foremost function lies in surfactant synthesis (23). In normal alveoli, there is always a minimal amount of alveolar lining fluid that exists between the apical surface of epithelial cells and the surfactant layer. As depicted in Figure 1.2, the amount of alveolar lining fluid is precisely regulated by active ion transport and passive water movement (22).

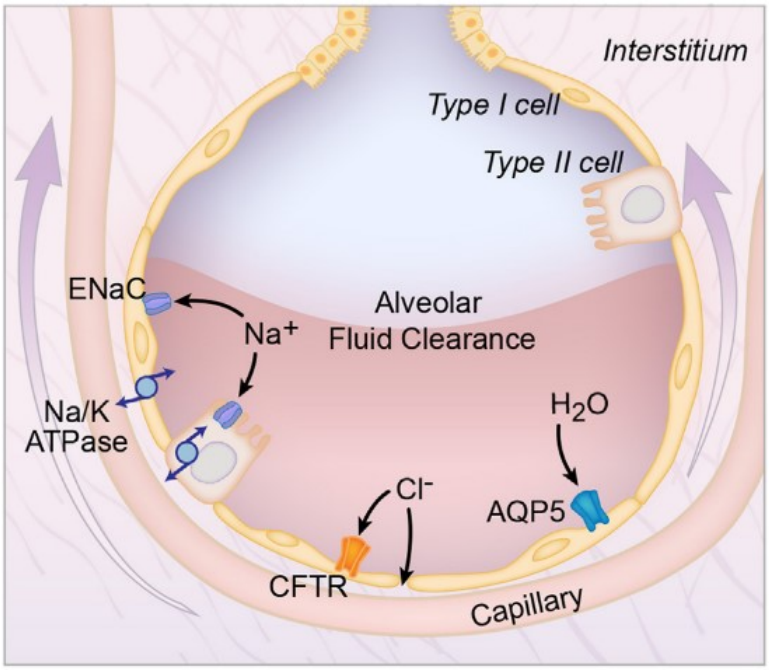

Figure 1.2 Alveolar fluid clearance pathways. The interstitial, capillary, and alveolar compartments, with pulmonary edema fluid in the alveolus are shown. Both type I and type II alveolar epithelial cells are involved in transepithelial ion transport. Sodium (Na^+) is transported across the apical side of epithelial type I and type II cells through the epithelial sodium channel (ENaC), and on the basolateral side via the sodium/potassium ATPase pump (Na/K-ATPase). Adapted from Huppert *et al,* Front Immunol, 2017 (24).

The main ions that are involved in these transport mechanisms are sodium (Na^+), potassium (K^+) and chloride (Cl^-). While Cl^- anions are actively secreted through apically localized

channels, Na^+ is actively transported across the epithelial cells via the apically localized epithelial sodium channel (ENaC) and the basolateral sodium/potassium ATPase (Na,K-ATPase). This vectorial Na^+ transport creates a transepithelial osmotic gradient that drives passive water movement to the interstitial space (7). For decades, it was thought that ATII cells were solely responsible for the above-described active fluid transport. However more recently, it became evident that that ATI cells play a central role in this process as well. (7,24,25).

During certain diseases, such as ARDS, the amount of alveolar fluid is increased in the alveolar space, leading to a condition termed alveolar edema. The increased amount of fluid restricts normal gas exchange, further aggravating the impaired lung function (14). The excess of fluid in the alveolar space is a consequence of increased hydrostatic pressures in the capillaries or by a decreased alveolar fluid clearance (AFC), as a result of alveolar-capillary barrier disruption or dysfunction of the Na^+ transporters (26). The restoration of the alveolar fluid homeostasis is critically dependent on the recovery of the alveolar-capillary barrier and the reestablishment of the Na^+-driven transepithelial osmotic gradient, which is in part determined by the Na,K-ATPase (27,28).

1.3 Structure of Na,K-ATPase

The Na,K-ATPase is a heterodimeric enzyme and a member of the P-type ATPase cation pump family that is widely expressed in various tissues (29). The Na,K-ATPase is localized on the basolateral side of polarized cells, where its primary function is the establishment of Na^+/K^+ intra- and extracellular gradient concentrations. This transporter mechanism is performed by pumping three Na^+ ions out of the cell and two K^+ ions into the cell while consuming a single ATP molecule (30). The function of the Na,K-ATPase is a highly ATP-dependent process, resulting in a consumption up to 50-70% of total cellular ATP, depending on the cell type and its origin (31).

Figure 1.3 shows the structure of the minimally required elements of a functional Na,K-ATPase pump, which consists of a catalytic α- and a regulatory β-subunit. Additionally, there is a γ-subunit, that represents a family of single-span transmembrane proteins containing the FXYD motif, which regulates the activity of the enzyme (32,33). The Na,K-ATPase subunits have different isoforms. Up to date, it has been shown that there are four α-subunits, three β-subunits, and seven FXYD subunits, which are expressed in a cell- and tissue-specific manner (29). The Na,K-ATPase α_1:β_1 subunit combination is the most widely expressed that dominates in epithelial cells (29,34). In alveolar epithelial cell types, two isoforms of the α-subunit (α_1, α_2)

and two of the β-subunit (β_1, β_3) are expressed. Of note, the α_2-subunitis only expressed in ATI cells (29,35).

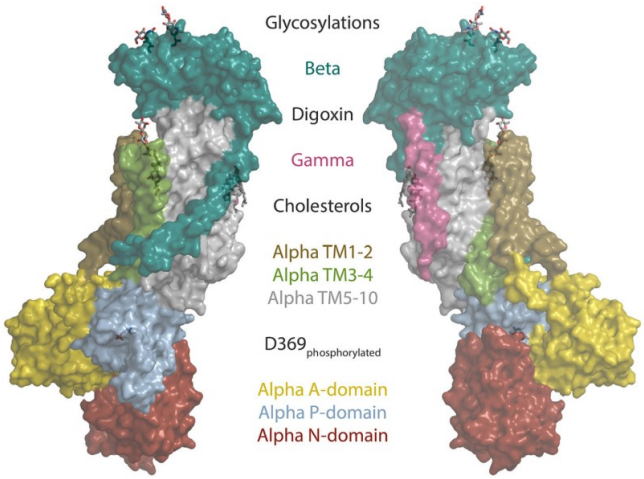

Figure 1.3 The structure of Na,K-ATPase. The structure of the sodium pump. Surface representation of the digoxin bound alpha1 isoform structure from pig. Sodium pump subunits and domains are shown in colors as indicated. The two beta glycosylations, digoxin, two cholesterols and the phosphorylated aspartate (D369) are shown as sticks. Adapted from Clausen *et al,* Front Physiol, 2017 (29).

The Na,K-ATPase α-subunit has a molecular mass of about 110 kDa. This subunit contains binding sites for Na^+, K^+ and ATP, thus maintaining the primary enzyme function – the catalytic exchange of Na^+ and K^+ (30). The α-subunit structurally comprises a large intracellular domain, ten transmembrane segments, and a simple extracellular domain (30). The Na,K-ATPase β-subunit is a type II membrane protein with a molecular mass depending on the glycosylation profile of about 35-55 kDa. It has a small N-terminus located in the cytoplasm, a single transmembrane and a large extracellular domain, the latter of which contains three N-glycosylation sites that are glycosylated (34). Acting as a chaperone, the central role of the Na,K-ATPase β-subunit is the delivery and the appropriate insertion of the Na,K-ATPase α-subunit into the plasma membrane. Recent publications have shown that the function of the Na,K-ATPase β-subunit is not limited to regulatory one. Rather, this subunit is additionally involved in the establishment of the epithelial cell polarity, the formation of the tight junction, desmosomes, actin dynamics, and thus may play a role in cancer progression (36-39).

Several publications have recently shown, that the Na,K-ATPase β-subunit acts as cell adhesion and tight junction molecule while forming adherence junctions in epithelial cells by direct interaction of the Na,K-ATPase β-subunit extracellular domains (34,40). Additionally, the Na,K-ATPase was found to influence the integral plasma-membrane tight junction protein,

occludin, by modifying its phosphorylation status and thus regulating tight junction permeability (41). Disruption of the Na,K-ATPase β:β interactions at the plasma membrane either by genetic manipulation with N-glycan amino acid sequences or blocking with antibodies against the Na,K-ATPase β-subunit results in downregulation of junctional complexes and elevated paracellular permeability (42,43). The critical role of the Na,K-ATPase β-subunit in the regulation of alveolar homeostasis was confirmed *in vivo*, where mice lacking the β-subunit in alveolar epithelial cells have a reduced alveolar fluid clearance (44).

1.4 Regulation of the Na,K-ATPase

The Na,K-ATPase represents a heterodimer where an α- and a β-subunit are assembled in the ER with a stoichiometric ratio of 1:1 and then delivered to the basolateral membrane where the functional Na,K-ATPase orchestrates active Na^+ and K^+ transport (45). Previous studies have reported that different stimuli regulate transcription, trafficking, and degradation of the Na,K-ATPase subunits, thus maintaining enzyme function (29,46). Mechanisms that regulate the pump activity can be classified as short- and long-term processes.

The short-term regulation of the transporter activity is regulated by the trafficking of the enzyme between the intracellular compartments, which is mediated by phosphorylation by intracellular kinases (35,47,48). This type of Na,K-ATPase regulation has been found for example after acute exposure of alveolar epithelial cells to hypoxia or hypercapnia (48-52). Additionally, ubiquitination has been suggested as a cross-talk mechanism that is involved in the regulation of the plasma membrane abundance of the enzyme (53,54).

In contrast, long-term regulation of the Na,K-ATPase includes changes in the RNA expression of the specific transporter subunits due to changes in the extra- and intracellular environmental conditions (46,55,56). Multiple factors affecting epigenetic mechanisms such as hypermethylation of the Na,K-ATPase-β subunit promoter also regulate expression of the enzyme (46,57). Accumulating evidence suggests that mineralocorticoids, glucocorticoids, thyroid hormones, insulin, progesterone, androgen, transforming growth factor-β, and fibroblast growth factors could activate or repress the transcription of the Na,K-ATPase subunits through the activation of specific signaling pathways, transcription factors and binding to the promoter regions of the subunits (46).

Moreover, it has been found that Na,K-ATPase activity can be directly modulated by changing the expression or composition of its subunits. For example, overexpression of the Na,K-ATPase β-subunit increases the translation of the α-subunit of the enzyme (58). Also, conformational

changes in the Na,K-ATPase β-subunit play a role in the ion-binding properties of the α-subunit (59). In addition, the γ-subunit may alter Na,K-ATPase activity by either modulating function or expression of the Na,K-ATPase α- or β-subunit (32,33). Furthermore, the Na,K-ATPase functions as a specific receptor for the cardiac glycosides, ouabain and digoxin, which are inhibitors of the pump activity (60). Interestingly, in contrast to high dosages (more than 1μM), low dosages (10-50 nM) of ouabain appear to upregulate tight and adherence junctions of epithelial cells (61,62).

1.5 CO_2 and hypercapnia

CO_2 is a by-product of cellular respiration and under physiological conditions should be eliminated from tissues and blood. Elevation of carbon dioxide levels over 45 mmHg in blood is termed hypercapnia. Hypercapnia occurs in pathological conditions that involve impairment of the alveolar-capillary barrier function (5). As such, it is often observed in patients with acute and chronic lung diseases such as ARDS, chronic obstructive pulmonary disease, cystic fibrosis, bronchial asthma and others (21,63). Additionally, changes in ventilation conditions including high alveolar ventilation-to-perfusion ratio (due to inhomogeneous distribution of ventilation) and increased dead space/tidal breath ratio often result in increased levels of CO_2 (64).

Recently, it became increasingly evident that lung cells are sensitive to changes in CO_2 levels (65,66). It has been shown several decades ago that in excitable cells, such as brainstem neurons or the glomus cells of the carotid body, CO_2 causes depolarization (67). Furthermore, numerous studies have revealed that in non-excitable cells, such as the alveolar epithelium, CO_2 sensing mechanisms are independent of intra- or extracellular pH, reactive oxygen species (ROS) and carbonic anhydrases (68,69). The lipid structure of the plasma membrane and presence of aquaporin channels are major determinants of cellular CO_2 entrance (70-72). However, the exact mechanism of CO_2 cellular permeability remains largely unknown.

Several mechanisms of CO_2 sensing have been suggested (65,73,74). Due to the fact that CO_2 rapidly dissociates into H^+ and HCO_3^-, it is difficult to distinguish between direct hypercapnia effects and effects of changes in intracellular pH or HCO_3^- levels (66). However, accumulating evidence suggests that cells may sense CO_2 by several distinct mechanisms, such as HCO_3^--dependent activation of soluble adenylyl cyclase (sAC) or by increasing intracellular levels of the second messenger 3,5-cyclic adenosine monophosphate (cAMP). Other potential mechanisms include CO_2 sensing by the action of the receptor protein tyrosine phosphatase-γ

(75), the role of increasing intracellular Ca^{2+} concentrations upon elevated CO_2 levels (51,76) as well as activation of intracellular kinases such as c-Jun N-terminal kinase (JNK), extracellular signal-regulated kinase (ERK1/2) and the central cellular metabolic sensor, AMP-activated protein kinase (AMPK) (51,77-79). Moreover, CO_2 can directly influence structure of proteins by carbamate modifications of amino acids that may lead to post-translational changes in the function of these proteins (80). Additionally, it has been found that CO_2 might be sensed by pH-sensitive ion channels and pH-sensitive G-protein coupled receptors (GPCRs). Furthermore, CO_2-sensitive connexin proteins, such as connexin 26, were found to be linked with respiratory chemo-sensitivity to CO_2 (65,81). However, the exact role of protein tyrosine phosphatase-γ, GPCRs, connexin 26 and protein carbamation in CO_2 sensing in the lung will need to be determined.

As mentioned above, disruption of alveolar gas exchange and ventilation with low V_t results in CO_2 retention in the alveolar space. The concept of "permissive hypercapnia" has been widely used in the treatment of patients with ARDS, which may be explained by the potentially beneficial anti-inflammatory effects of elevated CO_2 levels (82). In addition, two single-center studies investigating patients on mechanical ventilation or sepsis concluded that elevated CO_2 levels increased the odds of survival and had a positive effect on clinical outcomes (83,84). This could be explained by the fact, that increased CO_2 concentrations may decrease the inflammatory response by inactivating NF-κB signaling and aggravating cytokine production (82,85,86). In contrast to these advantageous effects of hypercapnia, a large international multicenter clinical trial showed that in patients with ARDS and severe hypercapnia ($PaCO_2$ ≥50 mmHg), elevated levels of CO_2, independently from acidosis, were associated with higher complication rates, more organ failures, worse outcomes and increased risk of ICU mortality (87). Subsequent translational studies showed that, indeed, elevated CO_2 levels may impair innate immunity and host defense by downregulating autophagy, phagocytosis and bacterial killing in macrophages through increasing the expression of apoptosis regulator Bcl-2 (Bcl-2) and Bcl2-associated agonist of cell death (Bcl-xL) (88). Hypercapnia also appear to decline neutrophil function (89) and decrease production of TNF-α and IL-6 (90), thus further aggravating lung injury. Moreover, short- and long-term exposure to hypercapnia were found to decrease epithelial cellular repair, impair mitochondrial function, alter cellular lipid metabolism, nucleosome assembly and increase airway smooth muscle contractility (76,91-93). Interestingly, although beneficial effects of CO_2 were linked to hypercapnia-induced acidosis, a recent multi-center retrospective study in mechanically-ventilated patients suggested that

hypercapnic acidosis also increases hospital mortality (94). Elevated levels of CO_2 have also been found to promote muscle wasting due to enhanced degradation, worsening cachexia in patients with chronic lung diseases (95,96). Indeed, in COPD patients, an elevated CO_2 concentration in the blood is an independent risk factor of mortality (97).

1.6 Hypercapnia and Na,K-ATPase

Notably, hypercapnia has been found to decrease alveolar fluid clearance and resolution of alveolar edema by decreasing plasma membrane abundance and function of ENaC and Na,K-ATPase (51,98). It has been previously described that *in vivo* and *in vitro* exposure to hypercapnia results in a significant reduction of alveolar fluid clearance and Na,K-ATPase plasma membrane expression (51). Several studies shed light on the mechanisms by which elevated CO_2 levels may downregulate Na,K-ATPase abundance on the cell surface (51,77-79). The main mechanisms that are involved in the hypercapnia-induced regulation of Na,K-ATPase are depicted in Figure 1.4.

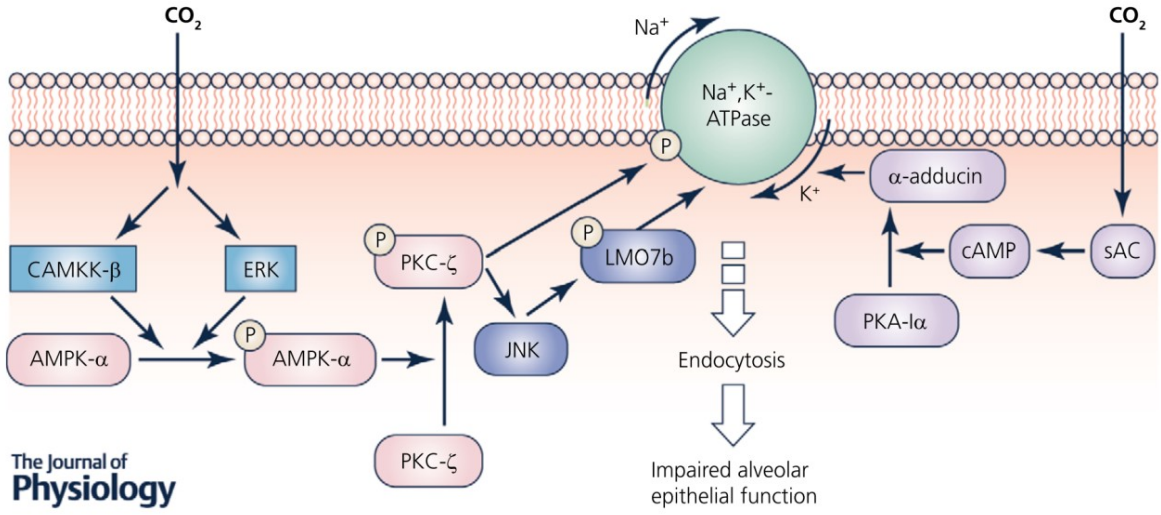

Figure 1.4 Mechanisms by which hypercapnia downregulates Na,K-ATPase cell surface abundance and alveolar fluid reabsorption. Endocytosis of the Na,K-ATPase from the plasma membrane of alveolar epithelial cells leads to decreased Na,K-ATPase activity and thus a reduction in lung edema clearance . During hypercapnia, protein kinase C (PKC)-ζ directly phosphorylates the Na,K-ATPase α_1-subunit, leading to endocytosis of the Na,K-ATPase. The activation of PKC-ζ is regulated by AMP-activated protein kinase (AMPK) via Ca^{2+}/calmodulin-dependent protein kinase kinase-β (CAMKK-β) and extracellular signal-regulated kinase (ERK). The endocytosis of the Na,K-ATPase by hypercapnia is also regulated by c-Jun-N-terminal kinase (JNK) via the AMPK-PKC-ζ signaling and by the protein kinase A (PKA)-Iα. Adapted from Shigemura *et al*, J Physiol, 2017 (66).

The CO_2 signaling pathway is initiated by a rapid elevation of intracellular Ca^{2+} and subsequent activation of the calcium/calmodulin-dependent protein kinase β (CaMKK-β), which then drives the phosphorylation of the AMP-activated protein kinase (AMPK) (51). Interestingly, ERK1/2 has been found to be upstream of AMPK, though the signaling stimuli for ERK1/2 activation remain unknown. Further downstream mechanisms involve translocation of protein kinase C zeta (PKC-ζ) and direct phosphorylation of the Na,K-ATPase-α subunit, thereby promoting endocytosis and retrieval of the pump from the plasma membrane (51). On the other hand, endocytosis of the Na,K-ATPase requires the phosphorylation of JNK, a downstream kinase that is involved in the AMPK-PKC-ζ signaling pathway. The subsequent activation of JNK leads to the phosphorylation of the LIM domain-only 7b (LMO7b), a scaffold protein, which is involved in the regulation of the actin cytoskeleton in the epithelial cells, at Ser-1295, thus driving the hypercapnia-induced endocytosis of the Na,K-ATPase (78). Of note, high CO_2-induced JNK activation has been found to be conserved among species such as *Drosophila melanogaster,* mice, rats and humans (77). Additionally, elevated CO_2 levels also increase intracellular cAMP levels, thereby activating protein kinase A (PKA) and inducing the phosphorylation of the actin cytoskeleton component α-adducin, thus decreasing Na,K-ATPase abundance in the plasma membrane (99). Interestingly, the hypercapnia-induced activation of ERK1/2, AMPK, and JNK have been shown to regulates another channel that is critically required for the establishment of the Na^+ gradient, ENaC. Direct phosphorylation of ENaC by ERK1/2, and E3 ubiquitin-protein ligase, neural precursor cell expressed developmentally down-regulated protein 4 (NEDD4-2) through AMPK leads to polyubiquitination of β-ENaC and further endocytosis of the ENaC complex (98). On another note, hypercapnia-induced elevation in cAMP has been found to downregulate another channel, the malfunction of which often aggravates alveolar fluid clearance disturbances, the cystic fibrosis transmembrane conductance regulator (CFTR) (100).

Most of the studies in the field of hypercapnia-induced downregulation of Na,K-ATPase have focused on the endocytosis of the assembled transporter from the plasma membrane. However, before trafficking to the cell surface, the Na,K-ATPase undergoes maturation processes, involving the synthesis of the nascent pump subunits by the ribosomes, and their further glycosylation and assembling in the ER and Golgi (101). This notion indicates an urgent need to understand the possible influence of elevated CO_2 levels on the mechanisms of the folding of the transporter.

1.7 Endoplasmic reticulum

Protein transcription, translation, and folding occur continuously in every living cell and are essential for a normal physiological function. About one-third of all proteins in the cellular proteome are interacting with the endoplasmic reticulum (ER) (102). The ER represents a large, dynamic cellular organelle that orchestrates synthesis, folding, and structural maturation of proteins, regulation of lipid metabolism and additionally functions as a calcium storage (103,104). Based on the structural composition, it is divided into two parts, smooth ER and rough ER, which are characterized by the presence or absence of ribosomes on the cytosolic surface of the ER (105). The ER has a specific intraorganellar environment that possesses specific molecular chaperons, ions and redox status that are required for proper protein folding (106). Therefore many co- and post-translational protein modifications occur in the ER, such as isomerization or reduction of disulfide-bond formations, signal sequence cleavage, isomerization of proline, N-linked glycosylation and glycophosphatidylinositol-anchor addition (106,107).

1.7.1 Regulation of the endoplasmic reticulum protein folding

Once the protein enters the ER, it undergoes three steps of a maturation process. In the first step, co-translational and co-translocational protein folding happens in a translocon complex, a specific channel where the nascent protein chain enters the ER lumen or the ER membrane. The second posttranslational folding event occurs after the completed chain has been released from the ribosome and translocon complex. During the last step, the final peptide folding and assembly of the oligopeptides takes place (106).

The ER tightly regulates protein folding through the coordinated action of the specific resident chaperones, calnexin, calreticulin, binding immunoglobulin protein (BiP, GRP78) and reductases, protein disulfide-isomerase A3 (ERp57), endoplasmic reticulum oxidoreductase-1α (Ero1α), DnaJ homolog subfamily B member (ERdj3-6) and others (108). During the maturation mechanisms, the binding of the nascent peptide to calnexin or calreticulin activates the leading primary folding cycle (Figure 1.5).

The calnexin/calreticulin cycle starts when a 14-oligosaccharide core (Glc3Man9GlcNAc2) is transferred from the phosphate precursor or lipid carrier and is added to the N-glycosylation site of the nascent folding protein by glycosyltransferases (101,106,109). This process results in the formation of a monoglucosylated glycoprotein that interacts with calnexin and calreticulin. Of note, N-glycosylation plays an important role in the determination of protein

localization, especially in the polarized epithelium (101). Subsequently, the association of calnexin or calreticulin with ERp57 catalyzes disulfide bond formations for proper protein folding (107,110). Alongside the assistance of lectin and the above-mentioned Ca^{2+}-dependent chaperones (calnexin and calreticulin), non-lectin chaperones, such as heat shock proteins are involved in protein maturation (110). An important member of this family of proteins is GRP78, which has multiple functions: it is involved in the co-translational folding/refolding of nascent proteins, prevents premature release of molecules from the ER, promotes the removal of the misfolded proteins and is an integral element of the unfolded protein response system (56,111).

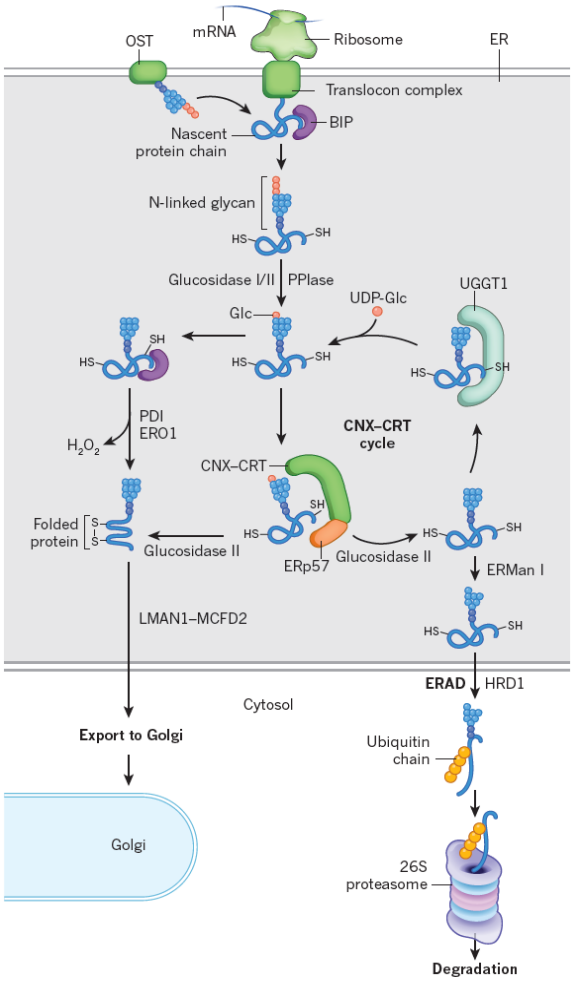

Figure 1.5 Calnexin/calreticulin cycle and quality control in the ER. Mature mRNA is loaded onto ribosomes to initiate protein synthesis. Nascent polypeptides enter the ER through the translocon complex in an unfolded state. Protein folding in the ER is facilitated by the many resident chaperones, such as BiP, GRP94, PDI, ERp57 and ERO1. Unfolded, misfolded or aggregated proteins are retrotranslocated to the cytosol for ubiquitination and degradation by the 26S proteasome through ER-associated protein degradation (ERAD). Adapted from Wang *et al,* Nat Rev Cancer, 2016 (112).

The maturation and folding continues until the remaining glucose on the nascent folding glycoprotein is trimmed by glucosidase II. This step terminates the interaction of the calnexin/calreticulin cycle with the folded protein and promotes further protein transport to the Golgi (106,113). However, removing the mannose residue in the middle of the oligosaccharide core by mannosyl-oligosaccharide 1,2-alpha-mannosidase (MAN1B1) leads to enhanced association with ER degradation-enhancing alpha-mannosidase-like protein 1 (EDEM1) and

elimination of the protein by a process termed ER-associated degradation (ERAD) (108,114,115). A detailed description of the degradation pathways will be discussed later.

1.7.2 Endoplasmic reticulum folding environment

The past decade of ER research revealed that in order to successfully fold proteins, the ER environment requires high Ca^{2+} levels, oxidizing conditions and high levels of ATP (116). The main pathways and signaling events that regulate ER homeostasis are depicted in Figure 1.6.

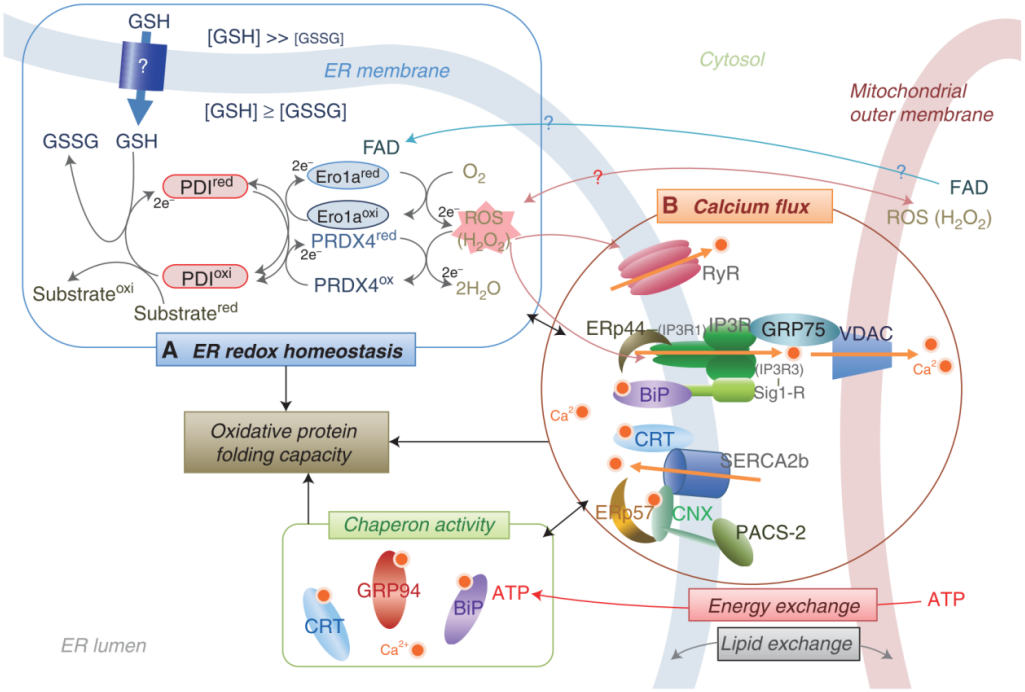

Figure 1.6 ER redox and calcium homeostasis. Endoplasmic reticulum oxidoreductase 1 alpha (Ero1a) serves as the primary oxidase of Protein disulfide-isomerase (PDI). Oxidized PDI family members drive oxidative protein folding, as well as modification of the Glutathione from reduced (GSH) into oxidized state (GSSG), thereby generating an oxidative environment. Mammalian cells contain two main channels responsible for Ca^{2+} efflux from the ER, inositol 1,4,5-trisphosphate receptors (IP3Rs) and ryanodine receptors (RyRs), and one pump responsible for Ca^{2+} influx into the ER, the sarcoplasmic reticulum Ca^{2+}-ATPase (SERCA). The mitochondria-associated membrane (MAM) is also the place where energy (ATP) and lipids are exchanged between ER and mitochondria. Ca^{2+} and ATP levels affect the activities of ER chaperones and foldases. Adapted from Araki *et al*, Cold Spring Harb Perspect Biol, 2011 (114).

Ca^{2+} ions act as second messengers and participate in many signaling pathways, which control protein synthesis, cell proliferation, metabolism and apoptosis (117). The ER is an important cellular calcium storage compartment and thus, plays a major role in the regulation of Ca^{2+} homeostasis and oscillations (118). The physiological concentration of Ca^{2+} in the ER is much

higher than in the cytoplasm and is modulated by the coordinated action of several mechanisms, such as ATP-dependent Ca^{2+} pumps (SERCA2A, SERCA2B) - that are increasing the cytosol-to-lumen concentrations, the ER membrane-localized inositol trisphosphate (IP3R) and the ryanodine (RyR) receptors - that release Ca^{2+} from the ER to the cytosol (119). In the ER, Ca^{2+} stores consist of a free Ca^{2+} fraction or bound to folding chaperons that contain Ca^{2+} binding motifs, such as calnexin, calreticulin, GRP94, and calumenin (118).

In addition to the Ca^{2+} regulation, the ER possesses a specific oxidizing environment in order to perform the oxidative protein folding and disulfide bond formation (Figure 1.6). The redox reactions are achieved by the coordinated action of glutathione disulfide, hydrogen sulfide, hydrogen peroxide, and nitric oxide, which are mediating the sulfenylation, sulfhydration and nitrosylation of the folded proteins (107). In contrast, the protein oxidative modifications are reduced by the oxidoreductases, ERO1a and ERO1b and protein disulfide isomerases (PDI) (114). In addition to the peptide modification, the ER-resident chaperones are subjected to redox reactions. Briefly, once the disulfide formation is completed, the PDI active center will be reduced and oxidized in order to restore its activity by Ero1 (120). Additionally, it has been reported that peroxiredoxin IV may reduce H_2O_2 production and oxidize members of the PDI family, thus equilibrating the redox homeostasis in the ER (114). Oxidative processing frequently results in the attachment of carbonyl groups to peptides, thereby causing an irreversible non-enzymatic protein carbonylation (121). It has been shown that protein and chaperone carbonylation that occurs in the ER, may disrupt the normal protein folding process (122,123).

Another critical requirement for ER homeostasis is a sufficient ATP supply. Most of the posttranslational processing in the ER including protein phosphorylation events, quality control, protein folding and translocation, calcium homeostasis, ERAD and unfolded protein response require energy. It has been shown that the ATP source depends on the metabolic state of the cell, more precisely, whether ATP is generated by oxidative phosphorylation or glycolysis. In cells, where the mitochondrial respiration is the predominant source of energy supply, ATP is directly transferred into the ER through mitochondria-associated ER membrane sites (MAM) (120). In contrast, when ATP is derived from the glycolysis pathways it enters the ER from the cytosol (120).

Furthermore, recent reports suggest that the $Ca^{2+}$and ATP levels and redox reactions are interdependent. It has been found that upon intracellular Ca^{2+} release, the levels of luminal ATP

increase (124). Furthermore, CCAAT/enhancer-binding protein-homologous protein (CHOP)-dependent stress response results in increased gene expression of ERO1a, hyperoxidizing ER environment, activation of IP3R receptors, thus increasing Ca^{2+} cytosol concentrations and eventually cell death (125).

1.7.3 Folding and maturation of the Na,K-ATPase in the endoplasmic reticulum

As previously mentioned, the Na,K-ATPase is a heterodimeric glycoprotein that minimally requires a catalytic α- and a glycosylated β-subunit to be functional (56). The catalytic Na,K-ATPase α-subunit cannot exit the ER (and thus cannot function at the plasma membrane) unless it had been assembled with the regulatory Na,K-ATPase β-subunit (45). The glycosylation processing of the Na,K-ATPase β-subunit in the ER is a critical step that affects folding, stability, subunit assembly and membrane integration of the Na,K-ATPase α/β-complex (126).

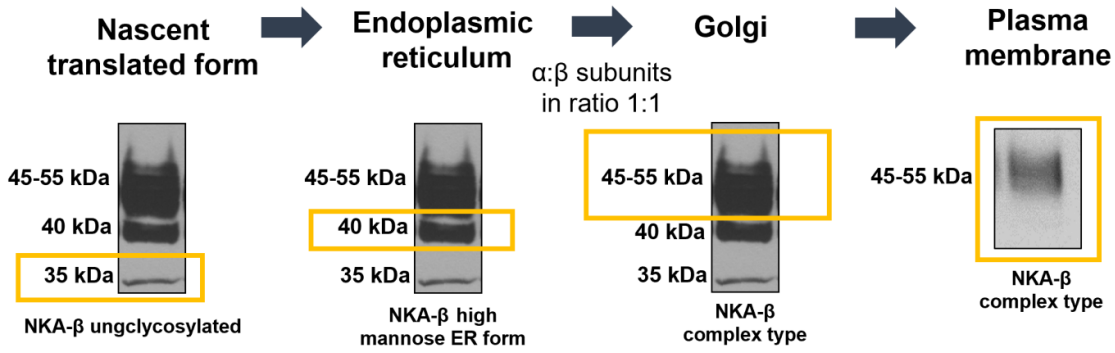

Figure 1.7 Different forms of the Na,K-ATPase β-subunit. A unglycosylated core of the Na,K-ATPase β-subunit (NKA-β) can be detected with a molecular weight of about 35 kDa. This form represents either nascent synthesized peptides by the ribosomes or subunits which will eventually be degraded. Further protein maturation in the ER and adding an oligosaccharide core results in a shift of the molecular mass up to 40 kDa, thus forming a high mannose ER-resident β-subunit. Subsequent addition of N-glycans in the Golgi to the NKA β-subunit shifts the molecular mass up to 55 kDa forming the complex type of the β-subunit. At the plasma membrane, only a complex type of the β-subunit is expressed.

As demonstrated in Figure 1.7, the Na,K-ATPase β-subunit undergoes various post-translational modifications until it can leave the ER and the Golgi and be transferred to the plasma membrane. The subsequent glycosylation results in the formation of Na,K-ATPase β-subunit peptides with different molecular weights, as assessed by electrophoresis. After being translated by the ribosomes, the unglycosylated Na,K-ATPase β-subunit has a molecular weight of approximately 35 kDa. In the first step of ER folding an oligosaccharide core is added, which results in Na,K-ATPase β-subunit molecular mass shift and the formation of a high mannose

type of N-glycans. Indeed, these specific Na,K-ATPase β-subunit forms reside exclusively in the ER (45). After leaving the ER, only Na,K-ATPase β-subunits assembled with Na,K-ATPase α-subunits, undergo further glycosylation reaching a molecular weight of up to 55 kDa. These glycosylation steps are driven by Golgi-resident glycosyltransferases and lead to the formation of hybrid- or complex-type N-glycans (45).

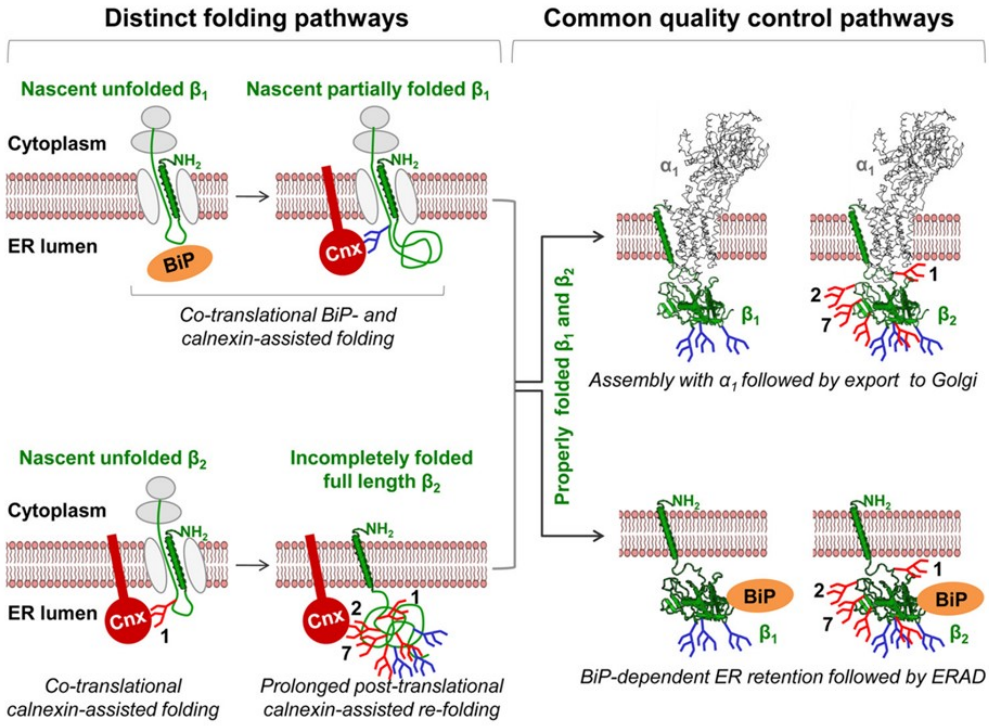

Figure 1.8 Maturation pathway for the Na,K-ATPase β1- and β2-subunits. The Na,K-ATPase β_1- and β_2-subunits are type II transmembrane proteins. The nascent β_1 subunit lacking N-glycans in the beginning of its luminal domain initially binds to BiP during translocation. Later, when N-glycosylation sites are translocated into the ER lumen and occupied by N-glycans, BiP is replaced by calnexin (Cnx). In contrast, the nascent β_2 subunit, binds directly to calnexin during translation. Once properly folded, the β_1- and β_2-subunits follow common maturation and trafficking pathways. Adapted from Tokhtaeva *et al*, J Cell Sci, 2012 (56).

Folded Na,K-ATPase-β_1 or β_2 subunits are either bound to Na,K-ATPase-α_1 and directed for further maturation in the Golgi or bound to BiP, retained and degraded in the ER (Figure 1.8). The folding of the NKA-β subunits is assisted by BiP and calnexin ER-resident chaperones (56).

Based on literature data, different isoforms of the Na,K-ATPase β-subunit have different rates of glycosylation and affinity in binding to ER chaperons. For example, the presence of N-glycans is more critical for the assembly of Na,K-ATPase-α with Na,K-ATPase-β_2, but not with

Na,K-ATPase-β_1 (127). It has been shown that inhibition of glycan-calnexin interactions or removal of the N-glycosylation sites does not affect assembly of the Na,K-ATPase-β_1 with Na,K-ATPase-α_1 but increases its retention and binding to the BiP chaperone, suggesting a minor involvement of calnexin in the maturation of the Na,K-ATPase-β_1 (56). In contrast, Na,K-ATPase-β_2 is directly bound to calnexin during translation and a prevention of this binding or a decrease in N-glycosylation completely prevents assembly of the two subunits. Mutations in the Na,K-ATPase α_1:β_1 or α_1:β_2 interacting regions result in their inability to assemble the enzyme complex and increase interactions of the Na,K-ATPase β-subunit with BiP (45,56).

1.8 Endoplasmic reticulum stress and unfolded protein response

Protein translation greatly varies among cell types and tissues, thereby different amounts of nutrients and energy supply are required for ER homeostasis and correct protein folding (112). Different physiological and pathological processes can interfere with the ER environment and its chaperone activity, thus causing accumulation of misfolded/unfolded proteins, which leads to ER stress (128). Perturbations in the calcium homeostasis of the ER (e.g. blocking of SERCA2 by its specific inhibitor thapsigargin), changes in the redox conditions (for example by DTT), or ATP depletion will result in an accumulation of misfolded/unfolded proteins and subsequently in ER stress (129-131). Recent reports show that the accumulation of unfolded proteins and ER stress is observed with aging and various illnesses, such as cancer, diabetes, autoimmune conditions, obesity, as well as liver, neurodegenerative and lung diseases (132-134). In lung pathology, ER stress has been found in pulmonary fibrosis and infections, lung cancer, cystic fibrosis, asthma, during cigarette smoke exposure and in the setting of hyperoxia-induced lung injury (133). Moreover, increased expression of ER stress markers are observed during instillation of ovalbumin into lungs. The chronic mechanisms of the ER stress during pulmonary fibrosis are related to surfactant mutations in ATII cells. The deletion of a specific sequence in the CFTR channel leads to its ER retention, ER stress and manifestation of cystic fibrosis (135,136).

In order to cope with ER stress, cells activate unfolded protein response pathways (UPR). Based on the mechanism of action and cellular outcome, these processes are classified as adaptive or maladaptive (Figure 1.9). During the acute (adaptive) phase of ER stress, the main function of the UPR is to restore the ER protein-folding homeostasis by decreasing protein synthesis and translation and by activation of ERAD and autophagy. However, if the initial UPR attempts for alleviating ER stress fails, a maladaptive response is triggered (112).

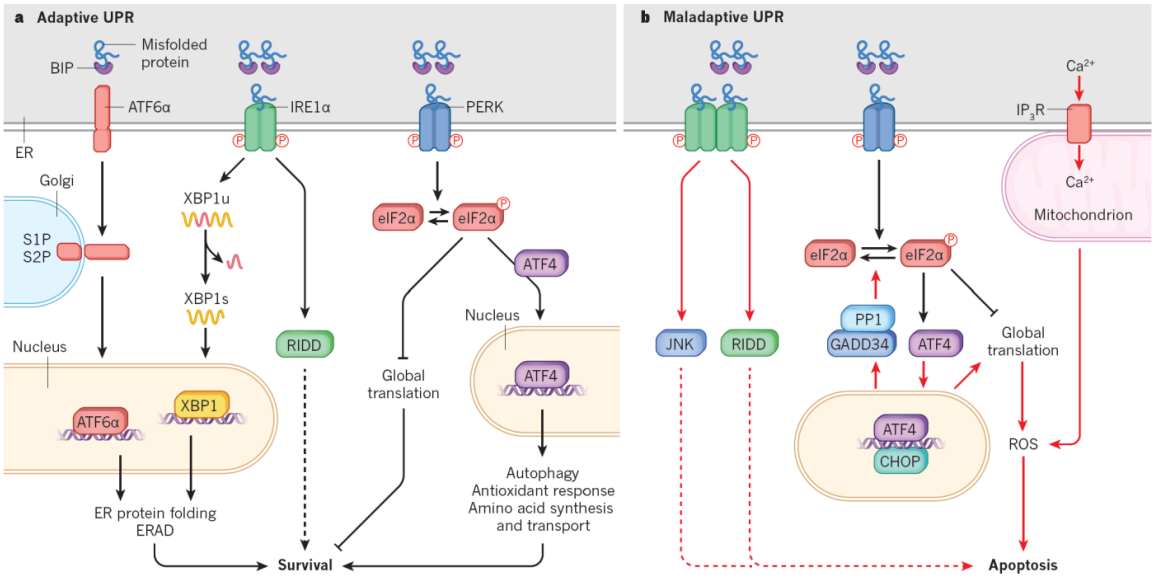

Figure 1.9 Adaptive and maladaptive UPR pathways. (A) The adaptive UPR comprises three parallel signaling branches: ATF6α, IRE1α–XBP1 and PERK–eIF2α. Misfolded proteins that accumulate in the ER bind to BiP, which causes it to be released from the UPR sensors and triggers their signaling pathways. On release from BiP, ATF6α is trafficked to the Golgi apparatus for processing by the enzymes S1P and S2P, to release a soluble cytosolic fragment that enters the nucleus to induce the expression of target genes. IRE1α and PERK homodimerize or oligomerize and trans-autophosphorylate to activate their downstream pathways and promote cell survival. **(B)** The maladaptive UPR is induced by sustained activation of the PERK pathway, which is the result of prolonged severe ER stress and leads to apoptosis. Adapted from Wang *et al,* Nature, 2016 (112).

Up to date, three main UPR pathways, named by ER-localized proteins have been characterized: inositol-requiring enzyme 1 (IRE1), protein kinase RNA-activated (PKR)-like ER kinase (PERK) and activating transcription factor-6 (ATF6). Under normal conditions, all three cellular sensors are bound to BiP. The accumulation of misfolded proteins leads to BiP dissociation from ER stress receptors, their autophosphorylation and their subsequent activation (137). Accumulating evidence suggests that UPR branches are not activated simultaneously during ER stress. While contribution of the PERK axis is more limited to the chronic ER stress, the activation of IRE1 and ATF6 appear to be more immediate (131,138).

Of note, a considerable amount of research studying the effects of unfolded/misfolded proteins in the ER is based on data obtained from irreversible chemical ER stress inducers, such as tunicamycin (which prevents N-glycosylation of peptides in ER), DTT (a reducing agent that prevents oxidation in ER) and thapsigargin (an irreversible inhibitor of the SERCA). The above-mentioned compounds have many pleiotropic effects and fully activate the UPR, which ultimately leads to cell death (139). In contrast, reports focusing on observations on

physiological ER stressors reveal non-classical responses of the UPR pathways that differ from their activation by chemical inducers and do not lead to immediate cell death (130,139-142).

1.8.1 The IRE1 pathway

As one of the most conserved UPR receptors, IRE1 represents a transmembrane protein that has two homologs, IRE1α and IRE1β. Based on previous research, IRE1α is ubiquitously expressed in all cells and tissues, whereas IRE1β expression is limited to the intestinal and pulmonary mucosal epithelium (119,143). IRE1α is mainly responsible for UPR signaling, while the role of IRE1β is still debated (143). As shown in Figure 1.10, IRE1α has a luminal domain connected with the ER membrane, a cytosolic kinase and an endoribonuclease domain (144).

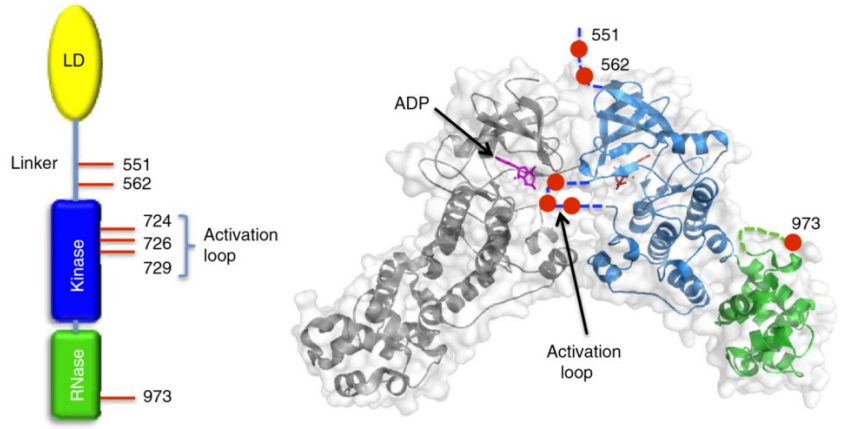

Figure 1.10 IRE1α structure and phosphorylation sites. The position of phospho sites relative to each other and mapped onto the X-ray structure of human IRE1 autophosphorylation complex (3P23). Adapted from Prischi *et al*, Nat Commun, 2014 (145).

After BiP dissociation under stress conditions, IRE1α undergoes oligomerization and activation of the cytosolic kinase domain by phosphorylation at Ser724, Ser726 and Ser729. Previous studies have reported that phosphorylation of IRE1α within the kinase domain increases the IRE1α RNAase splicing activity and induces the cleavage of cellular mRNA leading to subsequent degradation. This mechanism serves to decrease the ER overload by limiting mRNA transcription and protein synthesis and is termed IRE1-dependent decay (RIDD) (145,146). Additionally, the IRE1α endoribonuclease activity selectively cleaves a 26-nucleotide fragment from the XBP1 mRNA, thus producing the XBP1s transcription factor. This active form of XBP1s upregulates genes that are involved in enhancing and assisting protein folding, and also

stimulates protein degradation pathways (112). The schematic representation of IRE1α signaling is depicted in Figure 1.11.

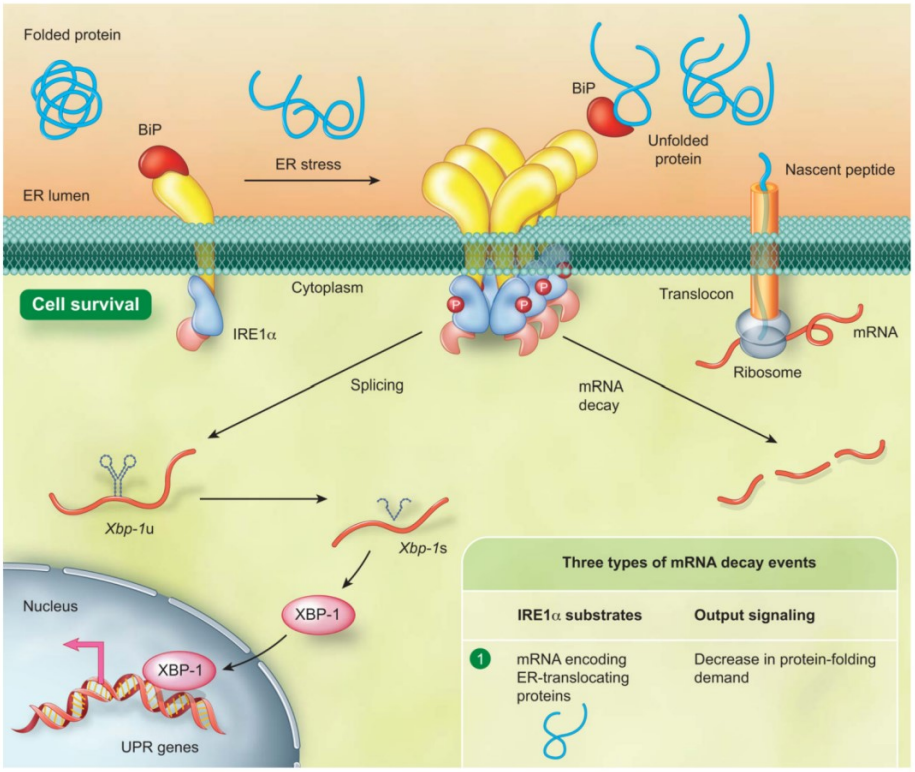

Figure 1.11 IRE1α regulatory mechanisms during ER stress. Mammalian IRE1α is repressed by physical interaction with BiP when demand and capacity of protein folding are balanced in the ER. A dissociation of IRE1α from BiP due to an elevated level of unfolded proteins in the ER leads to activation of IRE1α. In addition, IRE1α unconventionally splices the transcript of Xbp-1 transcription factor. The spliced XBP-1 enters into the nucleus to transcriptionally reprogram UPR target genes, including ER chaperones. Adapted from Chen *et al*, Trends Cell Biol, 2013 (147).

Accordingly, sustained IRE1α activation promotes pro-apoptotic pathways and cellular death via oligomerization and recruitment of the TNF receptor-associated factor 2 (TRAF2), apoptosis signal-regulating kinase 1 (ASK1), JNK and ERK1/2 (148,149). Interestingly, these IRE1 functions are not only limited to assisting the protein folding of the normal cellular proteome. It has been described that the IRE1 stress pathway is manipulated by viruses to increase their replication (150,151).

1.8.2 PERK pathway

PERK is a type I membrane protein located in the ER. It is ubiquitously expressed in all cells and consists of luminal and cytoplasmic kinase domains (119). Detachment of BiP from the ER

luminal domain leads to PERK autophosphorylation and activation of the specific UPR signaling pathway (Figure 1.12).

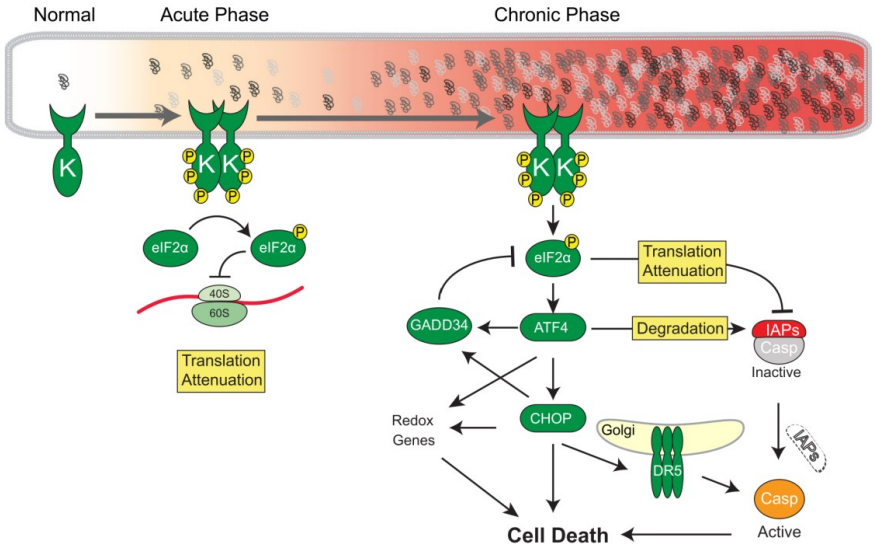

Figure 1.12 PERK activation and signaling pathway. Consequences of acute and chronic PERK activation. PERK has a kinase domain (K) and phosphorylates eukaryotic translation initiation factor 2 subunit alpha (eIF2α). In the acute phase, PERK-eIF2α attenuates overloading of proteins in the ER. Upon chronic activation of PERK signaling, expression of activating transcription factor-4 (ATF4) regulates cell fate. GADD34 dephosphorylates eIF2α, and protein translation is reinitiated. Adapted from Hiramatsu *et al*, Am J Pathol, 2015 (144).

Activation of PERK signaling leads to phosphorylation of eukaryotic translation initiation factor 2α (eIF2α) at Ser51 and repression of the global protein translation by blocking translation initiation (142,152). While eIF2α is phosphorylated the canonical eukaryotic initiation factor 4E (eIF4E) cap-dependent translation is attenuated and the alternative eIF4E non-dependent protein translation is activated (153). These alternative pathways more efficiently translate mRNA transcripts with short open reading frames in their 5'-regions, including the activating transcription factor 4 (ATF4). ATF4 acts as a transcription factor and thus helps the ER to cope with misfolded peptides by regulating gene expression of proteins involved in redox reactions, amino acid metabolism and ER chaperones (132). Alternatively, upon sustained activation, ATF4 may activate the transcription of C/EBP homologous protein (CHOP) and growth arrest and DNA damage-inducible protein (GADD34), which dephosphorylates eIF2α via the catalytic subunit of type 1 protein serine/threonine phosphatase (PP1) and restores protein synthesis (119,154). The mechanisms of PERK-mediated cell death were unknown until recently it has been discovered, that ATF4 and CHOP interact and upregulate the genes encoding protein synthesis and the UPR, but not apoptosis. Increased

expression of ATF4 and CHOP dramatically increase protein translation and cause ATP depletion, which results in oxidative stress and cell death (131,155). These results suggest that the status of eIF2α phosphorylation, but not ATF4 transcriptional activity, promotes cell survival and determines the switch between adaptive and maladaptive PERK responses (119).

1.8.3 ATF6 pathway

In addition to the IRE1 and PERK unfolded protein response pathways, the ER cell homeostasis can be restored through another UPR signaling pathway by activating transcription factor 6 (ATF6). ATF6 is a member of the leucine zipper protein transcription factors that are encoded in humans by two genes, ATF6A and ATF6B, where ATF6A represents the most powerful activator of the UPR (119). After ATF6 activation by dissociation from BiP, ATF6 is exported from the ER to the Golgi, where it is cleaved by the membrane-bound transcription factor peptidase site 1 and 2 (MBTPS1, MBTPS2), thus producing a transcriptionally active N-terminal cytosolic form of ATF6 (ATF6f) (134). The cleaved fragment contains a transcriptional activation domain and a nuclear localization sequence, thereby ATF6f is translocated to the nuclei and modulates the gene expression of cAMP response element-binding protein (CREB), XBP1, serum response factor, general transcription factor I and also other genes involved in protein folding (116,119,156). In addition, ATF6 may potentiate the effects of IRE1 and PERK signaling and increase the expression of XBP1 and CHOP (144).

1.8.4 Endoplasmic reticulum-associated degradation

Recent evidence suggests that in mammals, around 30% of all newly translated proteins are folded incorrectly (157). If the ER quality control machinery fails to correct these proteins, they need to be eliminated by the cell. Terminally unfolded or misfolded proteins are retrotranslocated, ubiquitinated and degraded by 26S proteasome in a process termed ER-associated degradation (ERAD) (158). While proteasomal ERAD is the most common mechanism of protein disposal, it is limited by the pore size of channels that are required for translocation. Thus, large protein aggregates and complexes undergo ER-to-lysosome-associated degradation (ERLAD) that include both autophagic and non-autophagic degradation (112,159). It has been shown that four ERAD pathway subforms exist, depending on the localization of the unfolded or misfolded proteins: ERAD-C (cytosolic), ERAD-L (luminal), ERAD-M (membrane) and ERAD-T (translocon-associated or preemptive degradation) (160).

Proteins that are subjected to degradation undergo a multistep process including recognition, targeting, extraction and ubiquitination. In the case of glycosylated proteins, the first step of

recognition begins after a mannose residue is trimmed by MAN1B1, which leads to the formation of Glc3Man8GlcNAc2 peptide and further binding by the EDEM family that contributes to ERAD acceleration (EDEM1-3) (115,161). Next, depending on the localization and of assisting chaperones, E3 ligases are recruited to the complex. It has been reported that proteins such as SEL1L, Derlin 1-3, HERP, OS9, XTP-B and the E3 ubiquitin ligases, HRD1 and gp78, are key components of the mammalian ERAD pathway (114,162). The schematic presentation of the mammalian ERAD complex is depicted in Figure 1.13.

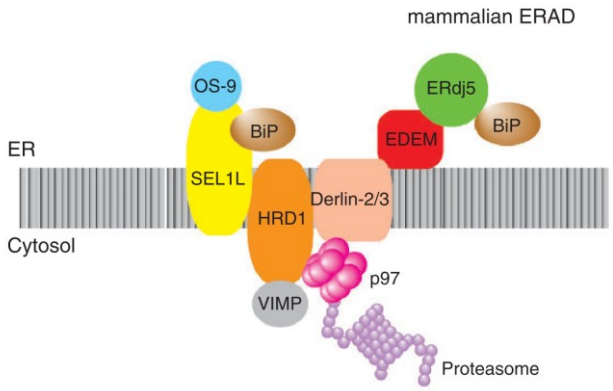

Figure 1.13 Mammalian ERAD complex. The mammalian HRD1/SEL1L ERAD complex. OS-9 recognizes N-glycans on misfolded proteins, which are then ubiquitinated by HRD1 in the cytosol and degraded by the proteasome. EDEM also recognizes N-glycans on misfolded proteins and recruits them to Derlin-2/3 and p97. ERdj5 interacts with EDEM and BiP and promotes dislocation of misfolded proteins from the ER by cleaving their incorrect disulfide bonds. Adapted from Hoseki *et al*, J Biochem, 2009 (163).

After being translocated and extracted to the cytosol, the substrate is transferred to the 26S proteasome for degradation with the help of E3 ligases, chain elongation factors, deubiquitinases and shuttle proteins (114). While the degradation of glycosylated proteins requires the formation of the above-mentioned complex, misfolded non-glycosylated peptides can be directly recruited to the ERAD machinery via BiP-assisted binding (163).

Accumulating evidence suggests that the UPR pathways are linked to ERAD. Treatment with tunicamycin affects the stability of the E3 ubiquitin ligase, gp78 and upregulates ERAD in cells (164). Furthermore, both spliced versions of ATF6 and XBP1, acting as transcription factors, can upregulate the ERAD components, SEL1L, Herp, EDEM1 and Derlin-3 (165,166). Finally, it has been shown that one of the UPR receptors, IRE1α can direct both proteasomal and lysosomal degradation of misfolded proteins and can also be a substrate for ERAD through the interaction with SEL1L and HRD1 (158,167,168).

1.9 Work hypothesis and aims

The main aim of the current work was to investigate how hypercapnia affects the maturation of the Na,K-ATPase β-subunit maturation in alveolar epithelial cells.

Based on the evidence that hypercapnia 1) impairs alveolar fluid clearance by downregulation of the plasma membrane expression of the Na,K-ATPase; 2) interferes with cellular homeostatic parameters that are essential for ER protein folding (e.g. increases intracellular Ca^{2+} levels, decreases ATP production, interferes with lipid metabolism and nucleosome assembly; 3) activates intracellular signaling kinases that are related to protein maturation in ER, including AMPK, ERK1/2, and JNK; and finally, 4) based on the fact that activated unfolded protein response has been found in various conditions accompanied with hypercapnia and decreased alveolar fluid clearance, such as pulmonary infections, cystic fibrosis and asthma;

we hypothesized that:

Elevated levels of CO_2 may alter the ER maturation of the Na,K-ATPase and thus influence delivery of the transporter to the plasma membrane in alveolar epithelial cells, thereby decreasing the function of the Na,K-ATPase.

To test this hypothesis, the following main questions were formulated:

1. Do elevated CO_2 levels alter the cell surface expression of the Na,K-ATPase in alveolar epithelial cells after short- and long-term exposure?
2. Does hypercapnia interfere with the turnover of the Na,K-ATPase β-subunit in the ER and does it prevent its exocytosis in alveolar epithelial cells?
3. Which molecular mechanisms are involved in the regulation of maturation of the Na,K-ATPase β-subunit in the ER upon exposure to elevated CO_2 levels?
4. Does hypercapnia activate unfolded protein response pathways in alveolar epithelial cells?
5. Does interfering with the identified ER pathways rescue the plasma membrane abundance and function of the Na,K-ATPase in alveolar epithelial cells upon hypercapnia?

2. Materials and methods

2.1 Instruments

Table 2.1 List of electronic devices used in this work

Device	Company
BioPhotometer, spectrophotometer	Eppendorf, Hamburg, Germany
Carl Zeiss Axio Observer Z1, fluorescent microscope	Carl Zeiss, Wetzlar, Germany
CASY Cell Counter and Analyzer Model TT	Roche Innovates, Reutlingen, Germany
CFX Connect Real-Time PCR Detection System	Bio-Rad, Munich, Germany
Curix 60 Processing Machine, film developer	Agfa, Morstel, Belgium
Electrophoresis and Blotting System	Bio-Rad, Munich, Germany
Gel imaging system	Bio-Rad, Munich, Germany
HeraCell 150, cell culture incubator	Thermo Scientific, Dreieich, Germany
Heraeus Fresco, centrifuge	Thermo Scientific, Dreieich, Germany
Humidified chamber, cell culture incubator	BioSpherix, Parish, NY, USA
Infinite 200 PRO, plate reader	TECAN, Männedorf, Switzerland
KNF Laboport vacuum pump flyer	KNF, Freiburg, Germany
Leica SP5, confocal microscope	Leica Microsystems, Wetzlar, Germany
Leica VT 1200S, vibratome	Leica Microsystems, Wetzlar, Germany
Mettler H20T Precision, laboratory scale	Mettler Toledo, Giessen, Germany
Milli-Q, water purification system	Millipore, Schwalbach, Germany
Mini-PROTEAN Tetra Cell, immunoblot	Bio-Rad, Munich, Germany
NanoDrop 1000, RNA and DNA measurement	Thermo Scientific, Dreieich, Germany
Optima MAX XP, ultracentrifuge	Beckman Coulter, Brea, CA, USA
pH-Meter 766	Knick, Berlin, Germany
Plymax 1040-Waving Platform Shaker	Heidolph, Schwabach, Germany
PowerPac Basic Power Supply, immunoblot	Bio-Rad, Munich, Germany
RapidLab Blood Gas Analyzer, CO_2 measurement	Siemens, Erlangen, Germany
T100 Thermal Cycler	Bio-Rad, Munich, Germany
Thermomixer	Eppendorf, Hamburg, Germany
Transblot SD Semi-Dry Transfer Cell	Bio-Rad, Munich, Germany

2.2 Chemicals and consumables

Table 2.2 List of common chemicals and consumables used in this work

Name	Company
BSA (bovine serum albumin)	Sigma-Aldrich, Taufkirchen, Germany
Cell culture plates, single- and multi-well	Greiner, Nürtingen, Germany
Cell scapers, 28cm and 40cm handle	Greiner, Nürtingen, Germany
D-mannitol	Sigma-Aldrich, Taufkirchen, Germany
DMEM	Thermo Fisher, Darmstadt, Germany
DMSO (Dimethyl sulfoxide)	Sigma-Aldrich, Taufkirchen, Germany
EDTA (Ethylenediaminetetraacetic acid)	Roth, Karlsruhe, Germany
Ethanol	Sigma-Aldrich, Taufkirchen, Germany
EZ-link Sulfo-NHS-SS-Biotin	Thermo Scientific, Waltham, MA, USA
FBS	PAA Laboratories, Egelsbach, Germany
Glacial acetic acid	Roth, Karlsruhe, Germany
Glycerol	Sigma-Aldrich, Taufkirchen, Germany
Glycine	Sigma-Aldrich, Taufkirchen, Germany
Ham's F-12 medium	Thermo Scientific, Dreieich, Germany
HEPES	Roth, Karlsruhe, Germany
Methanol	Roth, Karlsruhe, Germany
NaCl	Roth, Karlsruhe, Germany
NP-40	Sigma-Aldrich, Taufkirchen, Germany
Paraformaldehyde (PFA)	Sigma-Aldrich, Taufkirchen, Germany
PBS	PAN-Biotech, Aidenbach, Germany
Penicillin	PAN-Biotech, Aidenbach, Germany
Polystyrene tubes, 15ml and 50ml	BD Falcon, Heidelberg, Germany
Protease inhibitor cocktail	Roche, Basel, Switzerland
Reaction tubes 0.5ml and 1.5ml	Eppendorf, Hamburg, Germany
SDS (Sodiumdodecylsulfate)	Roth, Karlsruhe, Germany
Sodium chloride	Roth, Karlsruhe, Germany
Streptomycin	PAN-Biotech, Aidenbach, Germany
Sucrose	Sigma-Aldrich, Taufkirchen, Germany
Syringes: 1ml, 10ml and 20ml	B.Braun, Melsungen, Germany
Tris	Roth, Karlsruhe, Germany
Tris-Base	Roth, Karlsruhe, Germany
Triton-X-100	Roth, Karlsruhe, Germany
Trypsin-EDTA	Thermo Fisher, Darmstadt, Germany
β-Mercaptoethanol	Roth, Karlsruhe, Germany

The following chemicals were used during the inhibition or activation of the cellular organelles or specific pathways (Table 2.3).

Table 2.3 List of the chemical compounds used in this work

Compound	Application	Concentration	Vehicle	Company
2-APB	IPR3 channel inhibitor	100 µM	DMSO	Sigma-Aldrich
BAPTA-AM	Ca^{2+} chelator	25 µM	DMSO	Sigma-Aldrich
Chloroquine	Lysosomal inhibitor	100 µM	Water	Sigma-Aldrich
Kifunensine	Mannosidase inhibitor	20 µM	DMSO	Sigma-Aldrich
Kira6	IRE1α kinase inhibitor	1 µM	DMSO	Sigma-Aldrich
MG-132	Proteasome inhibitor	20 µM	DMSO	Calbiochem
Quercetin	IRE1α activator	100 µM	DMSO	Sigma-Aldrich
SP600125	JNK specific inhibitor	25 µM	DMSO	Sigma-Aldrich
STF-083010	IRE1α RNAase inhibitor	100µM	DMSO	Sigma-Aldrich
Thapsigargin	ER stress inducer	1µM	DMSO	Sigma-Aldrich
α-Ketoglutaric acid	ATP metabolite	10 mM	Water	Sigma-Aldrich

2.3 Buffers

Table 2.4 Common buffers used in this work

Buffer name	Compounds
mRIPA buffer	50 mM Tris-HCL, pH=8 150 mM NaCl 1% IGEPAL CA-630 (Sigma-Aldrich, St. Luis, MO, USA) 1% (w/v) Sodium deoxycholate (Sigma-Aldrich, St. Luis, MO, USA)
T-TBS	50 mM Tris 150 mM NaCl 0,05% Tween-20
2xLaemmli Buffer	100 mM Tris, pH=6.8 4% SDS 0,02% Bromophenol blue 20% Glycerol
SDS-Page running buffer	25 mM Tris 192 mM Glycine 0.1% SDS
SDS-Page transfer buffer	25 mM Tris 192 mM Glycine 20% [v/v] Methanol

2.4 Primary and secondary antibodies

Table 2.5 List of the antibodies used in this work

Antibody	Dilution rate	Species	Company
ATF4	1:1000	Rabbit	Cell Signaling
BiP (GRP78)	1:200 (IB)	Mouse	Santa Cruz Biotechnology
BiP (GRP78)	1:50 (IF)	Rabbit	Cell Signaling
Calnexin	1:500 (IF)	Rabbit	Abcam
CD29	1:1000	Mouse	BD Transduction Laboratories
CHOP	1:500	Mouse	Cell Signaling
EDEM1	1:1000	Rabbit	Sigma-Aldrich
eIF2α	1:5000	Rabbit	Cell Signaling
GADD34	1:500	Rabbit	Proteintech
GCN2	1:1000	Rabbit	Cell Signaling
GFP	1:1000; 1:50 (IP)	Rabbit	Santa Cruz Biotechnology
GM130	1:500	Rabbit	Cell Signaling
GRP94	1:1000	Rabbit	Cell Signaling
IRE1a	1:1000	Rabbit	Cell Signaling
MAN1B1	1:200	Mouse	Santa Cruz Biotechnology
Na,K-ATPase α-subunit	1:1000	Mouse	Merck Millipore
Na,K-ATPase β_1-subunit (clone M17-P5-F11)	1:5000; 1:100 (IF); 1:50 (IP)	Mouse	Thermo Scientific
Na,K-ATPase β_3-subunit	1:1000	Goat	Santa Cruz Biotechnology
PDI	1:1000	Rabbit	Cell Signaling
PERK	1:1000	Rabbit	Cell Signaling
Phospho-eIF2α	1:500	Rabbit	Cell Signaling
Phospho-IRE1α (S724)	1:2000	Rabbit	Novus Biologicals
Phospho-SAPK/JNK (Thr183/Tyr185)	1:500	Rabbit	Cell Signaling
PKR	1:1000	Rabbit	Cell Signaling
SAPK/JNK	1:1000	Rabbit	Cell Signaling
Transferrin receptor	1:1000	Mouse	Thermo Scientific
XBP1s	1:1000	Rabbit	Cell Signaling
β-actin	1:1000	Rabbit	Sigma-Aldrich
IgG, HRP mouse	1:10000	Mouse	Cell Signaling
IgG, HRP rabbit	1:10000	Rabbit	Cell Signaling
IgG, HRP goat	1:10000	Goat	Santa Cruz Biotechnology
Alexa Fluor 488, Alexa Fluor 594	1:500 (IF)	Rabbit	Thermo Fisher
Alexa Fluor 488, Alexa Fluor 594	1:500 (IF)	Mouse	Thermo Fisher

2.5 Murine precision-cut lung slices and cell lines

Murine precision-cut lung slices (PCLS) were isolated as previously described (169). Briefly, after the lung was removed from anesthetized mice, it was filled intratracheally with 0.3% agarose and embedded in agarose. Next, the lung lobes were cut into 200 µm sections using a vibratome and kept in culture media. After isolation, PCLS were cultured and used on day 3.

Epithelial cell lines:

- Primary rat alveolar epithelial type II cells were isolated as previously described (51,170). Briefly, after removal from male Sprague-Dawley rats, lungs were flushed and digested with elastase, DNAse and homogenized mechanically . Next, the lung homogenates were filtered through 100, 40 and 10 µm filters and the supernatant was plated on rat IgG (Sigma-Aldrich, Germany) pre-coated plates. After incubation, cells were collected and plated in conditioned media for further experiments.
- A549 cells were obtained from the American Type Culture Collection (ATCC-CCL-185).
- In some experiments, A549 cells stably expressing the Na,K-ATPase α_1-subunit fused to a green fluorescent protein (GFP) were used (A549-α_1-GFP cells; a generous gift from Profs. Sznajder and Dada, Northwestern University, Chicago, IL, USA).

2.6 Cell culture and growth conditions

Alveolar epithelial cells were cultured in a humidified incubator with an atmosphere of 5% CO_2 and 95% air at 37°C. Proliferative cells were subcultured once achieving 80% confluence. Cells were rinsed with sterile 1X PBS and detached by incubation with 0.25% trypsin-EDTA. The reaction was stopped by the addition of DMEM and cells were plated on cell culture dishes, 6- and 12-well plates or microscopy chamber slides. After defreezing, A549 cells were kept in culture from passages 4 to 12.

The following media compositions were used for PCLS and cell culturing (Table 2.6).

Table 2.6 Media composition for cell culture studies

Culture	Media composition
PCLS	DMEM/F12; 10% fetal bovine serum; 100 U/ml penicillin; 100 µg/ml streptomycin; 1% amphotericin B
Primary ATII cells	DMEM high glucose (4,5 g/L); 10% fetal bovine serum; 100 U/ml penicillin; 100 µg/ml streptomycin
A549 cells	DMEM high glucose (4,5 g/L); 10% fetal bovine serum; 100 U/ml penicillin; 100 µg/ml streptomycin

2.7 Hypercapnia treatment

In order to study the effects of hypercapnia on PCLS and cultured alveolar epithelial cells, the buffer capacity of the media was modified by changing the initial pH with MOPS-base to obtain a pH of 7.4 both at 40 mmHg (Control, "Ctrl") and 120 mmHg (Hypercapnia, "CO_2"). Compositions of the normocapnia and hypercapnia medium are shown in Table 2.7. The experimentally required CO_2 levels were obtained by incubating and equilibrating the media overnight in a humidified chamber. Afterwards, PCLS or cultured cells were exposed to normocapnia or hypercapnia in the humidified chamber. The levels of CO_2 and pH were controlled by using a Rapidlab blood gas analyzer.

Table 2.7 Composition of normocapnic and hypercapnic media

Normocapnic Media (Ctrl)	Hypercapnia Media (CO_2)
3 ml DMEM (DMEM/F12 for PCLS) with FCS 10%	3 ml DMEM (DMEM/F12 for PCLS) with FCS 10%
1 ml Ham´s F-12 medium	1 ml Ham´s F-12 medium
0.5 ml MOPS buffer solution 0.5 M (pH 7.4)	0.5 ml MOPS buffer solution 0.5 M (pH 13)

2.8 Analysis of protein expression

2.8.1 Cell lysis and protein quantification

To investigate the protein changes after treatment, cells were lysed by incubation with mRIPA buffer. After 10 min of incubation the samples were centrifuged at 10,000 rpm for 10 min at 4°C in order to remove cellular debris. Total protein concentrations from the cell lysates were measured by the Bradford assay. Briefly, samples were diluted 1:20 in Bradford reagent (Bio-Rad, Hercules, CA, USA) and after 15 minutes of incubation at room temperature protein concentrations were determined by the assessment of protein absorbance by using a spectrophotometer according to the instructions of the manufacturer.

2.8.2 SDS-PAGE, western immunoblotting and densitometry

For cell culture experiments, 25-50 µg of the protein supernatant was diluted with 2X Laemmli sample buffer and heated to 60°C for 20 min. The samples were cooled shortly, centrifuged and according to the expected molecular weight, the proteins were resolved in 7.5% and 10% polyacrylamide gels (Roth, Karlsruhe, Germany). The electrophoresis was preformed in running buffer at 100 V for 1.5 h. Then, the proteins were transferred to a nitrocellulose membrane (Bio-Rad, Hercules, CA, USA) by a semi-dry method at 400 mA for 60 min in transfer buffer. To prevent unspecific binding, the membranes were blocked in 5% skimmed milk (Sigma-Aldrich, St. Luis, MO, USA) in T-TBS buffer and, after washing, incubated overnight at 4°C with primary antibodies. The next day, after washing in T-TBS buffer, the blots were incubated with the secondary antibodies for 1 hour at room temperature. The membrane blots were developed with a SuperSignal west pico or a femto chemiluminescent substrate detection kit (Thermo Scientific, Waltham, MA, USA) according to the manufacturer's recommendations using the CP-1000 automatic film processor. Further, a densitometric analysis to quantify the band intensity was done in the ImageJ software (National Institutes of Health, Bethesda, MD, USA).

2.8.3 Coomassie staining

For some experiments, a loading control was performed through a Coomassie brilliant blue 250 (Sigma-Aldrich, St. Luis, MO, USA) staining of nitrocellulose membranes. After the proteins were detected by immunoblotting, the membranes were washed for 10min in distilled water and subsequently incubated in the following solution: 0.1% (v/v) Coomassie brilliant blue 250, 40% (v/v) methanol and 1% (v/v) glacial acetic acid for 10 min. Afterwards, the membranes were thoroughly rinsed with the washing solution: 50% (v/v) methanol and 1% (v/v) glacial acetic acid. At the end of the staining, the membranes were washed again with distilled water and scanned.

2.8.4 Cell surface biotinylation

To analyze the Na,K-ATPase plasma membrane abundance, a biotinylation of the cell surface proteins was performed. After the experimental treatment, the media was removed, the cells were rinsed with 1X PBS (Mg^{2+}, Ca^{2+}) and incubated in the dark with non-permeable EZ-link Sulfo-NHS-SS-Biotin (Pierce Biotechnology, Waltham, MA, USA) dissolved in 1X PBS (2 mg/ml) for 20 min at 4°C. Next, the cells were rinsed thoroughly three times by incubating for 10 min with 100 mM glycine. Afterwards, the cells were lysed in mRIPA buffer, scraped off

and the cell lysates were centrifuged at 10,000 rpm for 10 min at 4°C. After quantification, equal amounts of proteins (150-300 µg) were incubated overnight at 4°C with streptavidin-agarose beads (Pierce Biotechnology, Waltham, USA). The next day, after a brief centrifugation, the supernatants were aspirated and the beads were washed with the solutions A, B, C and 10 mM Tris pH=7.4 (Table 2.8). Biotin-labeled proteins were eluted from the beads by incubating with 2X Laemmli buffer at 60°C for 20 min. Finally, the biotinylated cell surface proteins were analyzed by SDS-PAGE and western immunoblotting.

Table 2.8 Biotinylation buffer composition

Buffer name	Composition
Solution A	150 mM NaCl, 50 mM Tris pH 7.4, 5 mM EDTA
Solution B	500 mM NaCl, 50 mM Tris pH 7.4, 5 mM EDTA
Solution C	500 mM NaCl, 20 mM Tris pH 7.4, 0.2% BSA

2.8.5 Co-immunoprecipitation

To test for protein-protein interactions between the Na,K-ATPase subunits or the oxidation status of the Na,K-ATPase β-subunit after hypercapnia, co-immunoprecipitation was used. At first, A549 cells were exposed to normocapnia (Ctrl, 40 mmHg of CO_2) or hypercapnia (120 mmHg of CO_2), washed three times in 1X PBS and lysed in IP lysis buffer (20 mM HEPES pH 7.4, 150 mM NaCl, 0.5% NP-40, 2 mM EDTA, 2 mM EGTA, 5% glycerol) containing freshly prepared protease and phosphatase inhibitors for 10 min on ice. Next, the cells were scraped off, centrifuged at 10,000 rpm for 10 min at 4°C and the protein concentrations were quantified. Cell lysates containing 150-300 µg of proteins were precleared with A/G agarose beads (Santa Cruz Biotechnology, Heidelberg, Germany). After pre-clearing, the supernatants were incubated with specific antibodies against Na,K-ATPase subunits, 2,4-DNPH, IgG negative control, and A/G agarose beads at 4°C overnight. After incubation, the supernatants were aspirated and the A/G agarose beads were washed thoroughly three times in IP lysis buffer containing protease and phosphatase inhibitors. Precipitated complexes were eluted from the beads by adding 2X Laemmli buffer, heated to 60°C for 20 min and then subjected to SDS-PAGE and western immunoblotting.

2.8.6 Measurement of protein oxidation

Total protein oxidation was measured by using the OxyBlot Protein Oxidation Detection Kit (Merck Millipore, Darmstadt, Germany) according to the manufacturer's instructions. Briefly, after the normocapnia or hypercapnia treatment, the cells were washed three times in 1X PBS and lysed using the mRIPA buffer supplemented with 1% (v/v) 2-mercaptoethanol. The cells

were then scraped off, centrifuged at 10,000 rpm for 10 min at 4°C and the protein concentrations were measured. Equal amounts of proteins were adjusted to 5 µl of the sample and 5µl of the 12% SDS. Next, the samples were derivatized by adding 10 µl of the 1X DNPH solution and then incubated for 15 min. Afterwards, the neutralization solution was added, samples were subjected to SDS-PAGE and transferred to nitrocellulose membranes. The membranes were incubated with the primary antibody stock solution of the kit for 1 h at room temperature, and then the secondary antibody stock solution from the kit was applied for 1 h. Next, protein oxidation was determined by a chemiluminescent method by developing the blots with the SuperSignal west pico or femto chemiluminescent substrate detection kit (Thermo Scientific, Waltham, MA, USA) according to manufacturer's recommendations using the CP-1000 automatic film processor. The obtained protein oxidation was quantified by densitometric analyses, calculated by using the ImageJ software (National Institutes of Health, Bethesda, MD, USA) and normalized to the total protein amounts after assessing by Coomassie staining.

2.8.7 Isolation of soluble cellular membrane protein fractions

The soluble fractions of plasma membrane proteins were obtained by ultracentrifugation as previously described (171). Briefly, after normocapnia or hypercapnia treatment, the cells were detached by incubation with 0.25% trypsin-EDTA for 5 min at 37°C and homogenized in the buffer (HB) (10 mM; 1 mM EDTA; 1 mM EGTA; 100 µg/ml N-tosyl-l-phenylalanine chloromethyl ketone, phosphatase and protease inhibitors), collected in a tube and centrifuged at 500×g at 4°C. The supernatants were then collected and subsequently centrifuged at 100,000×g for 1 h at 4°C. Next, the supernatants were aspirated and the pellets which contained crude membrane fractions were resuspended in HB buffer supplemented with 1% Triton X-100 and then centrifuged at 100,000×g for 30 min at 4°C. After centrifugation, the supernatants containing soluble membrane fraction were collected and used for the experiments.

2.8.8 Endoplasmic reticulum purification

The assessment of the endoplasmic reticulum (ER) folding protein environment was performed by isolation of the ER fraction from the whole cell lysate by using sucrose gradients followed by ultracentrifugation. The current protocol is an adaptation of previously described methods for ER isolation by Graham and Williamson *et al.* (172,173). The ER sucrose gradients were prepared by adding 2 M, 1.5 M and 1.3 M sucrose to the bottom of a sterile Beckman polyallomer ultracentrifuge tube.

After treatment, the cells were washed with 1X PBS, detached by incubating with 0.25% trypsin-EDTA for 5 min at 37°C and then pelleted by centrifugating at 200×g for 5 min at 4°C. Afterwards, the cells were collected in a tube, resuspended in MTE buffer solution (270 mM D-mannitol; 10 mM Tris-base; 0.1 mM EDTA; phosphatase and protease inhibitors), disrupted by homogenizing and passed through a 26 G needle. Then, the cell homogenates were centrifuged at 15,000×g for 10 min at 4°C. The supernatants were transferred to a 0.5 ml tube and were labeled as "total protein" fraction. Afterwards, using a micropipette, the supernatants were layered on top of the ER sucrose gradients and ultracentrifuged by using the Optima MAX XP ultracentrifuge with the MLA-55 fixed-angle rotor (Beckman Coulter, CA, USA) at 152,000×g for 70 min at 4°C. After centrifugation, the upper layer was transferred by using a micropipette into a sterile tube and was labeled as "Cytosol" fraction. Next, a large band at the interface of the 1.3 M sucrose gradient layer was extracted by using a 20G needle, transferred to a Beckman polyallomer ultracentrifuge tube and then diluted with an additional MTE buffer solution. Thereafter, the homogenates were centrifuged at 126,000×g for 45 min, the supernatants were discarded, and the pellets were resuspended in 50 µL of 1X PBS and labeled as "ER" fraction. Samples were used immediately for analysis or stored at -80°C.

2.9 Analysis of gene expression

2.9.1 RNA isolation

Total RNA was isolated by using the standard protocol of the RNeasy Kit (Qiagen, Hilden, Netherlands). Briefly, after treatment cells were washed with 1X PBS and then lysed in 350 µl RLT buffer. The lysates were then applied to the RNeasy spin columns and washed with the kit buffers. Finally, RNA was eluted by RNA-free water and the concentrations were measured using the NanoDrop 1000. The samples were used immediately for analysis or stored at -80°C.

2.9.2 cDNA synthesis (reverse transcription)

For cDNA synthesis 1 µg of the total RNA was used. The cDNA was obtained by using the iScript cDNA synthesis kit (Bio-Rad, Hercules, CA, USA) following the manufacturer's protocol. The reaction mix is shown in Table 2.10. The reverse transcription reaction was performed in a thermocycler under the following conditions: 25°C for 5 min, 42°C for 30 min, 85°C for 5 min and finally kept at 4°C.

Table 2.9 Master mix employed in the cDNA synthesis

Compound	Volume
Reaction buffer (5x)	4 µl
RNA (1 µg)	measured by NanoDrop
Reverse transcriptase	1 µl
Nuclease free water	up to 20 µl

2.9.3 Quantitative Real-Time Polymerase Chain Reaction (qRT-PCR)

To detect transcriptional changes, qRT-PCR was performed by using SYBR Green Master Mix (Bio-Rad, Hercules, CA, USA) according to the manufacturer's instructions. The primers used in the analysis were produced by Eurofins Genomic (Ebersberg, Germany) and are listed in Table 2.10.

Table 2.10 Primers used for qRT-PCR

Gene	Forward sequence 5'-3'	Reverse sequence 5'-3'
ATP1A1	AGCTACCTGGCTTGCTCTGTCC	GCTGACTCAGAGGCATCTCCTGC
ATP1B1	AAAAGTACAAAGATTCAGCCCAGAGGG	AGCTTGAATCTGCAGACCTTTCGC
GAPDH	AGCACCAGGTGGTCTCCTCT	CTCTTGTGCTCTTGCTGGGG

The cDNA was diluted 1:10 and the qRT-PCR was performed by using the iTaq Universal SYBR Green Supermix (Bio-Rad, Hercules, CA, USA) according to manufacturer's instructions on the CFX Connect Real-Time PCR Detection System and by using the cycle conditions as shown below:

Initial Denaturation	60 s	95°C
Denaturation	60 s	95°C
Primer annealing and elongation	30 s	55°C
Cooling down	-	4°C
Melting curve		

The mRNA expression levels of the Na,K-ATPase subunits were normalized to glyceraldehyde 3-phosphate dehydrogenase (GAPDH) expression by using the delta Ct (ΔCt) method.

2.10 Transfection with siRNA

To study the role of specific proteins in the regulation of the Na,K-ATPase, siRNA transfection using Lipofectamine RNAiMAX (Invitrogen, Waltham, MA, USA) was applied. The siRNA (concentrations are shown in Table 2.11) and Lipofectamine RNAiMAX (6µl per reaction) were diluted in Opti-MEM (Life Technology, Darmstadt, Germany) and incubated at room temperature for 20 min. After incubation, the lipofectamine-siRNA mix was added on top of the cells. After 6 hours, the culture medium was aspirated, replaced with fresh conditioned culture DMEM and the cells were incubated at 37°C for 36 or 48 hours.

Table 2.11 List of siRNAs used in knockdown studies

siRNA	Concentration (nM)	Company
si-EDEM	100	Santa Cruz Biotechnology
si-eIF2α	60	Santa Cruz Biotechnology
si-GCN2	100	Santa Cruz Biotechnology
si-HRI	100	Santa Cruz Biotechnology
si-IRE1α	60	Santa Cruz Biotechnology
si-MAN1B1	100	Santa Cruz Biotechnology
si-PERK	100	Santa Cruz Biotechnology
si-PKR	100	Santa Cruz Biotechnology
si-XBP1	100	Santa Cruz Biotechnology

2.11 Microscopy

2.11.1 Confocal and immunofluorescent imaging

Immunofluorescent microscopy was performed to analyze the subcellular localization of ER chaperons and plasma membrane expression of the Na,K-ATPase. Murine PCLS or alveolar epithelial cells were exposed to normal or elevated CO_2 levels for specified times and then were washed with 1X PBS and fixed by incubating with 4% paraformaldehyde for 30 min. After fixation, PCLS or cells were permeabilized with 0.01% Triton X-100 for 5 min, blocked by 3% BSA and incubated with primary antibodies at 4°C overnight. The next day, the treated cultures were washed three times with 1X PBS and the secondary antibodies were applied subsequently for 1 h. For visualizing of F-actin and the cellular plasma membrane, a phalloidin staining (Thermo Scientific, Eugene, OR, USA) was performed. After reconstitution according to the manufacturer's instructions, phalloidin was applied to the cells at a 1:40 dilution for 30 min prior to the nuclear staining. Next, the treated cultures were washed thoroughly three times with PBS. Finally, the nuclei were stained with Hoechst 33342 (Thermo Scientific, Eugene, OR,

USA) for 30 min. Fluorescence detection and capturing of images were performed by using the confocal Leica TCS SP5 (Leica Microsystems, Wetzlar, Germany) or the Carl Zeiss Axio Observer Z1 (Carl Zeiss, Wetzlar, Germany) immunofluorescent microscopes. The pictures were analyzed using the LAS AF (Leica) and the ZEN (Carl Zeiss) softwares. The co-localization was quantified by using the Fiji software (NIH, Bethesda, MD, USA).

2.11.2 Measurement of total intracellular calcium levels

The measurement of the intracellular Ca^{2+} levels was performed by using the Fluo-4 Calcium imaging kit (Life Technology, Darmstadt, Germany) according to the manufacturer's instructions. The Fluo-4 AM loading solution was prepared according to the supplied protocol. The cell culture medium from murine PCLS or alveolar epithelial cells was removed, washed three times with 1X PBS and the Fluo-4 AM loading solution was applied on top of the cells followed by an incubation at 37°C for 30 min. Afterwards the cultures were incubated for 15 min at room temperature. Next, the Fluo-4 loading solution was aspirated, the cells were washed in 1X PBS and exposed to normal or elevated CO_2 levels in the appropriate buffer culture media. The murine PCLS or the alveolar epithelial cells were fixed, the nuclei were stained with Hoechst 33342 (Thermo Scientific, Eugene, OR, USA) and the Ca^{2+} fluorescence intensity was detected by using a confocal or immunofluorescent microscope. The captured fluorescence signals were normalized to the nuclei counts and analyzed in the ImageJ software (NIH, Bethesda).

2.12 ATP measurement

To measure ATP levels after hypercapnia exposure, an ATP bioluminescence assay kit HSII (Roche Diagnostics, Mannheim, Germany) was used following the manufacturer's instructions. Briefly, the cells were treated with normal or elevated CO_2 levels, detached by an incubation with 0.25% trypsin-EDTA and diluted to a have a final concentration of 10^6 cells/ml. Afterwards, the lysis buffer provided in the kit was applied to the cells for 5 min at 25°C. Next, the samples were centrifuged at 10,000×g for 60 sec and the supernatant was transferred to a fresh tube. Afterwards, 50 µl of the supernatant was transferred to 96-well plates, 50 µl of the luciferase reagent was added to the samples and the luminescence was measured immediately by the Infinite M200 Pro reader. The obtained values were normalized to the protein amount, as assessed by the Bradford assay.

2.13 Measurement of Na,K-ATPase enzymatic activity

To measure the Na,K-ATPase activity, a high-sensitivity ATPase assay kit (Innova Biosciences, Cambridge, United Kingdom) was used, which determines the P_i released by ATP hydrolysis. Assessment of ouabain-sensitive ATPase activity was performed as previously described (171). Briefly, after the treatment with normocapnia or hypercapnia, the cells were detached by incubating with 0.25% trypsin-EDTA and the soluble plasma membrane fraction was isolated. Next, by using isolated soluble protein fractions as a substrate, the ATPase colorimetric assay was performed according to the manufacturer's instructions. To measure the ouabain-sensitive ATPase activity 10 mM of ouabain was applied to the samples. The absorbance was measured by the Infinite M200 Pro reader at 600 nm. The Na,K-ATPase-specific activity was quantified by the subtraction of the ouabain-sensitive from the total ATPase activity.

2.14 Assessment of cellular viability and cell counting

Cell number and viability were assessed by using the CASY Cell Counter and the Analyzer Model TT according to manufacturer's instructions. After the cells were exposed to normal or elevated CO_2 levels, they were detached by incubation with 0.25% trypsin-EDTA and diluted in culture medium. Afterwards, the cell suspension was diluted in a ratio of 1:100 in a CASY tone solution and placed to the measuring capillaries. The cellular viability was assessed by an automatic measurement of plasma membrane integrity upon an electric impulse. The preequilibrated specific cellular program was used to assess the cellular viability and amount.

2.15 Statistical analysis

All results shown in the graphs were expressed as mean ± standard deviation (SD). The statistical comparisons between two groups were analyzed by the unpaired Students t-test. The statistical significance of differences among more than two groups was calculated by using the one-way analysis of variance (ANOVA) with the Dunnet test for multiple comparisons. A *p*-value below 0.05 was considered as statistically significant. For the statistical analysis and data visualizing GraphPad Prism 6 (GraphPad Software, San Diego, CA) was used.

3. Results

In order to study the function and plasma membrane abundance of the Na,K-ATPase most of the experimental studies were performed in human alveolar epithelial A549 cells. These cells are fully characterized and have been shown to express the main channels and (co)transporters that drive the vectorial Na^+ transport similarly to primary alveolar epithelial type II cells (28,174,175). The key experiments were confirmed by using two primary cell models: the 3D *ex vivo* cultured mouse precision-cut lung slices and the primary rat alveolar epithelial type II cells. Since the Na,K-ATPase α_1:β_1 is the most common combination of the enzyme subunits, we focused in our experiments on the β_1-subunit in the epithelial cells. However, since the β_1-subunit was barely detectable in mouse tissues, we determined the β_3-subunit in the studies involving murine samples.

Since transfection of primary cultures is challenging, we used human A549 cells, to investigate the downregulation of specific targets via siRNA transfections and to determine the hypercapnia-induced effects on the ER machinery. Previously, it was shown that the UPR and the Na,K-ATPase are differentially regulated by various short- and long-term stimuli. Therefore, we have defined short-term hypercapnia as up to 60 min and long-term exposure to CO_2 as up to 12 h. The plasma membrane abundance of the Na,K-ATPase was characterized by biotinylation of the cell surface and confocal microscopy. To measure the Na,K-ATPase function, we studied the ouabain-sensitive ATPase activity of the enzyme by using a colorimetric method.

Studies with hypercapnia on the alveolar epithelium were performed by exposing cells to up to 120 mmHg of CO_2. This reflects clinically-relevant CO_2 levels that are occasionally observed in mechanically ventilated patients with ARDS or during exacerbations of uncontrolled asthma or COPD (21). However, such marked elevations in CO_2 concentrations result in a significant decrease in cellular pH and lead to acidosis. In order to exclude the effects of the associated acidosis, the levels of extracellular pH were maintained at the pH_e=7.4. It is worth mentioning, that the intracellular pH (pH_i) was not controlled in our current experiments, as we have previously reported that buffered hypercapnia, in a comparable setting, induces only minor changes in pH_i, which rapidly returns to normal levels without affecting the function of the Na,K-ATPase (69).

3.1 Short- and long-term hypercapnia exposure decreases Na,K-ATPase plasma membrane abundance

The Na,K-ATPase apart from playing a central role in the formation of adherens junctions in alveolar epithelial cells, is the main transporter that creates a Na^+-driven transepithelial osmotic gradient that drives alveolar fluid reabsorption (27,28,37). Further to this line, it has been previously shown that a decreased plasma membrane abundance of the Na,K-ATPase impairs alveolar fluid clearance (21,51). The enzyme can only effectively establish a Na^+ gradient and maintain junctions if it is properly expressed at the plasma membrane of cells. To test whether short-term hypercapnia affects the Na,K-ATPase plasma membrane abundance, we exposed murine PCLS to elevated CO_2 levels for 60 min and assessed the localization of the Na,K-ATPase β-subunit by confocal microscopy (Figure 3.1).

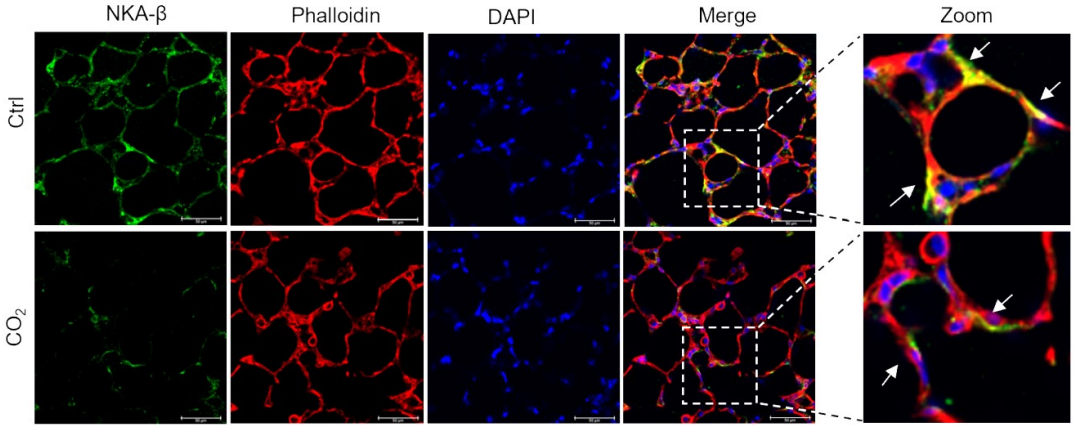

Figure 3.1 Short-term hypercapnia exposure decreases plasma membrane abundance of the Na,K-ATPase β-subunit in murine PCLS. Murine PCLS were exposed to normal (Ctrl, 40 mmHg; pH_e=7.4) or elevated CO_2 levels (CO_2, 120 mmHg; pH_e=7.4) and Na,K-ATPase β-subunit (NKA-β) localization was assessed by immunofluorescence. Immunofluorescence staining of the NKA-β (green), phalloidin (red) and nuclei (DAPI, blue) are shown. Scale bar – 50 µM.

Our results revealed that in contrast to normocapnic controls, in PCLS treated with hypercapnia, co-localization of the Na,K-ATPase β-subunit with phalloidin was markedly reduced, suggesting a decreased cell surface expression of the enzyme. To test whether elevated CO_2 levels impaired the cell surface localization of the β-subunit in AEC, we measured plasma membrane abundance of the enzyme by performing biotin-streptavidin pull-down assays in A549 cells. Indeed, short-term exposure of AEC to elevated CO_2 levels decreased cell surface expression of both the Na,K-ATPase-β and the Na,K-ATPase-α subunits by approximately 30% (Figure 3.2).

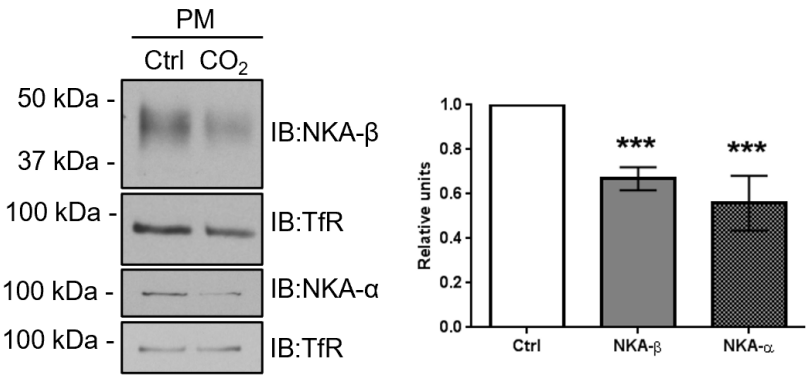

Figure 3.2 Short-term hypercapnia decreases Na,K-ATPase cell surface abundance in A549 cells. A549 cells were exposed to normal (Ctrl, 40 mmHg; pH_e=7.4) or elevated CO_2 levels (CO_2, 120 mmHg; pH_e=7.4) for 60 min. Afterwards, surface proteins were labeled with biotin and the streptavidin pull-down was performed. Plasma membrane abundance and total cell lysate levels of Na,K-ATPase α- (NKA-α) and β-subunits (NKA-β) were analyzed by immunoblotting (IB). Representative western blots are shown. Bars represent NKA-α or NKA-β/TfR ratio. Values are expressed as mean ± SD, ***p<0.001 (n=5).

After establishing that short-term elevated CO_2 levels decreased the Na,K-ATPase plasma membrane abundance, we next focused on the long-term effects of hypercapnia. For this purpose, we exposed primary rat ATII and A549 cells to the elevated CO_2 levels for 12 h and assessed the function of the enzyme by measuring the ouabain-sensitive ATPase activity. As shown in Figure 3.3, hypercapnia significantly decreased the ouabain-sensitive ATPase activity of the transporter by approximately 50%.

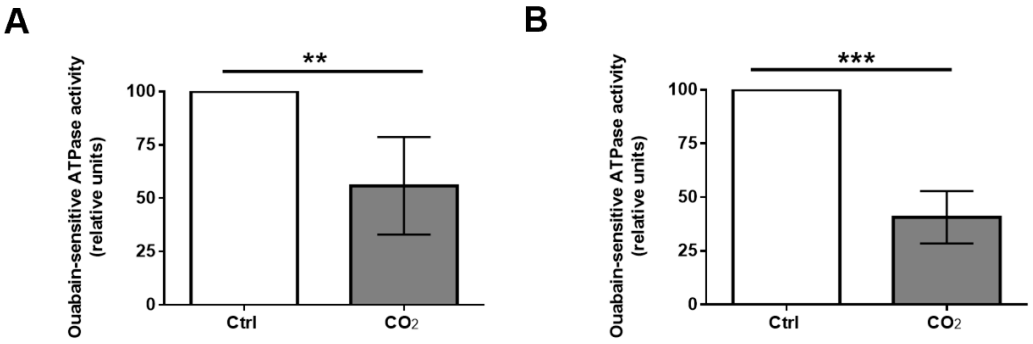

Figure 3.3 Long-term hypercapnia decreases Na,K-ATPase function in ATII and A549 cells. (A) Primary rat ATII and **(B)** A549 cells were exposed to normal (Ctrl, 40 mmHg; pH_e=7.4) or elevated CO_2 levels (CO_2, 120 mmHg; pH_e=7.4) for 12 h. Afterwards, the ouabain-sensitive activity of the Na,K-ATPase was measured in isolated membranes by using the colorimetric ATP Bioluminescence assay kit. Data are expressed as mean ± SD, **p<0.01, ***p<0.001 (n=5).

We further analyzed the cell surface expression of the Na,K-ATPase subunits after long-term treatment with elevated CO_2 levels. Exposure for up to 12 h revealed a significant decrease in the NKA-β and NKA-α abundance at the plasma membrane, as assessed by the cell-surface biotinylation and streptavidin pulldown assays (Figure 3.4). These findings are line with the previously determined reduction in the ouabain-sensitive ATPase activity of the transporter upon hypercapnic exposure.

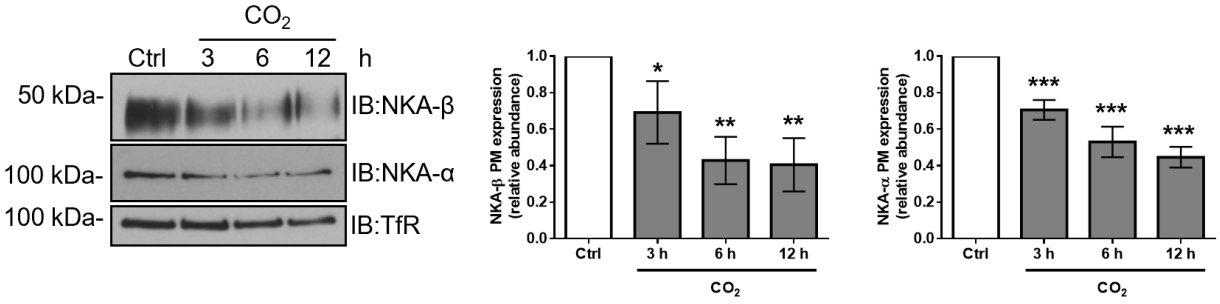

Figure 3.4 Long-term hypercapnia decreases Na,K-ATPase cell surface abundance in alveolar epithelial cells. A549 cells were exposed to normal (Ctrl, 40 mmHg; pH_e=7.4) or elevated CO_2 levels (CO_2, 120 mmHg; pH_e=7.4) for different time points. Afterwards, the surface proteins were labeled with biotin and the streptavidin pull-down was performed. Na,K-ATPase α- (NKA-α) and β-subunit (NKA-β) plasma membrane abundance and total cell lysate levels were analyzed by IB. Representative western blots are shown. Graph bars represent NKA-α or NKA-β/TfR ratio. Values are expressed as mean ± SD, *p<0.05; **p<0.01; ***p<0.001 (n=3).

3.2 Hypercapnia does not decrease mRNA levels of the Na,K-ATPase subunits

To uncover the cause of the decreased plasma membrane abundance of the enzyme upon hypercapnia, we next measured the transcriptional expression of the transporter subunits. To this end, A549 cells were exposed to normocapnia (Ctrl) or hypercapnia (CO_2) for 60 min or 12 h at a constant extracellular pH of 7.4. After exposure, mRNA was isolated, converted to cDNA, and analyzed by real-time qPCR (Figure 3.5).

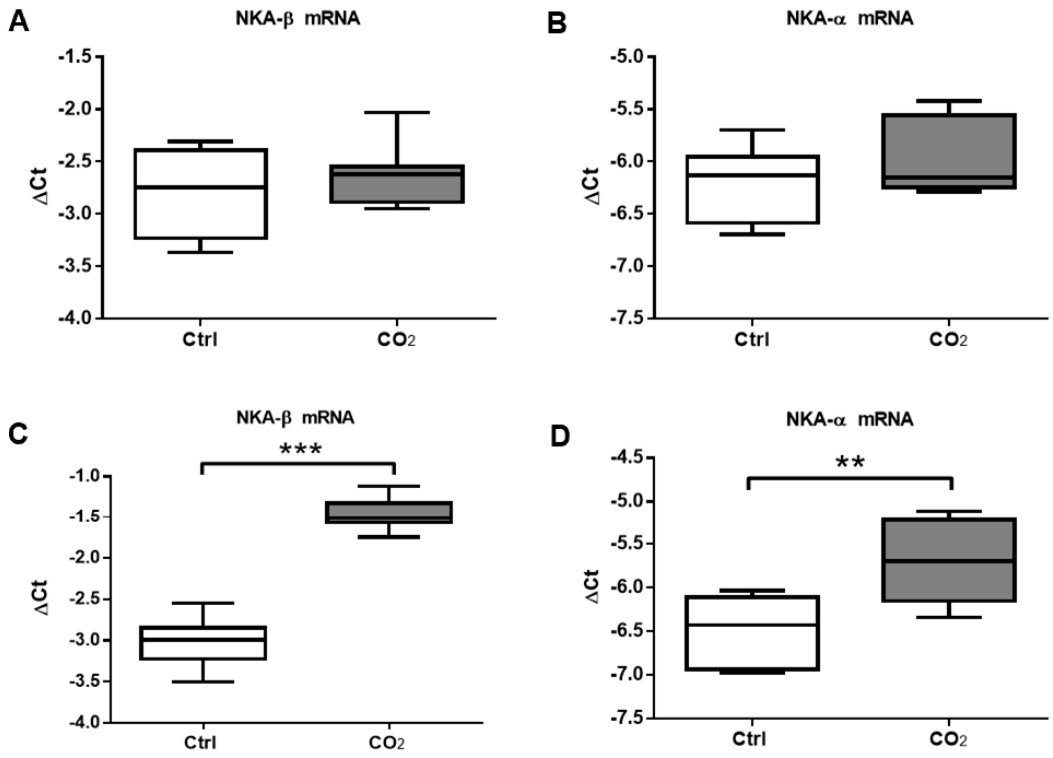

Figure 3.5 Relative mRNA levels of Na,K-ATPase subunits upon short- and long-term hypercapnic exposure. A549 cells were exposed to normal (Ctrl, 40 mmHg; pH_e=7.4) or elevated CO_2 levels (CO_2, 120 mmHg; pH_e=7.4) for **(A, B)** 60 min or **(C, D)** 12 h. Afterwards, total mRNA was isolated and the expression levels of NKA-α and NKA-β were analyzed by real-time qPCR. GAPDH was used as a reference gene. Graph bars represent ΔCt and expressed as mean ± SD, **p<0,01; ***p<0,001 (n=5-8).

Our studies revealed no changes in the transcription levels of the transporter subunits after the short-term hypercapnia exposure, as shown in Figure 3.5A and 3.5B. In contrast, the long-term exposure to elevated CO_2 levels (Figure 3.5C,D) led to an upregulation of the mRNA expression for both Na,K-ATPase-β and Na,K-ATPase-α subunits. This upregulation of the Na,K-ATPase at the transcriptional level was clearly not the reason for a decreased protein expression level, thus we hypothesized that post-translational modifications were probably driving the decreased plasma membrane abundance of the transporter.

3.3 Hypercapnia dynamically changes the levels of the ER-resident Na,K-ATPase β-subunit

Cell surface expression of the Na,K-ATPase is regulated by its trafficking between the plasma membrane and intracellular compartments. In the context of hypercapnia, it has been shown that elevated CO_2 levels decrease the Na,K-ATPase plasma membrane abundance by activation

of intracellular kinases, involving AMPK, ERK, JNK1/2, thereby promoting the phosphorylation of the Na,K-ATPase α-subunit and its retrieval from the plasma membrane (51,77,79). Subsequently, the retrieved forms of the enzyme are either immediately degraded or retained in endosomal compartments.

Therefore, we further analyzed the expression of the endogenous Na,K-ATPase subunits in A549 cells upon exposing cells to hypercapnia for different time points (Figure 3.6).

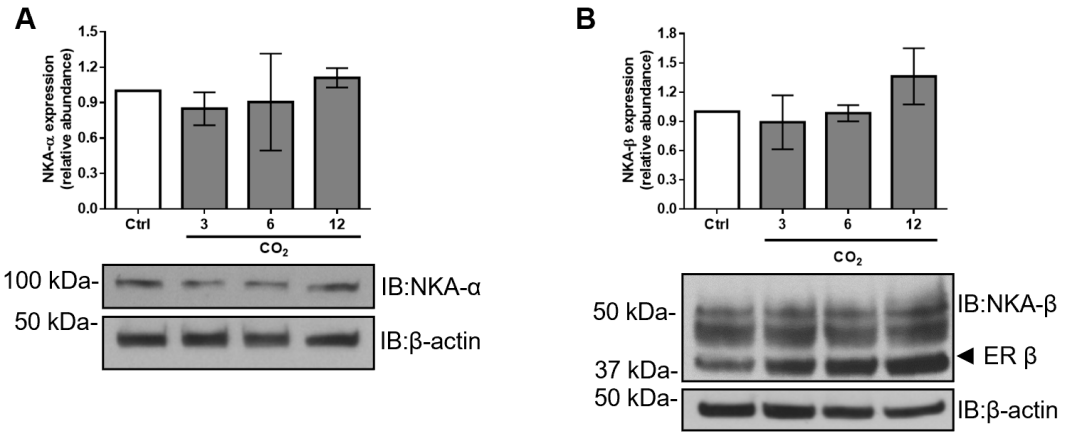

Figure 3.6 Total intracellular levels of the Na,K-ATPase subunits are not downregulated by hypercapnia. A549 were exposed to normal (Ctrl, 40 mmHg; pH_e=7.4) or elevated CO_2 levels (CO_2, 120 mmHg; pH_e=7.4) for different time points. **(A)** Na,K-ATPase α- (NKA-α) and **(B)** β-subunit (NKA-β) total cell lysate levels were analyzed by IB. Representative western blots are shown. Graph bars represent NKA-α or NKA-β/β-actin ratio. Values are expressed as mean ± SD (n=3).

After exposure of the alveolar epithelial cells to normocapnia (Ctrl) or hypercapnia (CO_2) for the different time points, we found no changes in the expression levels of the Na,K-ATPase α-subunit (Figure 3.6A). Similarly, when comparing the expression of the complex-type isoforms of the Na,K-ATPase β-subunit, no differences were evident (Figure 3.6B). In sharp contrast, the amount of high mannose N-glycan isoforms of the Na,K-ATPase β-subunit, which are exclusively localized in the ER, were found to be markedly increased.

Accumulating evidence suggests that the levels of the Na,K-ATPase β-subunit high mannose fraction are affected by stress stimuli and may either be degraded or retained under certain conditions (56). To further characterize the ER-resident Na,K-ATPase-β expression after hypercapnia, we exposed epithelial cells to elevated CO_2 levels and quantified the high mannose ER subunit fraction (Figure 3.7).

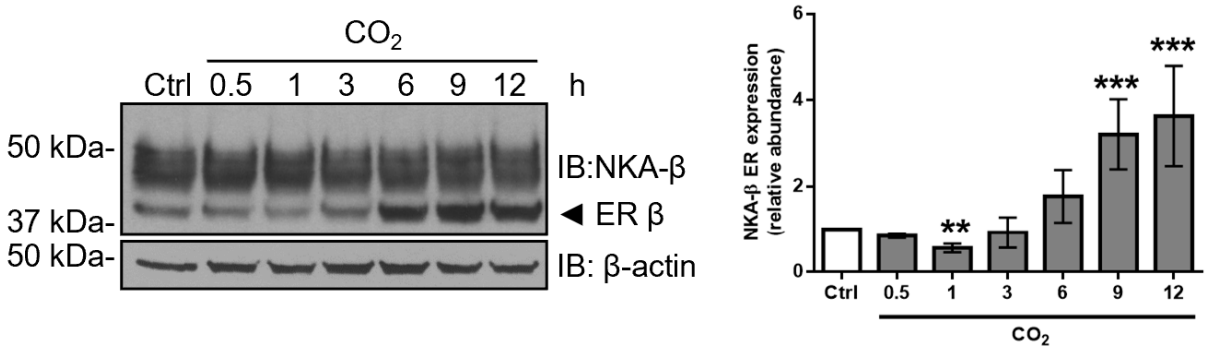

Figure 3.7 Hypercapnia exposure dynamically changes the ER-resident Na,K-ATPase β-subunit. A549 cells were exposed to normal (Ctrl, 40 mmHg; pH_e=7.4) or elevated CO_2 levels (CO_2, 120 mmHg; pH_e=7.4) for different time points up to 12 h. Total cell lysate levels of the Na,K-ATPase β-subunit (NKA-β) were analyzed by IB. Representative western blots are shown. Graph bars represent ER NKA-β/β-actin ratio. Values are expressed as mean ± SD, **p<0.01; ***p<0.001 (n=3-5).

Our results revealed that high levels of CO_2 regulated the ER-resident fraction of the Na,K-ATPase β-subunit in a time-dependent manner. As shown in Figure 3.7, short-term exposure (up to 60 min) to hypercapnia led to a significant decrease in the amount of high mannose type Na,K-ATPase β-subunit molecules. In contrast, long-term treatment with elevated CO_2 levels resulted in ER retention of this isoform of the enzyme.

3.4 Dose-dependent hypercapnic effects on the Na,K-ATPase β-subunit and the role of acidosis

It is well known that hypercapnia, if not buffered, results in acidosis. Moreover, we have previously shown that markedly elevated CO_2 levels may lead to a transient intracellular acidosis even when buffering pH_e to 7.4. (69). To further investigate whether the changes in the Na,K-ATPase β-subunit expression in the ER were linked to acidosis, we treated A549 cells with different levels of CO_2 (40, 80 and 120 mmHg) and with either a normal (pH_e=7.4) or an acidic (pH_e=7.2) extracellular pH. As depicted in Figure 3.8, the exposure to short- or long-term hypercapnia resulted in dose-dependent changes in the ER-resident fraction of the Na,K-ATPase. Interestingly, exposure to the acidic pH *per se* for 1 h decreased the number of ER-localized Na,K-ATPase-β subunits, although the effect of buffered high CO_2 (120 mmHg) was markedly larger. In contrast, after 12 h of hypercapnia treatment, the acidic environment did not any effects on the ER-localized Na,K-ATPase-β subunits, when compared to control.

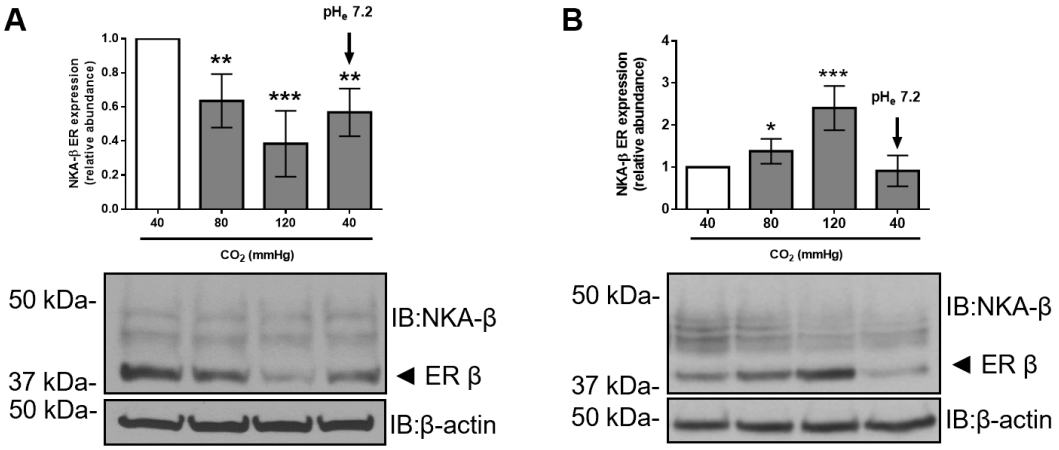

Figure 3.8 Dose-dependent CO_2 effects on the ER-resident Na,K-ATPase β-subunit. A549 cells were exposed to 40, 80 and 120 mmHg CO_2 with a pH_e=7.4 or to 40mmHg CO_2 with a pH_e=7.2 for **(A)** 1 h or **(B)** 12 h. Total cell lysate levels of the Na,K-ATPase β-subunit (NKA-β) were analyzed by IB. Representative western blots are shown. Graph bars represent ER NKA-β/β-actin ratio. Values are expressed as mean ± SD, *p<0.05; **p<0.01; ***p<0.001 (n=3-4).

To further investigate the effects of hypercapnia on the Na,K-ATPase β-subunit in the ER and a potential relation of these findings with the decreased plasma membrane abundance of the enzyme upon hypercapnia, we divided our further studies into short- (up to 1 hour) and long-term (up to 12 hours) experiments based on the time points where we found the most significant effects of CO_2 on the Na,K-ATPase.

3.5 Effects of short-term hypercapnia on the maturation of the Na,K-ATPase β-subunit in the endoplasmic reticulum

3.5.1 Acute hypercapnia decreases the high mannose ER-resident form of the Na,K-ATPase β-subunit

In the next phase of our studies, we examined the putative mechanisms underlying the decrease of the ER-resident Na,K-ATPase β-subunit after short-term exposure to hypercapnia. First, we exposed murine PCLS and A549 cells to normocapnia (Ctrl) or hypercapnia (CO_2) for 60 min and analyzed the expression of the ER fraction of the Na,K-ATPase β-subunit by immunoblotting (Figure 3.9).

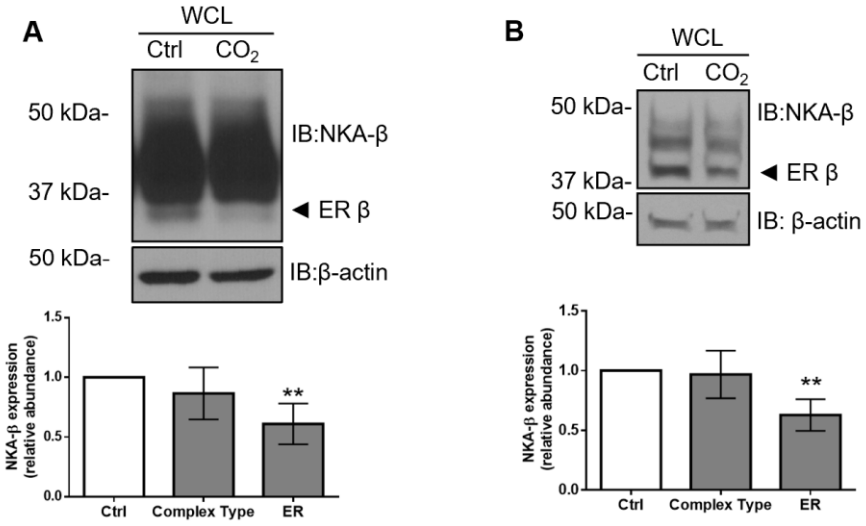

Figure 3.9 Short-term hypercapnia decreases ER-resident Na,K-ATPase β-subunit in PCLS and A549 cells. **(A)** PCLS and **(B)** A549 cells were exposed to normal (Ctrl, 40 mmHg; pH_e=7.4) or elevated CO_2 levels (CO_2, 120 mmHg; pH_e=7.4) for 60 min. Total cell lysate levels of the Na,K-ATPase β-subunit (NKA-β) were analyzed by IB. Representative western blots are shown. Graph bars represent the ER NKA-β/β-actin ratio. Values are expressed as mean ± SD, **p<0.01 (n=5).

Our results revealed that in PCLS exposed to hypercapnia, the amount of high mannose ER-resident Na,K-ATPase-β was decreased by approximately 40% (Figure 3.9A). These findings were reproducible in A549 cells, suggesting common hypercapnia-driven pathways between these models (Figure 3.9B).

3.5.2 Short-term hypercapnia induces endoplasmic reticulum-associated degradation of the Na,K-ATPase β-subunit

It has been previously shown that under stress conditions unfolded NKA-β molecules or those that remain disassembled with NKA-α, are substrates for faster degradation (56). As mentioned above, several steps are required prior to targeted degradation of proteins. First, the ERAD process is controlled by trimming a mannose residue in the oligosaccharide core of the nascent folded protein by mannosidase MAN1B1. Then, the substrate translocates to the cytoplasm to and interacts with EDEM proteins for further proteasomal degradation (176). Theoretically, the decrease in the ER-resident fraction of the NKA β-subunit upon hypercapnia may be a consequence of its accelerated export to the Golgi or its degradation via the ERAD pathway. However, an accelerated traffic of the NKA β-subunit from the ER to the Golgi would in turn have led to increased plasma membrane abundance of the Na,K-ATPase, which was clearly not

the case in our studies. Thus, next we focused on ER degradation pathways as potential mediators of CO_2-induced downregulation of the NKA-β in the ER.

To uncover the role of ERAD in the downregulation of ER-resident NKA-β upon short-term exposure to hypercapnia, A549 cells were pretreated with a permeable inhibitor of mannosidase activity, kifunensine and were exposed to 40 mmHg (Ctrl) or 120 mmHg of CO_2 (CO_2) for 60 min (Figure 3.10A) at a pH_e of 7.4. Our results revealed that a pretreatment with kifunensine was sufficient to stabilize the amount of the ER-resident Na,K-ATPase-β forms.

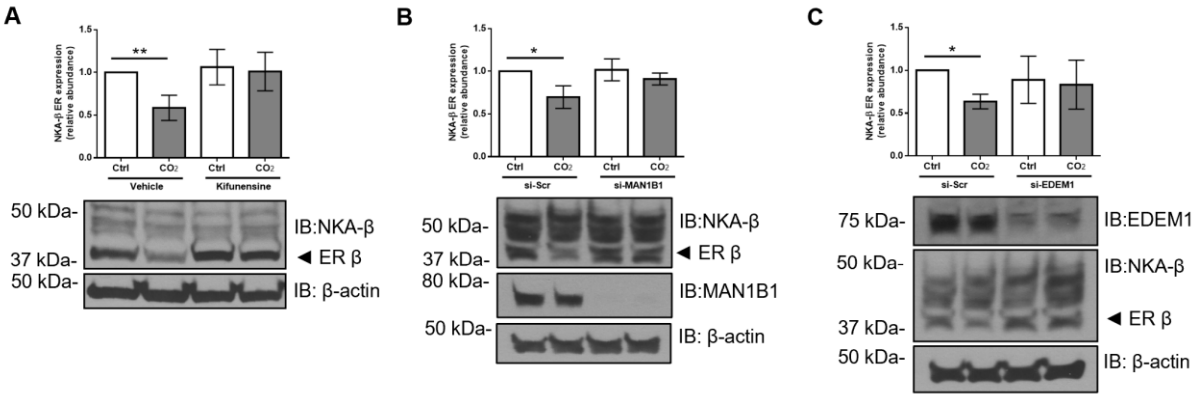

Figure 3.10 Short-term hypercapnia induces endoplasmic reticulum associated degradation of the ER-resident Na,K-ATPase β-subunit. A549 cells were exposed to normal (Ctrl, 40 mmHg; pH_e=7.4) or elevated CO_2 levels (CO_2, 120 mmHg; pH_e=7.4) for 60 min in the presence or absence of **(A)** mannosidase inhibitor kifunensine (20 µM, pretreatment 30 min); **(B)** siRNA targeting MAN1B1 (si-MAN1B1) or scrambled siRNA (si-Scr); **(C)** siRNA targeting EDEM1 (si-EDEM1) or scrambled siRNA (si-Scr) 48 h after transfection. Total cell lysate levels of Na,K-ATPase β-subunit (NKA-β), MAN1B1 and EDEM1 were analyzed by IB. Representative western blots are shown. Graph bars represent the ER NKA-β/β-actin ratio. Values are expressed as mean ± SD, *p<0.05; **p<0.01 (n=3-5).

Next, we tested whether silencing of MAN1B1 influenced the amount of the ER-resident Na,K-ATPase β-subunit upon hypercapnia treatment. A549 cells were transfected for 48 h with a siRNA targeting MAN1B1 or a scrambled siRNA. Afterwards, the cells were subjected to normocapnia (Ctrl) or hypercapnia (CO_2) treatment for 60 min (Figure 3.10B). Indeed, our data demonstrated that the downregulation of MAN1B1 expression significantly prevented the decrease in the ER forms of the Na,K-ATPase β-subunit. Finally, the role of EDEM1 in ERAD of the Na,K-ATPase β-subunit was determined. To test this, we performed a specific knock-down by siRNA targeting EDEM1 in A549 cells and exposed them to normal or elevated CO_2 levels for 60 min (Figure 3.10C). Of note, the knock-down of EDEM1 also prevented the decrease of the ER-resident Na,K-ATPase β-forms. These results suggest that during short-term

hypercapnic exposure pharmacological inhibition of mannosidase by kifunensine or genetic knock-down of either MAN1B1 or EDEM1 was sufficient to stabilize the ER-resident amount of the NKA-β subunit, indicating their critical requirement for the ERAD process.

Once tagged for ERAD, immature Na,K-ATPase β-subunits undergo deglycosylation and degradation through the proteasomal pathway. However, mechanisms involving the lysosomal machinery could potentially be involved in these processes as well (56,159). To assess whether hypercapnia affects proteasomal or lysosomal degradation of the ER-resident Na,K-ATPase β-subunits, A549 cells were preincubated with a proteasomal (MG132) or a lysosomal inhibitor (chloroquine) and then exposed to different levels of CO_2 with constant pH_e=7.4 (Figure 3.11).

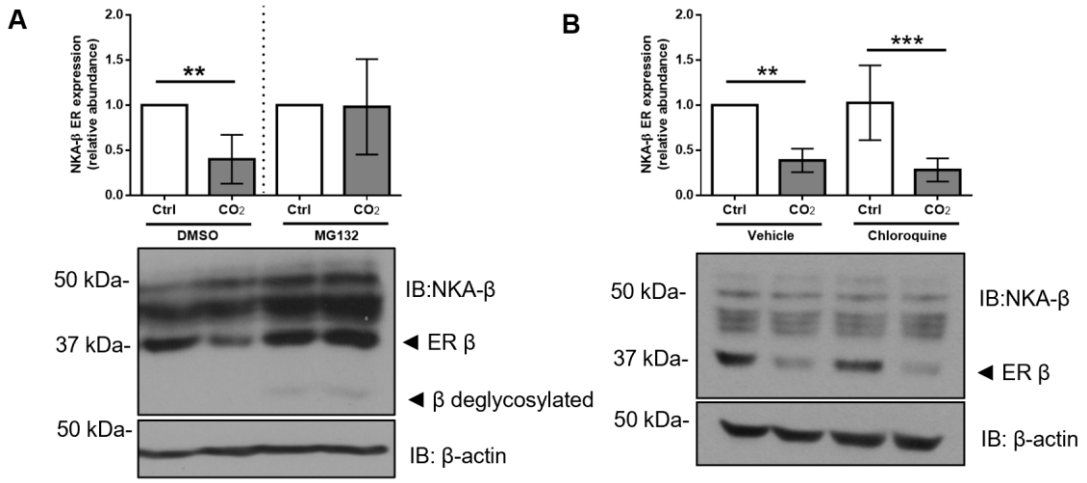

Figure 3.11 Short-term hypercapnia induces proteasomal degradation of the ER-resident Na,K-ATPase β-subunit. A549 cells were exposed to normal (Ctrl, 40 mmHg; pH_e=7.4) or elevated CO_2 levels (CO_2, 120 mmHg; pH_e=7.4) for 60 min in the presence or absence of **(A)** the proteasomal inhibitor, MG132 (20 μM, pretreatment 30 min) or **(B)** the lysosomal inhibitor, chloroquine (100 μM). Total cell lysate levels of the Na,K-ATPase β-subunit (NKA-β) were analyzed by IB. Representative western blots are shown. Graph bars represent the ER NKA-β/β-actin ratio. Values are expressed as mean ± SD, **p<0.01; ***p<0.001 (n=4).

We identified that the inhibition of proteasomal, but not lysosomal activity, prevented the hypercapnia-induced degradation of the ER-resident Na,K-ATPase β-subunits. Thus, we confirmed that short-term hypercapnia induced the ERAD of the NKA β-subunit, thereby preventing its further export to the Golgi.

3.5.3 IRE1α activation is required for the ERAD of the Na,K-ATPase β-subunit

It has been previously demonstrated that protein folding in the ER is tightly regulated and controlled. If the homeostatic parameters of the ER are disturbed and thus misfolding occurs, a

mechanism known as the unfolded protein response (UPR) becomes active (119). IRE1α, PERK, and ATF6 are the central UPR receptors. Among them, IRE1α has been shown to specifically control the mechanisms of protein degradation (137,147,158). Based on these findings, we hypothesized that IRE1α might regulate the hypercapnia-induced decrease in the ER-resident forms of the Na,K-ATPase β-subunit.

First, we examined whether elevated CO_2 levels activate IRE1α. To further asses this, we measured the levels of phosphorylated IRE1α in murine PCLS and A549 cells that were exposed to hypercapnia and indeed, we observed a rapid and transient increase in the phosphorylation of IRE1α in both models, suggesting its activation (Figure 3.12).

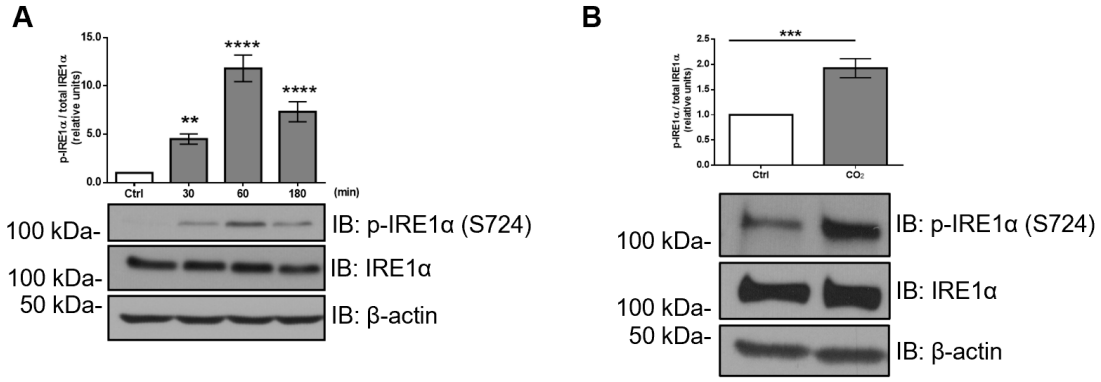

Figure 3.12 Hypercapnia activates IRE1α by its phosphorylation at S724. (A) A549 cells were exposed to normal (Ctrl, 40 mmHg; pH_e=7.4) or elevated CO_2 levels (CO_2, 120 mmHg; pH_e=7.4) for 30, 60 and 180 min. Phosphorylated (p-IRE1α) and total IRE1α (IRE1α) levels were analyzed by IB. **(B)** Murine PCLS were exposed to normal (Ctrl, 40 mmHg; pH_e=7.4) or elevated CO_2 levels (CO_2, 120 mmHg; pH_e=7.4) for 30, 60 and 180 min. Phosphorylated (p-IRE1α) and total IRE1α (IRE1α) levels were analyzed by IB. Representative western blots are shown. Graph bars represent the p-IRE1α/IRE1α ratio. Values are expressed as mean ± SD, **p<0,01; ***p<0.001; ****p<0.0001 (n=3-5).

We next examined whether the activation of IRE1α was required for the ERAD of the Na,K-ATPase β-subunit upon hypercapnia. To assess that, A549 cells were transfected with a siRNA targeting IRE1α for 48 h and then exposed to normal (Ctrl) or hypercapnic CO_2 levels (CO_2) for 60 min (Figure 3.13A). Of note, downregulation of IRE1α protein expression by a siRNA stabilized the levels of the ER-resident NKA-β subunit. To further confirm that the activation of the IRE1α kinase domain was necessary for the hypercapnia-induced ERAD, A549 cells were pretreated with the IRE1α kinase inhibitor, KIRA6 for 30 min and then exposed to elevated CO_2 levels for 60 min(Figure 3.13B). Indeed, inhibition of the IRE1α activity by KIRA6 prevented the hypercapnia-induced ERAD of the NKA β-subunit.

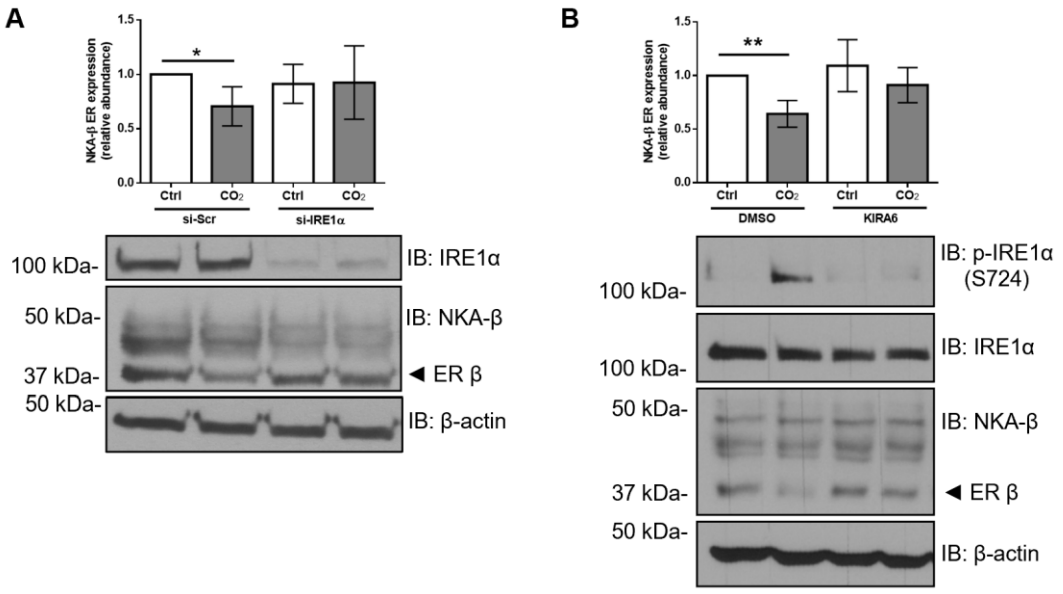

Figure 3.13 Hypercapnia-induced activation of the IRE1α triggers the degradation of the ER-resident Na,K-ATPase β-subunit. A549 cells were exposed to normal (Ctrl, 40 mmHg; pH_e=7.4) or elevated CO_2 levels (CO_2, 120 mmHg; pH_e=7.4) for 60 min in the presence or absence of **(A)** a siRNA targeting IRE1α (si-IRE1α) or a scrambled siRNA (si-Scr) 48 h after transfection or **(B)** the IRE1α kinase domain inhibitor, KIRA6 (1 μM). Na,K-ATPase β-subunit (NKA-β), phosphorylated (p-IRE1α) and total IRE1α (IRE1α) cell lysate levels were analyzed by IB. Representative western blots are shown. Graph bars represent the ER NKA-β/β-actin ratio. Values are expressed as mean ± SD, *p<0.05; **p<0.01 (n=4-5).

3.5.4 ERAD of the Na,K-ATPase β-subunit is independent of XBP1 or JNK activation.

It has been previously reported that the ER protein degradation, which is regulated by IRE1α, can be driven either by its direct influence on mRNA degradation (RIDD) or by the activation of its downstream targets, such as XBP1 and JNK (137,177). While we did not find any differences in the mRNA expression of the Na,K-ATPase subunits, as discussed above and shown in Figure 3.5A, we next focused on the potential role of XBP1 and JNK in the degradation of the ER-resident Na,K-ATPase β-subunit during CO_2 exposure.

First, we investigated whether the inhibition of the IRE1α endonuclease and the mRNA splicing activity, which is required for the formation of the active XBP1 spliced version, XBP1s affected the degradation of the Na,K-ATPase β-subunit. To test this, A549 cells were pretreated with the specific IRE1α endonuclease inhibitor, STF-083010 and then exposed to normal (Ctrl) or elevated (CO_2) concentrations of CO_2 for 60 min (Figure 3.14A). Our results revealed that pretreatment with STF-083010 failed to prevent ERAD of the ER-resident Na,K-ATPase β-subunit. Next, to further assess the role of XBP1, we used a genetic approach through a siRNA

protein knock-down (Figure 3.14B). Based on our results, silencing of XBP1 was not sufficient to abolish the ERAD of the Na,K-ATPase β-subunit. These results suggest that the degradation mechanism might be directly controlled by activation of IRE1α.

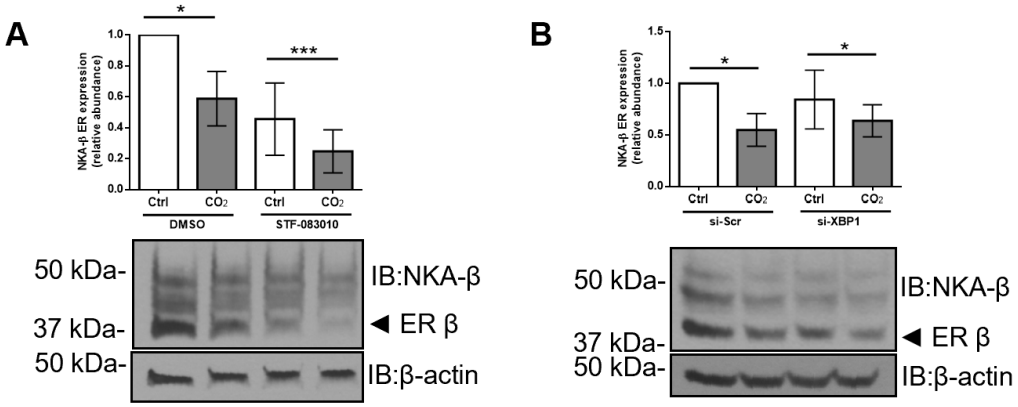

Figure 3.14 ERAD of the ER-resident Na,K-ATPase β-subunit is independent of XBP1 activity. A549 cells were exposed to normal (Ctrl, 40 mmHg; pH_e=7.4) or elevated CO_2 levels (CO_2, 120 mmHg; pH_e=7.4) for 60min in the presence or absence of **(A)** the specific IRE1α endonuclease inhibitor, STF-083010 (100μM) or **(B)** a siRNA targeting XBP1 (si-XBP1) or a scrambled siRNA (si-Scr) 48 h after transfection. Total cell lysate levels of the Na,K-ATPase β-subunit (NKA-β) were analyzed by IB. Representative western blots are shown. Graph bars represent the ER NKA-β/β-actin ratio. Values are expressed as mean ± SD, *p<0.05; ***p<0.001 (n=4).

It has been shown that JNK1/2 is involved in the CO_2-induced signaling pathway in alveolar epithelial cells and is implicated in the downregulation of the plasma membrane expression of the Na,K-ATPase and ENaC (77,78,98). Interestingly, JNK1/2 was found to be a downstream target of IRE1α in the ER stress signaling pathway. Upon activation, IRE1α can recruit TRAF2 and thus activate the apoptosis signal-regulating kinase 1 (ASK1) and subsequently JNK1/2 (129,148). To further investigate the role of JNK1/2 during the degradation of the Na,K-ATPase β-subunit, A549 cells were pretreated with the specific JNK1/2 inhibitor SP600125 and then exposed to normal (Ctrl) or elevated CO_2 (CO_2) levels for 60 min (Figure 3.15). Consistent with our previous observations, hypercapnia induced the activation of JNK1/2, as assessed by its phosphorylation levels. However, the inhibition of JNK1/2 activity by SP600125 was insufficient to stabilize the levels of the ER-resident Na,K-ATPase β-subunit, suggesting that JNK is not involved in the IRE1α-driven downregulation of the transporter.

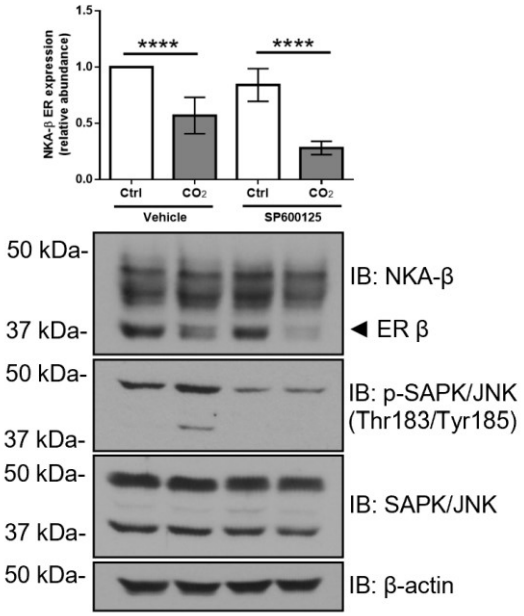

Figure 3.15 ERAD of the ER-resident Na,K-ATPase β-subunit is independent of JNK1/2 activity A549 cells were exposed to normal (Ctrl, 40 mmHg; pH_e=7.4) or elevated CO_2 levels (CO_2, 120 mmHg; pH_e=7.4) for 60 min in the presence or absence of the JNK inhibitor, SP600125 (25μM). Na,K-ATPase β-subunit (NKA-β), total and phosphorylated JNK levels in total cell lysates were analyzed by IB. Representative western blots are shown. Graph bars represent the ER NKA-β/β-actin ratio. Values are expressed as mean ± SD, ****p<0.0001 (n=5).

3.5.5 Treatment with the ER stress inducer, thapsigargin or the IRE1α activator, quercetin mimics the effects of hypercapnia on ERAD.

The above-mentioned experiments confirmed that hypercapnia activates IRE1α by its phosphorylation and affects the ERAD of the ER-resident Na,K-ATPase β-subunit independent of XBP1s and JNK activity. Next, we investigated the activation of the ER stress pathways by thapsigargin (TG)-mediated depletion of ER Ca^{2+} stores. A549 cells were treated with TG (1 μM) for various time points up to 180 min. Our results showed a time-dependent increase in the phosphorylation of IRE1α, which returned to basal levels after 180 min of TG treatment (Figure 3.16A). Furthermore, an increase in IRE1α activation was associated with a decrease of the ER-resident Na,K-ATPase β-subunit, suggesting that ER Ca^{2+} depletion affects the degradation of NKA-β (Figure 3.16B). Notably, protein levels of XPB1s did not correlate with IRE1α activation and reduction in the ER fraction of the Na,K-ATPase β-subunit. These data further confirmed that the IRE1α-XBP1s axis does not play a role in the ERAD of the Na,K-ATPase β-subunit upon short-term hypercapnia.

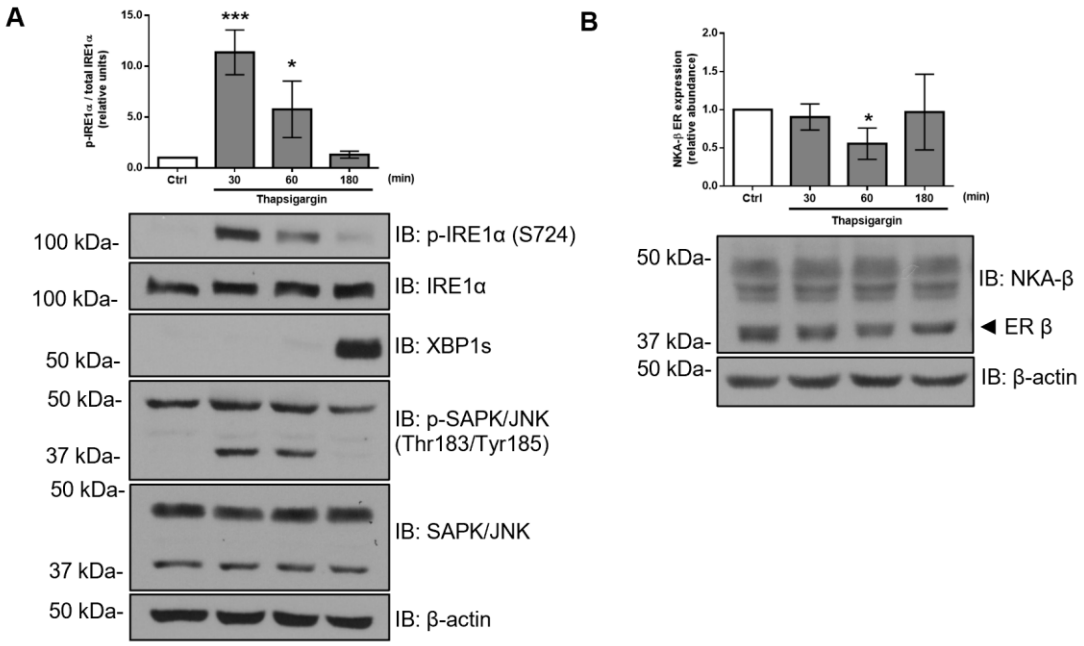

Figure 3.16 Thapsigargin activates the phosphokinase domain of IRE1α and decreases ER-resident Na,K-ATPase β-subunit abundance. A549 were treated with thapsigargin (1 µM) for 30, 60 and 180min in normocapnic conditions. **(A)** Phosphorylated IRE1α (p-IRE1α), total IRE1α (IRE1α), XBP1s, phosphorylated JNK1/2 (p-SAPK/JNK) and total JNK1/2 (SAPK/JNK) levels were analyzed by IB. Representative western blots are shown. Graph bars represent p-IRE1α/IRE1α ratio. Values are expressed as mean ± SD, *p<0.05; ***p<0.001 (n=3) **(B)** Levels of the Na,K-ATPase β-subunit (NKA-β) in total cell lysates were analyzed by IB. Representative western blots are shown. Graph bars represent the ER NKA-β/β-actin ratio. Values are expressed as mean ± SD, *p<0.05 (n=5).

Recently, a member of the flavonols family, quercetin was shown to activate IRE1α (178). To further uncover the role of IRE1α activation in the degradation of the ER-resident Na,K-ATPase β-subunit, we treated A549 cells with quercetin (Figure 3.17). Cells treated with thapsigargin were used as a positive control for ER stress markers and loaded in the same gel. Treatment of alveolar epithelial cells with quercetin increased phosphorylation of IRE1α and subsequently induced the degradation of the ER-resident Na,K-ATPase β-subunit. Similarly to TG treatment, these effects quercetin on the ER abundance of the Na,K-ATPase β-subunit were independent of XBP1s levels or JNK1/2 activation.

Taken together, these data indicate that ERAD of the Na,K-ATPase β-subunit is dependent on IRE1α activation but independent from XBP1s or JNK1/2 activity.

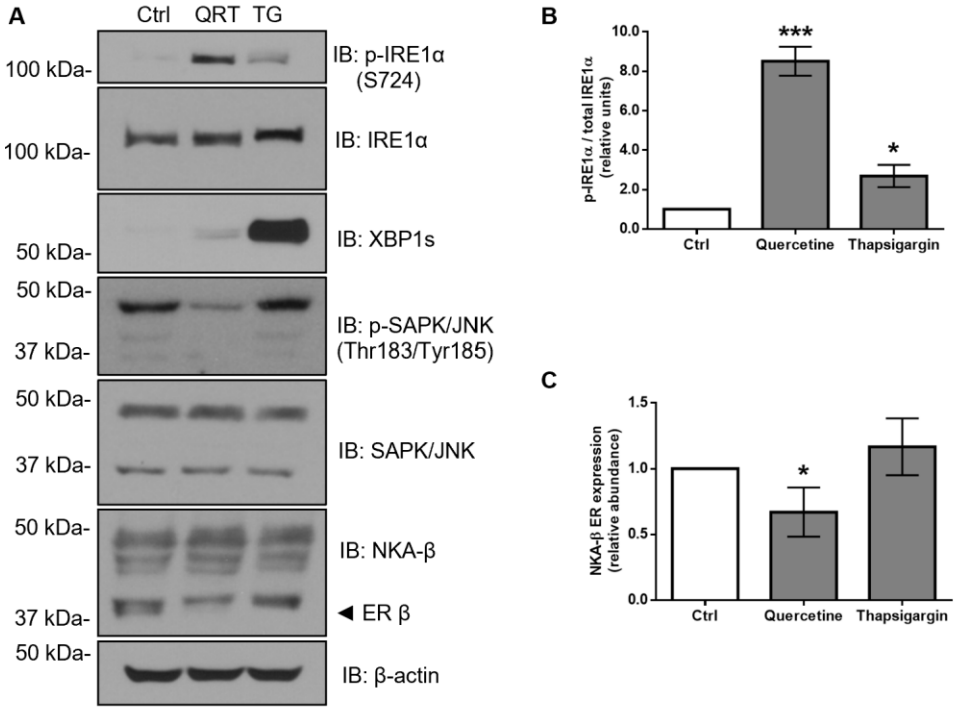

Figure 3.17 Treatment with quercetin induces IRE1α activation and ERAD of the ER-resident Na,K-ATPase β-subunit. (A) A549 cells were treated with quercetin (QRT, 100 µM) for 1 h and thapsigargin (TG, 1 µM) for 3 h (positive control) in normocapnic conditions. Na,K-ATPase β-subunit (NKA-β), phosphorylated IRE1α (p-IRE1α), total IRE1α (IRE1α), phosphorylated JNK1/2 (p-SAPK/JNK), total JNK1/2 (SAPK/JNK) and XBP1s levels were analyzed by IB. Representative western blots are shown. **(B)** Graph bars represent p-IRE1α/IRE1α ratio. Values are expressed as mean ± SD, *p<0.05; ***p<0.001 (n=3). **(C)** Graph bars represent the ER NKA-β/β-actin ratio. Values are expressed as mean ± SD, *p<0.05 (n=3).

3.5.6 Hypercapnia increases intracellular calcium concentrations in murine PCLS and A549 cells

Calcium is one of the main cellular signal transduction messengers that control cellular functions, such as gene expression, metabolism, survival and death (117). Previous reports indicated that acute and chronic hypercapnia increase intracellular Ca^{2+} concentrations (51,76). Since showed in our current studies that the treatment with thapsigargin decreased the ER-resident fraction of the Na,K-ATPase β-subunit, we hypothesized that the activation of ERAD was Ca^{2+} dependent. To address this question, next the effects of short-term hypercapnia on Ca^{2+} levels were evaluated. Murine PCLS and A549 cells were preloaded with the Ca^{2+} indicator, Fluo-4 AM for 30 min and subsequently treated with normal (Ctrl) or elevated CO_2 levels (CO_2) at a pH_e=7.4 for 60 min. PCLS and A549 cells were then fixed and analyzed using

fluorescent microscopy (Figure 3.18). Our results revealed that upon hypercapnic exposure, intracellular Ca^{2+} levels were markedly elevated in both PCLS and A549 cells.

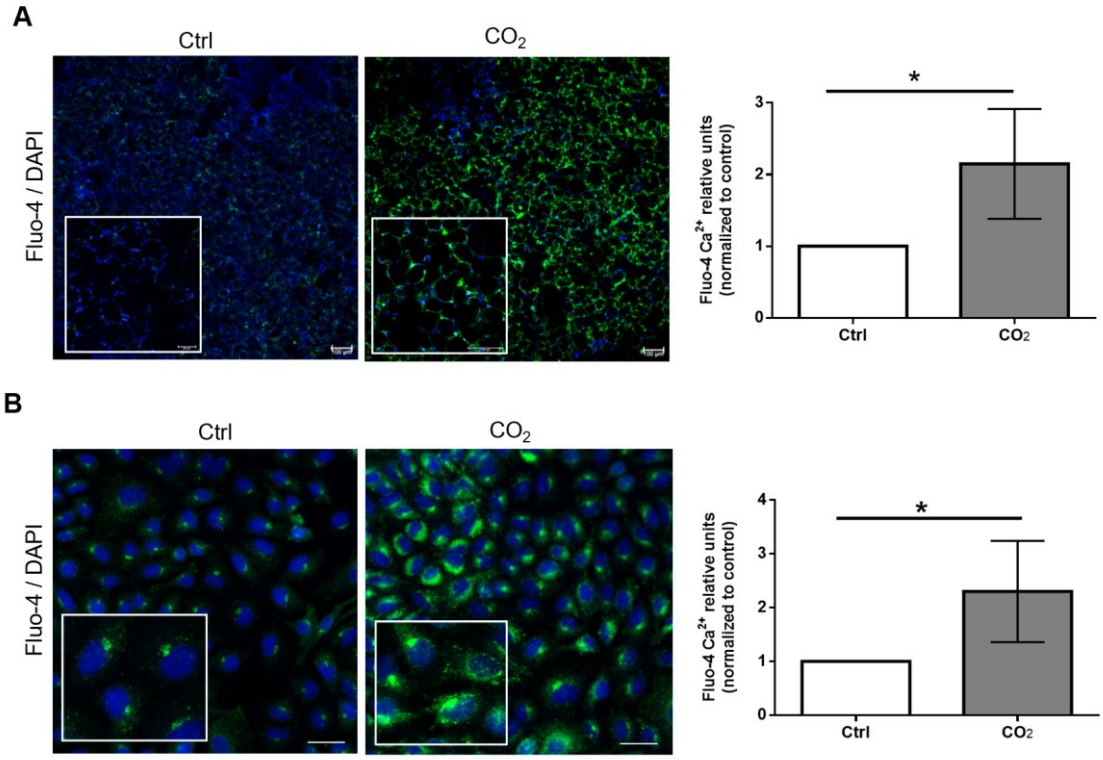

Figure 3.18 Hypercapnia increases intracellular Ca^{2+} concentrations. Intracellular Ca^{2+} concentrations were measured in **(A)** murine PCLS or **(B)** A549 cells by Fluo-4 assay. Fluo-4 AM was added in DMEM at 37°C for 30 min. Afterwards, cultures were exposed to normal (Ctrl, 40 mmHg; pH_e=7.4) or elevated CO_2 levels (CO_2, 120 mmHg; pH_e=7.4) for 60 min and Ca^{2+} fluorescence was captured using fluorescent microscopy and analyzed by the ImageJ software. Graph bars represent relative Fluo-4 levels normalized to the normocapnic control. Scale bar: (A) - 100 µM, (B) – 50 µM. Values are expressed as mean ± SD, *p<0.05 (n=4).

3.5.7 Treatment with BAPTA-AM aggravates ERAD of the ER-resident Na,K-ATPase β-subunit

To determine whether the increase of intracellular Ca^{2+} was upstream of IRE1α activation and ERAD of the Na,K-ATPase β-subunit, we employed the cell-permeant Ca^{2+} chelator, 1,2-bis(2-aminophenoxy)ethane-N,N,N′,N′-tetraacetic acid–acetoxymethyl ester (BAPTA-AM). A549 cells were preincubated with BAPTA-AM for 30 min and then exposed to normocapnia (Ctrl) or hypercapnia (CO_2) for 60 min in the presence or absence of BAPTA-AM. Indeed, chelating total intracellular Ca^{2+} by BAPTA-AM was insufficient to prevent the degradation of the Na,K-ATPase β-subunit in the ER (Figure 3.19). Of note, treatment with BAPTA-AM significantly enhanced IRE1α phosphorylation and led to a further reduction in the levels of the ER-resident

Na,K-ATPase β-subunit. Based on these results, we hypothesized that hypercapnia may pathologically increase the ER Ca^{2+} release and thus disrupt Ca^{2+} homeostasis.

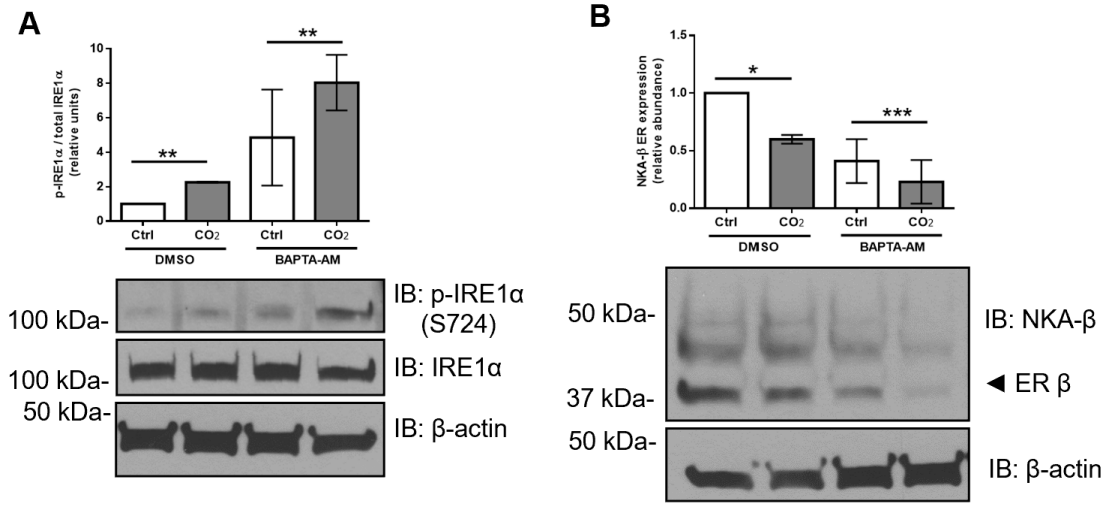

Figure 3.19 Chelating intracellular Ca^{2+} with BAPTA-AM aggravates ERAD of the ER-resident Na,K-ATPase β-subunit. A549 cells were exposed to normal (Ctrl, 40 mmHg; pH_e=7.4) or elevated CO_2 levels (CO_2, 120 mmHg; pH_e=7.4) for 60 min in the presence or absence of BAPTA-AM (20 μM). **(A)** Phosphorylated (p-IRE1α) and total IRE1α (IRE1α) levels were analyzed by IB. Representative western blots are shown. Graph bars represent p-IRE1α/IRE1α ratio. Values are expressed as mean ± SD, **p<0.01 (n=3). **(B)** Na,K-ATPase β-subunit (NKA-β) total cell lysate levels were analyzed by IB. Representative western blots are shown. Graph bars represent the ER NKA-β/β-actin ratio. Values are expressed as mean ± SD, *p<0.05; ***p<0.001 (n=3).

3.5.8 Treatment with 2-APB prevents the hypercapnia-induced increase of intracellular calcium levels and phosphorylation of IRE1α

Previous studies have reported that elevation of intracellular Ca^{2+} levels might be mediated by several mechanisms, either affecting the extracellular space or intracellular compartments (e.g. ER, mitochondria) (117,179). Opening of calcium release-activated channels (CRAC) or transient receptor potential channels (TRP) promotes Ca^{2+} influx from the extracellular space into the cell. Also, the release of Ca^{2+} from the ER through activation of inositol trisphosphate receptors (IP3R) or ryanodine receptors channels (RyR) might increase Ca^{2+} concentrations from intracellular stores. It has been shown that IP3R channels are ubiquitously expressed, while RyR are mainly present in muscles (179).

Thus, to test whether the hypercapnia-induced Ca^{2+} release involved IP3R receptors, we employed the IP3R receptor antagonist, 2-aminoethoxydiphenyl borate (2-APB). Murine PCLS and A549 cells were preloaded with Fluo-4 AM, pretreated with 2-APB, exposed to normal

(Ctrl) or elevated CO_2 (CO_2) levels for 60 min and then analyzed by confocal and immunofluorescent microscopy (Figure 3.20). Indeed, we were able to show that the hypercapnia-induced elevation in Ca^{2+} concentrations were largely prevented in 2-APB treated samples, suggesting that calcium was mobilized from intracellular ER stores via IP3R channels.

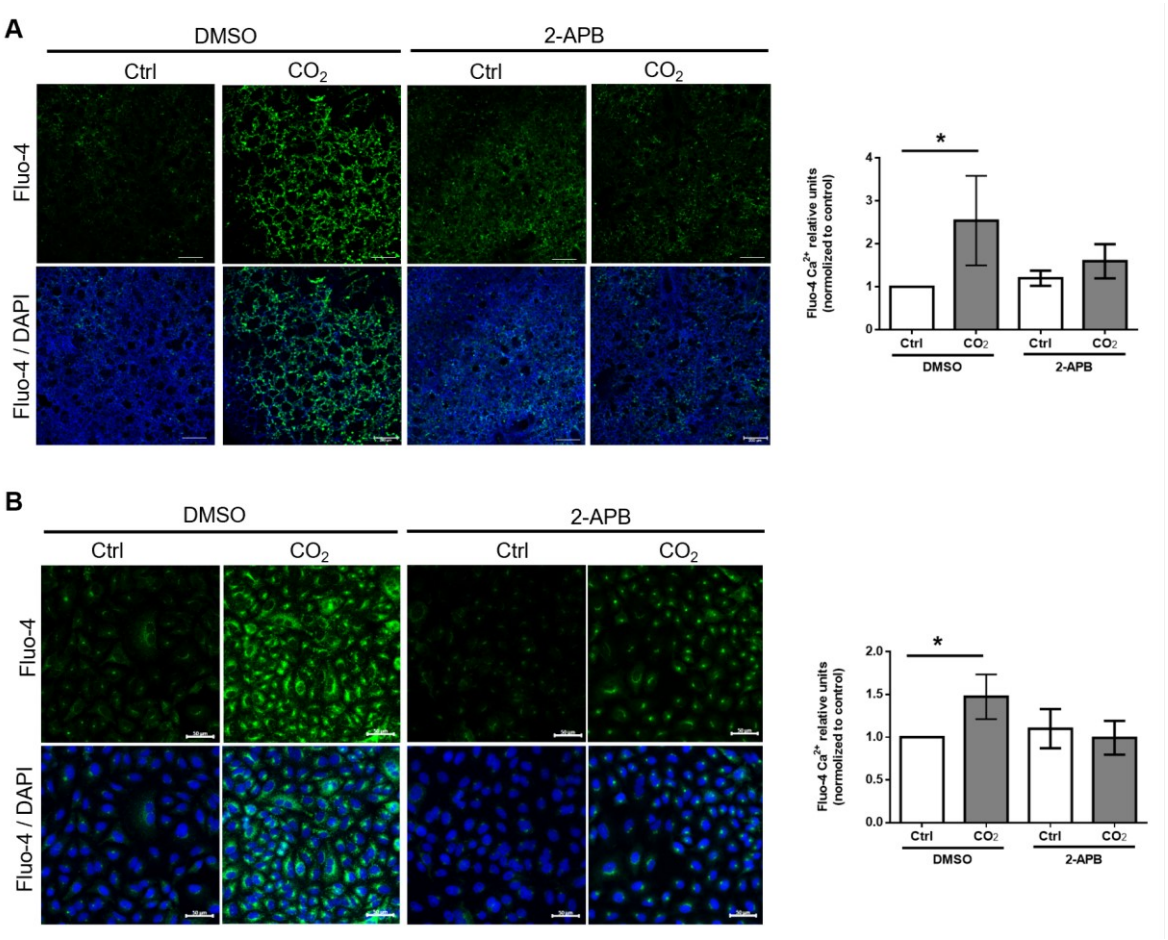

Figure 3.20 Treatment with the IP3R receptor antagonist, 2-APB decreases the elevation of intracellular Ca^{2+} levels induced by hypercapnia. (A) Murine PCLS and **(B)** A549 cells were pretreated with 2-APB (100 µM) for 30 min. Afterwards, intracellular Ca^{2+} was measured by the Fluo-4 assay. Fluo-4 AM was added in DMEM at 37°C for 30 min. Cultures were exposed to normal (Ctrl, 40 mmHg; pH_e=7.4) or elevated CO_2 levels (CO_2, 120 mmHg; pH_e=7.4) in the presence or absence of 2-APB (100 µM) for 60 min and Ca^{2+} fluorescence was captured by fluorescent microscopy and analyzed by the ImageJ software. Graph bars represent relative Fluo-4 units normalized to the control. Scale bar: (A) - 200 µM, (B) – 50 µM. Values are expressed as mean ± SD, *p<0.05 (n=3).

To further determine whether Ca^{2+} efflux from the ER was responsible for the hypercapnia-induced activation of IRE1α, we measured the levels of phosphorylated IRE1α after 2-APB treatment. As shown in Figure 3.21A and Figure 3.21B, phosphorylation of IRE1α was attenuated in both murine PCLS and human A549 cells treated with 2-APB, further suggesting the involvement of IP3R receptors in the activation of the IRE1α.

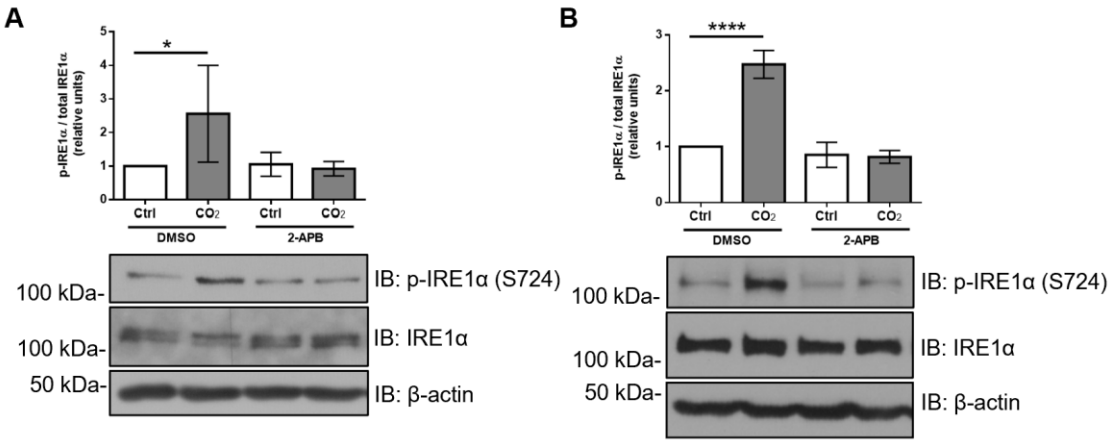

Figure 3.21 Treatment with the IP3R receptor antagonist, 2-APB, attenuates the hypercapnia-induced phosphorylation of IRE1α. (A) Murine PCLS and **(B)** A549 cells were exposed to normal (Ctrl, 40 mmHg; pH_e=7.4) or elevated CO_2 levels (CO_2, 120 mmHg; pH_e=7.4) for 60 min in the presence or absence of 2-APB (100 µM). Phosphorylated (p-IRE1α) and total IRE1α (IRE1α) levels were analyzed by IB. Representative western blots are shown. Graph bars represent p-IRE1α/IRE1α ratio. Values are expressed as mean ± SD, *p<0.05; ****p<0.0001 (n=4-5).

3.5.9 Treatment with 2-APB prevents ERAD of the Na,K-ATPase β-subunit and increases its plasma membrane abundance

Next, we aimed to determine whether the inhibition of Ca^{2+} release prevents the ERAD of the ER-resident Na,K-ATPase β-subunit. We measured the amount of the ER fraction of the Na,K-ATPase β-subunit upon treatment with 2-APB. In both murine PCLS and A549 cells, pretreatment with 2-APB stabilized the levels of the Na,K-ATPase β-subunit (Figure 3.22A,B).

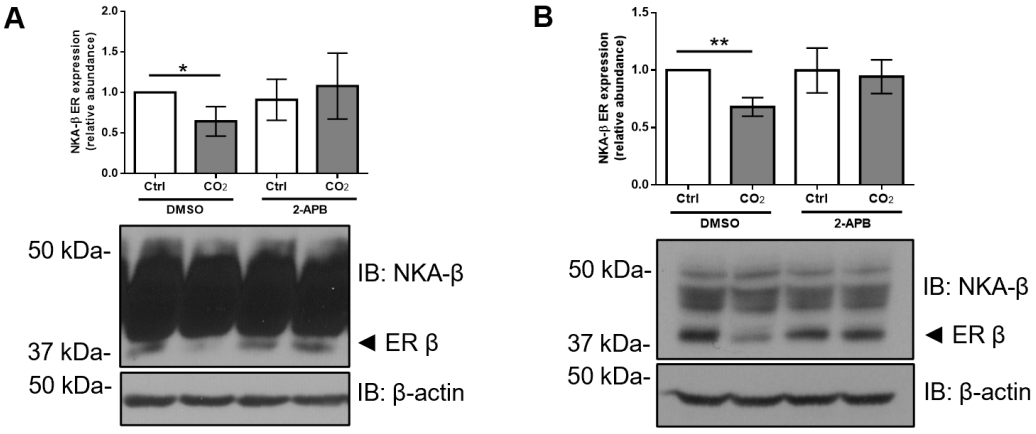

Figure 3.22 Hypercapnia-induced ERAD of the ER-resident Na,K-ATPase β-subunit is rescued by 2-APB. (A) Murine PCLS and **(B)** A549 cells were exposed to normal (Ctrl, 40 mmHg; pH_e=7.4) or elevated CO_2 levels (CO_2, 120 mmHg; pH_e=7.4) for 60 min in the presence or absence of 2-APB (100 µM). Total cell lysate levels of the Na,K-ATPase β-subunit (NKA-β) were analyzed by IB. Representative western blots are shown. Graph bars represent the ER NKA-β/β-actin ratio. Values are expressed as mean ± SD, *p<0.05; **p<0.01 (n=5).

Furthermore, to determine whether blocking ERAD activity by 2-APB affected the Na,K-ATPase plasma membrane abundance upon elevated CO_2 concentrations, confocal imaging and biotin-streptavidin pull down assays were performed. PCLS were treated with 2-APB for 30 min and then exposed to normocapnia (Ctrl) or hypercapnia (CO_2) for 60 min in the presence or absence of 2-APB. Consistent with our previous findings, inhibition of IPR3R activity remarkably increased the cell surface abundance of NKA-β in PCLS compared to DMSO-treated hypercapnic controls, as assessed by confocal microscopy (Figure 3.23).

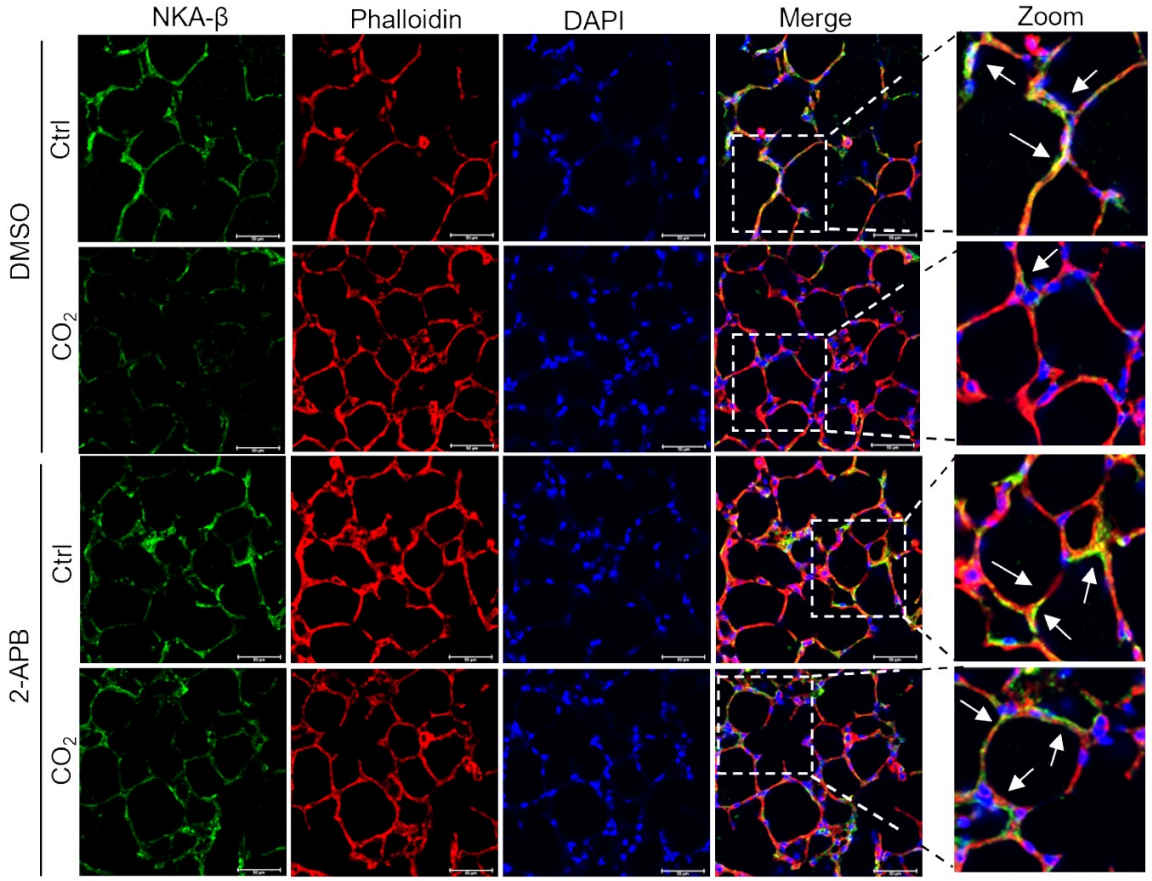

Figure 3.23 Treatment with 2-APB stabilizes the plasma membrane abundance of the Na,K-ATPase β-subunit after short-term hypercapnic exposure in murine PCLS. Murine PCLS were exposed to normal (Ctrl, 40 mmHg; pH_e=7.4) or elevated CO_2 levels (CO_2, 120 mmHg; pH_e=7.4) for 60 min in the presence or absence of DMSO or 2-APB (100 µM). The localization of the Na,K-ATPase β-subunit (NKA-β) was assessed by immunofluorescence. Immunofluorescence staining of the NKA- β (green), phalloidin (red) and nuclei (blue) are shown. Scale bar – 50 µM.

In line with the data obtained from murine PCLS, pharmacological inhibition of IP3R by 2-APB in A549 cells stabilized plasma membrane levels of the Na,K-ATPase subunits after hypercapnic exposure (Figure 3.24).

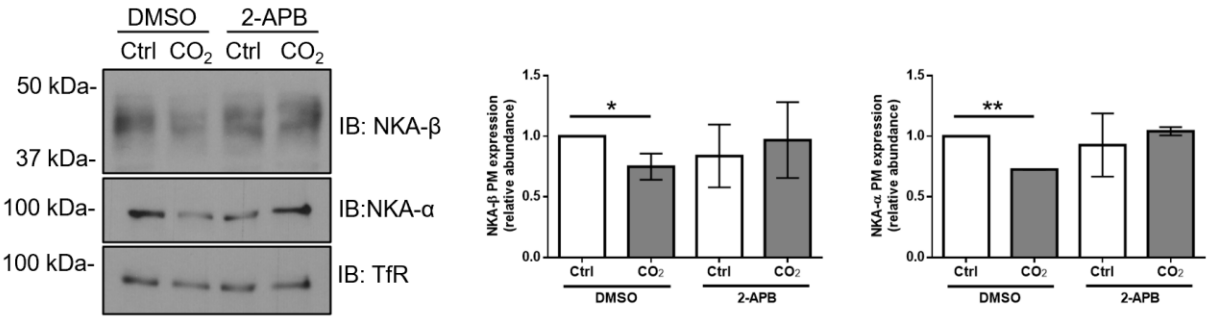

Figure 3.24 Treatment with 2-APB prevents the hypercapnia-induced downregulation of the Na,K-ATPase plasma membrane expression. A549 cells were exposed to normal (Ctrl, 40 mmHg; pH_e=7.4) or elevated CO_2 levels (CO_2, 120 mmHg; pH_e=7.4) for 60 min in the presence or absence of DMSO or 2-APB (100 µM). Afterwards, surface proteins were labeled with biotin and a streptavidin pull-down was performed. **(A)** Na,K-ATPase α- subunit (NKA-α) and Na,K-ATPase β-subunit **(**NKA-β**)** plasma membrane abundance were analyzed by IB. Representative western blots are shown. Graph bars represent NKA-α or NKA-β/TfR ratio. Values are expressed as mean ± SD, *p<0.05; **p<0.01 (n=3).

Collectively, these studies established that short-term hypercapnia transiently decreases the amount of the ER-resident Na,K-ATPase β-subunit, thereby reducing the plasma membrane abundance of the transporter. Our results showed that acute hypercapnia induced ERAD of the Na,K-ATPase β-subunit by depleting the ER Ca^{2+} stores and activating IRE1α.

3.6 Effects of long-term hypercapnia on the folding of the Na,K-ATPase β-subunit in the endoplasmic reticulum

3.6.1 Long-term hypercapnia induces ER retention of the Na,K-ATPase in alveolar epithelial cells

As described above, both short- and long-term exposure to hypercapnia decrease the Na,K-ATPase plasma membrane abundance. We have previously shown that in contrast to short-term, the exposure to elevated CO_2 levels for up to 12 h increased the amount of the ER-resident Na,K-ATPase β-subunit. Therefore, we hypothesized that in alveolar epithelial cells hypercapnia may cause retention of the Na,K-ATPase in the ER, thus preventing its delivery to the cell surface.

Thus, we next investigated whether the hypercapnia-induced ER retention of the Na,K-ATPase β-subunit was a transient or a sustained event. To answer this question, A549 cells were exposed to normal (Ctrl) or elevated CO_2 levels (CO_2) for up to 72 h and levels of the Na,K-ATPase β-subunit were analyzed by immunoblotting (Figure 3.25).

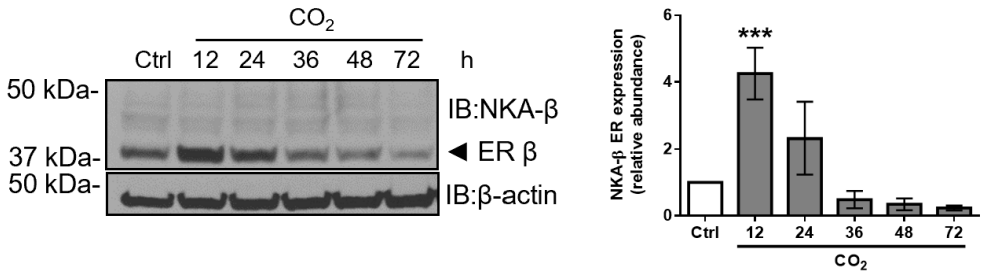

Figure 3.25 Elevated CO_2 levels transiently induce ER retention of the Na,K-ATP β-subunit. A549 cells were exposed to normal (Ctrl, 40 mmHg; pH_e=7.4) or elevated CO_2 levels (CO_2, 120 mmHg; pH_e=7.4) for different time points up to 72 h. Na,K-ATPase β-subunit (NKA-β) total cell lysate levels were analyzed by IB. Representative western blots are shown. Graph bars represent the ER NKA-β/β-actin ratio. Values are expressed as mean ± SD, ***p<0.001 (n=4).

Indeed, we detected a time-dependent ER retention of the Na,K-ATPase β-subunit, which reached its maximum after 12 h. Next, we performed subcellular fractionation of A549 cells exposed to hypercapnia for 12 h and isolated total, ER and Golgi protein fractions by ultracentrifugation (Figure 3.26).

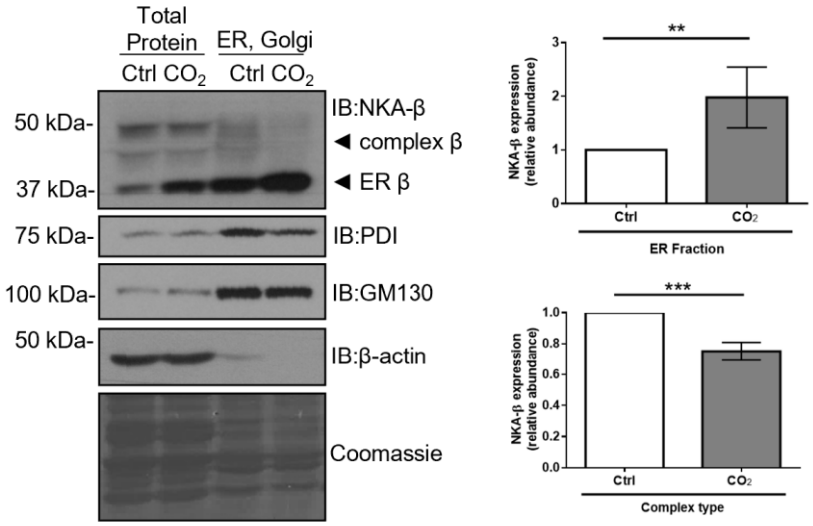

Figure 3.26 Long-term hypercapnia exposure increases the levels of the ER-resident Na,K-ATPase β-subunit. A549 cells were exposed to normal (Ctrl, 40 mmHg; pH_e=7.4) or elevated CO_2 levels (CO_2, 120 mmHg; pH_e=7.4) for 12 h. Afterwards, cellular fractions were isolated by ultracentrifugation. Protein levels of Na,K-ATPase β-subunit (NKA-β), PDI (an ER marker) and GM130 (a Golgi marker) were analyzed by IB. Representative western blots are shown. Graph bars represent the ER NKA-β/Coomassie protein ratio or complex type NKA- β/Coomassie protein ratio. Values are expressed as mean ± SD, **p<0.01; ***p<0.001 (n=4).

Our results showed an increase in the ER-resident Na,K-ATPase β-subunit in the isolated ER fraction, paralleled by a decreased amount of complex Na,K-ATPase β-subunit forms that are located in the Golgi and at the plasma membrane.

3.6.2 Hypercapnic exposure increases co-localization of the Na,K-ATPase β-subunit with the ER-resident chaperons, calnexin and BiP

Recent studies have reported that BiP and calnexin are chaperones that assist the folding of the Na,K-ATPase β-subunit in the ER under both physiological and stress conditions (56). Therefore, we exposed alveolar epithelial cells to normal (Ctrl) or elevated CO_2 (CO_2) levels and detected the localization of the Na,K-ATPase β-subunit, calnexin, and BiP by immunofluorescent microscopy to assess which chaperone was involved in the hypercapnia-induced ER retention of NKA-β.

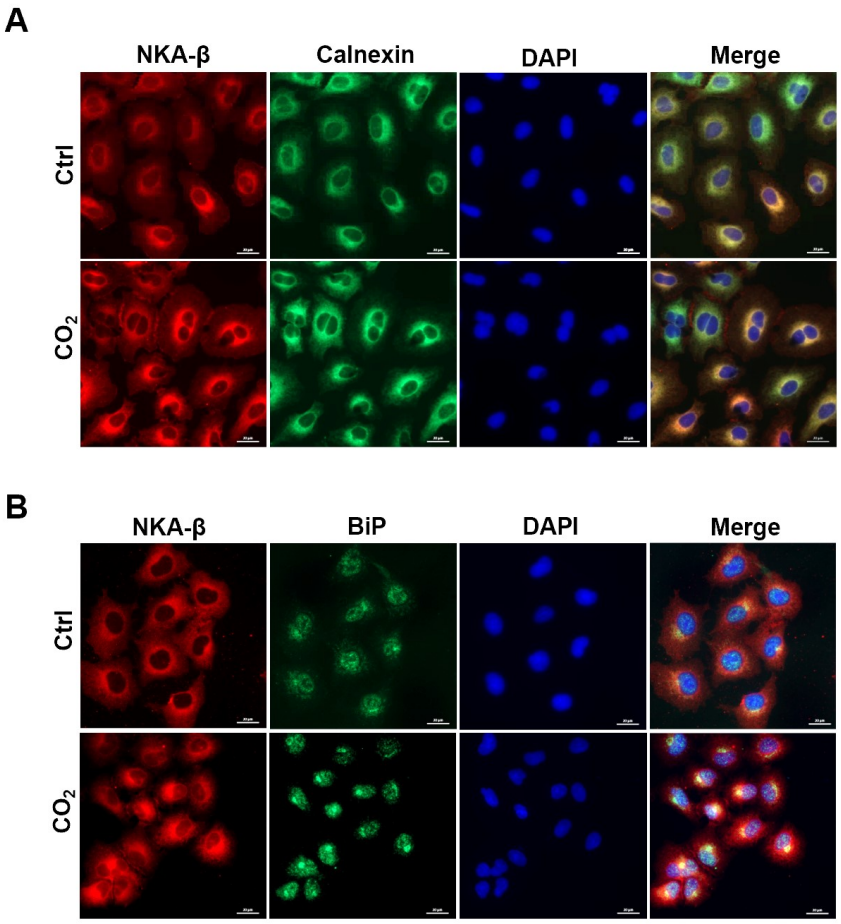

Figure 3.27 Hypercapnia induces the ER retention of the Na,K-ATPase β-subunit and increases its co-localization with ER chaperons. A549 cells were exposed to normal (Ctrl, 40 mmHg; pH_e=7.4) or elevated CO_2 levels (CO_2, 120 mmHg; pH_e=7.4) for 12h. Afterwards, cellular localization of **(A)** the Na,K-ATPase β-subunit (NKA-β) and calnexin or **(B)** NKA-β and BiP was assessed by immunofluorescence. Immunofluorescence staining of the NKA-β (red), calnexin/BiP (green) and nuclei (blue) are shown. Scale bar – 20 µM.

As shown in Figure 3.26, upon hypercapnia co-localization of the ER-resident Na,K-ATPase β-subunits increased with both calnexin and BiP, when compared to normocapnic controls. The results of this experiment suggest that both calnexin and BiP may be involved in the mechanisms of Na,K-ATPase β-subunit retention upon elevated CO_2 levels.

3.6.3 Hypercapnia decreases assembly of the Na,K-ATPase α:β complex

Based on previously published data, the ER quality control only allows assembled Na,K-ATPase α:β complexes to be exported to the Golgi and subsequently to the plasma membrane (45,127). After showing that hypercapnia induced the retention of the Na,K-ATPase β-subunit, we next asked whether elevated CO_2 levels led to disruption of the α:β complexes. To test this, we used A549-α_1-GFP-tagged cells in which a green fluorescent protein (GFP) was bound to the Na,K-ATPase α-subunit and exposed them to normal (40 mmHg, pH_e=7.4) or elevated CO_2 (120 mmHg, pH_e=7.4) levels for 12 h. Afterwards, we immunoprecipitated the Na,K-ATPase β-subunit from total cell lysate or ER-isolated fraction by using specific antibodies and the amount of the co-immunoprecipitated NKA-α was detected by immunoblotting.

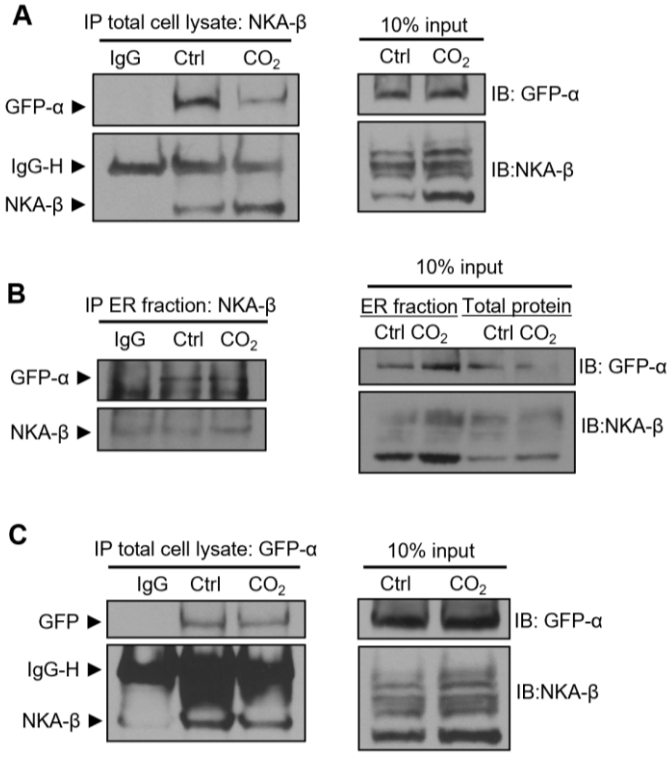

Figure 3.28 Hypercapnia decreases the formation of the Na,K-ATPase α:β complexes. A549-α_1-GFP cells were exposed to normal (Ctrl, 40 mmHg; pH_e=7.4) or elevated CO_2 levels (CO_2, 120 mmHg; pH_e=7.4) for 12 h. Afterwards, cellular fractions were isolated by ultracentrifugation. Na,K-ATPase β-subunit (NKA-β) or α-subunit (NKA-α) were immunoprecipitated from the total or ER fraction with specific antibodies and were analyzed by IB. Representative western blots of the assessed co-immunoprecipitated proteins are shown.

As shown in Figure 3.28, the co-immunoprecipitation of the Na,K-ATPase β-subunits from the total lysate (Figure 3.28A) or the ER fraction (Figure 3.28B), resulted in a decreased amount of precipitated NKA-α, suggesting that a greater amount of the ER retained Na,K-ATPase β-

subunits were not assembled with Na,K-ATPase-α. Similar results were obtained when a reverse co-immunoprecipitation with GFP antibodies was preformed(Figure 3.28C).

3.6.4 Long-term hypercapnia decreases ATP production and increases protein oxidation in the ER

As mentioned above, the ER environment requires several parameters in order to successfully perform protein folding, including optimal levels of ATP and Ca^{2+} and an oxidizing environment (106). To further test whether elevated CO_2 levels decrease the ATP production in alveolar epithelial cells, we treated cells in normocapnia (Ctrl) or hypercapnia (CO_2) for the different time points up to 12 h and determined ATP levels by measuring luciferase activity (Figure 3.29).

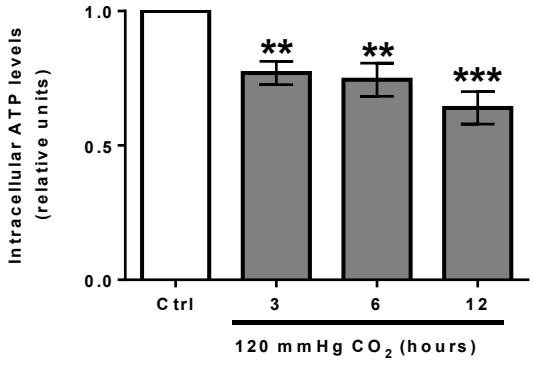

Figure 3.29 Long-term hypercapnia decreases ATP levels in alveolar epithelial cells. A549 cells were exposed to normal (Ctrl, 40 mmHg; pH_e=7.4) or elevated CO_2 levels (CO_2, 120 mmHg; pH_e=7.4) for different time points. Afterwards, ATP levels were detected by using the ATP Bioluminescence assay kit HSII. Graph bars represent total ATP/total protein ratio. Values are expressed as mean ± SD, **p<0.01; ***p<0.001 (n=3).

We found that exposure to hypercapnia significantly inhibited ATP production by approximately 25%. It has been shown that reduced cellular ATP levels can increase protein oxidation by activating redox reactions (180,181). Thus, to further investigate whether elevated CO_2 levels affected redox processes in the ER, we exposed A549 cells to normocapnia or hypercapnia for 12 h and detected protein oxidation in purified total, cytosolic and ER protein fractions by ultracentrifugation. Protein oxidation was measured by using the OxyBlot Detection Kit, which is based on the detection of carbonyl groups attached to proteins by oxidative reactions.

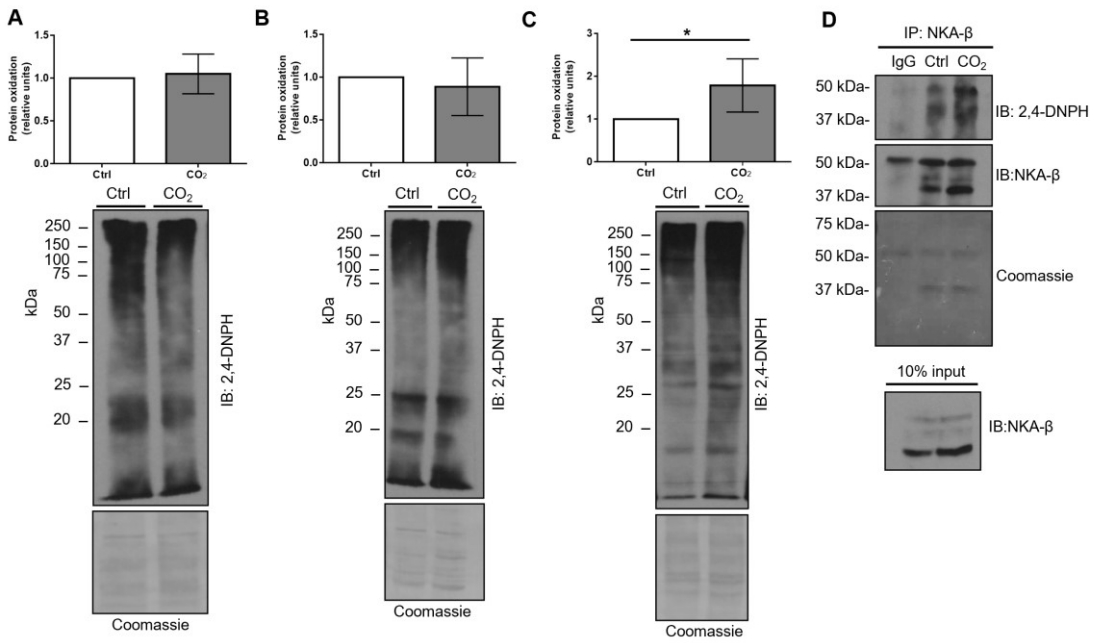

Figure 3.30 Long-term hypercapnia increases oxidation of ER proteins and specifically of the Na,K-ATPase β-subunit. A549 cells were exposed to normal (Ctrl, 40 mmHg; pH_e=7.4) or elevated CO_2 levels (CO_2, 120 mmHg; pH_e=7.4) for 12 h. Afterwards, cellular fractions were isolated by ultracentrifugation and protein oxidation in **(A)** total, **(B)** cytosolic and **(C)** ER/Golgi fractions were determined by using the OxyBlot Protein Oxidation Detection Kit. Total protein oxidation was detected by using antibodies against 2,4-dinitrophenylhydrazone (2,4-DNPH). Graph bars represent 2,4-DNPH/Coomassie protein ratio. Values are expressed as mean ± SD, *p<0.05 (n=5). **(D)** A549 cells were exposed to normal (Ctrl, 40 mmHg; pH_e=7.4) or elevated CO_2 levels (CO_2, 120 mmHg; pH_e=7.4) for 12 h. Na,K-ATPase β-subunits were immunoprecipitated using specific antibodies and protein oxidation was determined by using the OxyBlot Protein Oxidation Detection Kit. Total protein oxidation was detected by using antibodies against 2,4-dinitrophenylhydrazone (2,4-DNPH) and were analyzed by IB. Representative western blots of co-immunoprecipitated proteins are shown.

As shown in Figure 3.30A, the hypercapnia treatment increased global protein oxidation in the purified ER, but not total or cytosolic protein fractions. Next, we evaluated if the Na,K-ATPase β-subunit was a substrate for the oxidative reactions. Na,K-ATPase β-subunits were immunoprecipitated with a specific antibody after hypercapnic exposure and the protein oxidation in immunoprecipitated samples was detected by immunoblotting with the 2,4-dinitrophenylhydrazone antibody (Figure 3.30D). We found that the levels of Na,K-ATPase β-subunit oxidation were increased in alveolar epithelial cells. Collectively, these results suggest that hypercapnia dysregulates ATP production and the redox environment of the ER, thus inducing oxidation of the Na,K-ATPase β-subunit and disrupting the normal maturation of the enzyme.

3.6.5 Long-term hypercapnia induces ER stress by promoting phosphorylation of eIF2a by PERK kinase

Next, we aimed to determine whether the elevation in ER protein oxidation activated the UPR upon long-term exposure to hypercapnia. For this purpose, we exposed A549 cells to normal (Ctrl) or elevated CO_2 levels (CO_2) with a pH_e=7.4 for 12 h and tested the levels of proteins involved in the UPR pathway. Cells treated with the ER stress inducer, thapsigargin (TG) for 12 h were used as positive controls (Figure 3.31A).

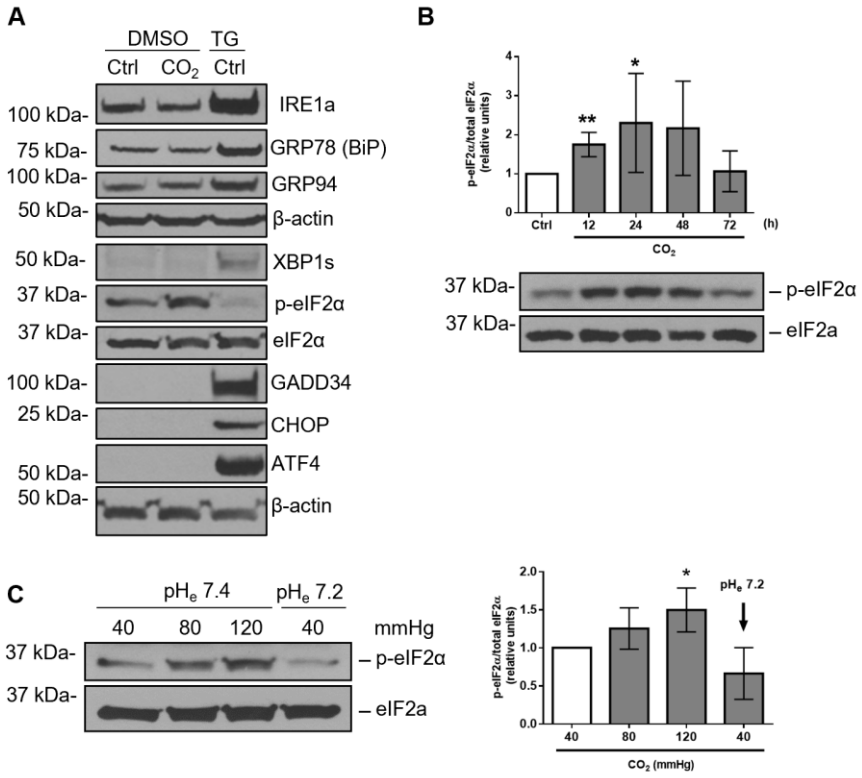

Figure 3.31 Long-term hypercapnia activates the PERK branch of the unfolded protein response and increases eIF2α phosphorylation. (A) A549 cells were exposed to normal (Ctrl, 40 mmHg; pH_e=7.4), elevated CO_2 levels (CO_2, 120 mmHg; pH_e=7.4) or to thapsigargin (1 µM) for 12 h. Total IRE1α, BiP, GRP94, XBP1s, GADD34, CHOP, ATF4, phosphorylated eIF2α (p-eIF2α) and total eIF2α (eIF2α) protein levels were analyzed by IB. Representative western blots are shown. **(B)** A549 cells were exposed to normal (Ctrl, 40 mmHg; pH_e=7.4) or elevated CO_2 levels (CO_2, 120 mmHg; pH_e=7.4) for different time points. p-eIF2α and eIF2α protein levels were analyzed by IB. Graph bars represent p-eIF2α/eIF2α ratio. Values are expressed as mean ± SD, *p<0.05; **p<0.01 (n=3). **(C)** A549 cells were exposed to 40, 80 and 120 mmHg CO_2 with a pH_e=7.4 or to 40 mmHg CO_2 with a pH_e=7.2 (gray bar) for 12 h. p-eIF2α and eIF2α protein levels were analyzed by IB. Representative western blots are shown. Graph bars represent p-eIF2α/eIF2α ratio. Values are expressed as mean ± SD, *p<0.05 (n=3).

In contrast to thapsigargin treatment, we found no upregulated protein levels of the ER stress markers, BiP, IRE1α, GRP94, XBP1s, GADD34, CHOP or ATF4 upon exposure to

hypercapnia in A549 cells. However, we observed that elevated CO_2 levels induced the phosphorylation of eiF2α a downstream target of PERK, a prominent modulator of ER stress. We detected a time-dependent eIF2α phosphorylation induced by CO_2, which returned to the basal level after 72 h (Figure 3.31B). Next, in order to test whether acidic pH or CO_2 *per se* affected phosphorylation of eIF2α, we treated A549 cells with elevated CO_2 concentrations or with physiological CO_2 but acidic media (pH_e=7.2). As shown in Figure 3.31C, decreased extracellular pH did not increase the phosphorylation of eIF2α, suggesting direct activation of the kinase by elevated CO_2 levels.

It has been previously described that in response to ER stress, viral infection, heme and amino acid deprivation, four upstream kinases converge to phosphorylate eIF2α, heme-regulated eIF2a kinase (HRI), double-stranded RNA-dependent protein kinase (PKR), PKR-like ER kinase (PERK) and general control nonderepressible 2 (GCN2) (154). To further investigate which kinase may be responsible for activation of eIF2α, specific knockdown experiments using siRNAs targeting HRI, PKR, PERK, and GCN2 were employed (Figure 3.32).

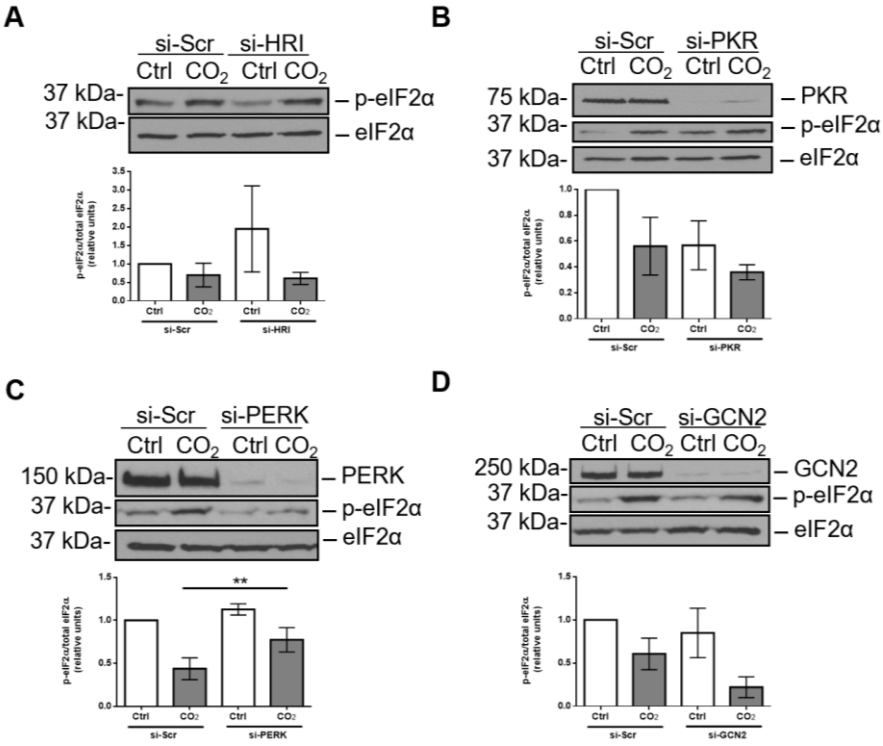

Figure 3.32 PERK kinase is involved in the hypercapnia-induced phosphorylation of eIF2α. A549 cells were transfected with **(A)** a siRNA targeting HRI (si-HRI) or **(B)** a siRNA targeting PKR (si-PKR) or **(C)** a siRNA targeting PERK (si-PERK) or **(D)** a siRNA targeting GCN2 (si-GCN2). 36 h after transfection, cells were exposed to normal (Ctrl, 40 mmHg; pH_e=7.4) or elevated CO_2 levels (CO_2, 120 mmHg; pH_e=7.4) for 12 h. Phosphorylated eIF2α (p-eIF2α) and total eIF2α (eIF2α) protein levels were analyzed by IB. Representative western blots are shown. Graph bars represent p-eIF2α/eIF2α ratio. Values are expressed as mean ± SD, **p<0.01 (n=4).

Our results revealed that, in contrast to HRI, PKR and GCN2, transfection of A549 cells with a siRNA against PERK (Figure 3.32C) prevented the hypercapnia-induced phosphorylation of eIF2α, thus suggesting the involvement of ER stress and unfolded protein response mechanisms.

3.6.6 Phosphorylation of eIF2α by PERK is an adaptive unfolded protein response

Upon ER stress, the UPR pathways aim to restore the protein-folding homeostasis of the ER. It has been previously reported that PERK activation and subsequent phosphorylation of eIF2α at Ser51 initiate a transient attenuation of protein synthesis by halting initiation of mRNA translation, thereby decreasing the protein overload of the ER (112). Therefore, we next asked whether inhibition of protein translation by the hypercapnia-induced phosphorylation of eiF2α is an adaptive or maladaptive UPR event and whether it is involved in the mechanisms of ER retention of the Na,K-ATPase β-subunit. To address this question, A549 cells were transfected with a siRNA against PERK or eiF2α and then exposed to normal or elevated CO_2 levels (Figure 3.33).

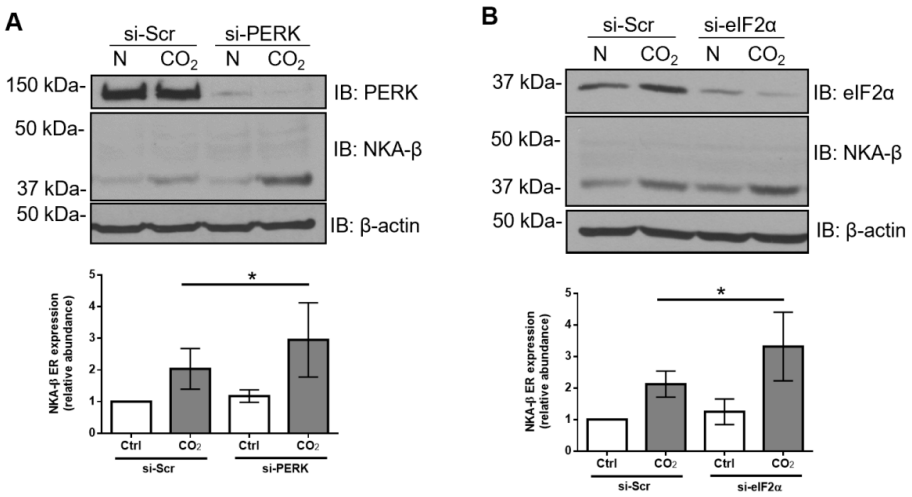

Figure 3.33 Knock-down of PERK or eIF2α increases the retention of the ER-resident Na,K-ATPase β-subunit after long-term hypercapnia exposure. A549 cells were transfected with **(A)** a siRNA targeting PERK (si-PERK) or **(B)** a siRNA targeting eIF2α (eIF2α). 36 h after transfection, cells were exposed to normal (Ctrl, 40 mmHg; pH_e=7.4) or elevated CO_2 levels (CO_2, 120 mmHg; pH_e=7.4) for 12 h. Total cell lysate levels of the Na,K-ATPase β-subunit (NKA-β) were analyzed by IB. Representative western blots are shown. Graph bars represent the ER NKA-β/β-actin ratio. Values are expressed as mean ± SD, *p<0.05 (n=4).

Our results revealed that downregulation of either PERK (Figure 3.33A) or eiF2α (Figure 3.33B) increased the amount of the Na,K-ATPase-retained β-subunits, suggesting that the

hypercapnia-induced activation of eIF2α is part of an adaptive ER stress response that aims to decrease the overload of the ER with newly synthesized proteins.

Recent studies have shown that under various stress conditions the duration of eIF2α phosphorylation directly correlates with ER adaptation mechanisms and cell fate decisions, such as cell death (152,182,183). Next, we assessed cellular viability after exposure to hypercapnia. A549 cells were treated with normal (Ctrl) or elevated CO_2 levels (CO_2) for different time points (up to 72 h) and then cellular viability was assessed by using the CASY Cell Counter and Analyzer Model TT (Figure 3.34). Indeed, elevated CO_2 levels did not increase cell death, which confirmed an adaptive ER stress response and a protective role of eIF2α phosphorylation in hypercapnia-exposed cells.

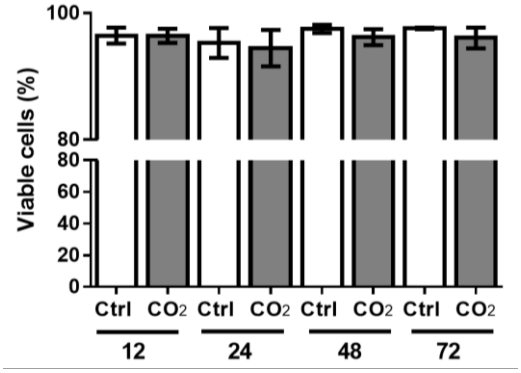

Figure 3.34 Cell viability after hypercapnia exposure. A549 cells were exposed to normal (Ctrl, 40 mmHg; pH_e=7.4) or elevated CO_2 levels (CO_2, 120 mmHg; pH_e=7.4) for different time points up to 72 h. Afterwards, cellular viability was determined by using the CASY Cell Counter and Analyzer Model TT. Graph bars represent the percentage of viable cells. Values are expressed as mean ± SD (n=3).

3.6.7 Treatment with α-ketoglutaric acid reverses the hypercapnia-induced ER protein oxidation and phosphorylation of eIF2α

Up to this point, we were able to show that hypercapnia enhances the retention of oxidized ER-resident NKA-β-molecules, thus disrupting the formation of the functional Na,K-ATPase-α:β complex. Furthermore, we have shown that a long-term exposure to elevated CO_2 levels activates the UPR and results in the phosphorylation of eiF2α by PERK. Previously, elevated levels of CO_2 were shown to cause mitochondrial dysfunction and ATP depletion by inhibiting the expression of isocitrate dehydrogenase 2 (IDH2), a key enzyme in the tricarboxylic acid cycle (TCA). This inhibitory effect could be rescued by the treatment with α-ketoglutaric acid (93). Thus we next pretreated A549 cells with α-ketoglutaric acid (10 mM) and subsequently exposed cells to normal (Ctrl) or elevated CO_2 levels (CO_2) for 12 h. Importantly, pretreatment of cells with α-ketoglutaric acid prevented the hypercapnia-induced increase in ER protein oxidation (Figure 3.35A). Furthermore, as shown in Figure 3.35B, treatment with α-ketoglutaric acid attenuated the hypercapnia-induced phosphorylation of eIF2α, suggesting that the ER stress response was attenuated by restoring normal protein folding.

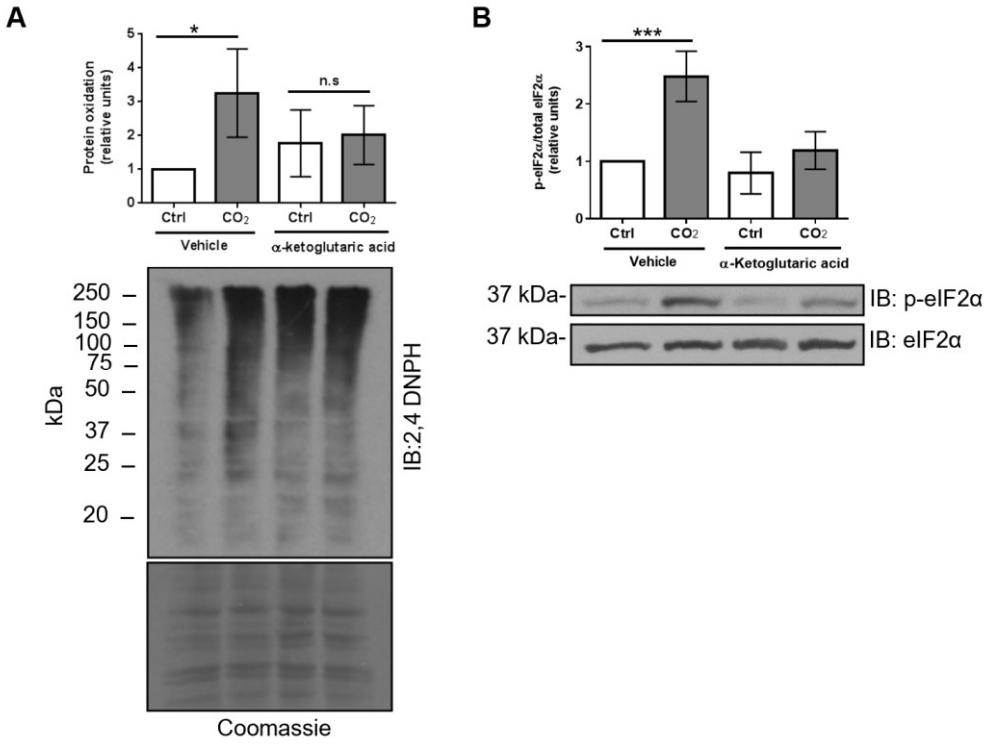

Figure 3.35 Treatment with α-ketoglutaric acid decreases ER protein oxidation and eIF2α phosphorylation. **(A)** A549 cells were exposed to normal (Ctrl, 40 mmHg; pH_e=7.4) or elevated CO_2 levels (CO_2, 120 mmHg; pH_e=7.4) for 12 h in the presence or absence of vehicle or α-ketoglutaric acid. Afterwards, cellular fractions were isolated by ultracentrifugation and protein oxidation in the ER/Golgi fraction was determined by using the OxyBlot Protein Oxidation Detection Kit. Total protein oxidation was detected by using antibodies against 2,4-dinitrophenylhydrazone (2,4-DNPH). Graph bars represent 2,4-DNPH/Coomassie protein ratio. Values are expressed as mean ± SD, *p<0.05 (n=3). **(B)** A549 cells were exposed to normal (Ctrl, 40 mmHg; pH_e=7.4) or elevated CO_2 levels (CO_2, 120 mmHg; pH_e=7.4) for 12 h in the presence or absence of vehicle or α-ketoglutaric acid. Phosphorylated eIF2α (p-eIF2α) and total eIF2α (eIF2α) protein levels were analyzed by IB. Representative western blots are shown. Graph bars represent p-eIF2α/eIF2α ratio. Values are expressed as mean ± SD, ***p<0.001 (n=4).

3.6.8 Treatment with α-ketoglutaric increases plasma membrane abundance and function of the Na,K-ATPase after hypercapnia exposure.

As we demonstrated that α-ketoglutaric acid attenuates the hypercapnia-induced changes in the ER, we next aimed to assess the potential effects of α-ketoglutaric acid on the maturation of the Na,K-ATPase β-subunit. We exposed A549 cells to normal (Ctrl) or elevated levels of CO_2 (CO_2) in the presence or absence of α-ketoglutaric acid for 12 h, and then cell surface abundance and total cell lysate levels of the Na,K-ATPase β-subunit were measured (Figure 3.36). As anticipated, the treatment with α-ketoglutaric acid prevented the hypercapnia-induced ER retention of the NKA-β subunit (Figure 3.36A), which paralleled with an increased cell surface expression of the transporter (Figure 3.36B).

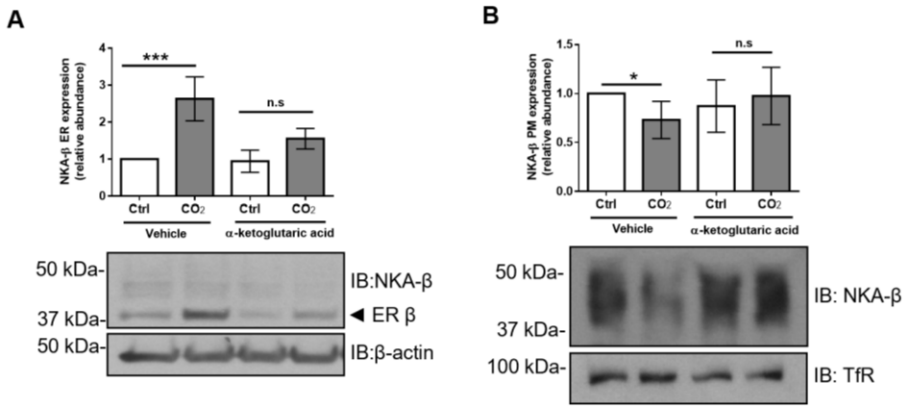

Figure 3.36 Treatment with α-ketoglutaric acid rescues the Na,K-ATPase β-subunit plasma membrane abundance after long-term hypercapnia. A549 cells were exposed to normal (Ctrl, 40 mmHg; pH_e=7.4) or elevated CO_2 levels (CO_2, 120 mmHg; pH_e=7.4) for 12 h in the presence or absence of α-ketoglutaric acid (10 mM). **(A)** Total cell lysate levels of the Na,K-ATPase β-subunit (NKA-β) were analyzed by IB. Representative western blots are shown. Graph bars represent the ER NKA-β/β-actin ratio. Values are expressed as mean ± SD, ***p<0.001 (n=5). **(B)** NKA-β plasma membrane abundance levels were analyzed by IB. Representative western blots are shown. Graph bars represent NKA-β/TfR ratio. Values are expressed as mean ± SD, *p<0.05 (n=5).

To complement these findings, functional studies were preformed to measure the function of the Na,K-ATPase. Primary rat ATII and A549 cells were exposed to normocapnia or hypercapnia and then the ouabain-sensitive ATPase activity was measured (Figure 3.37).

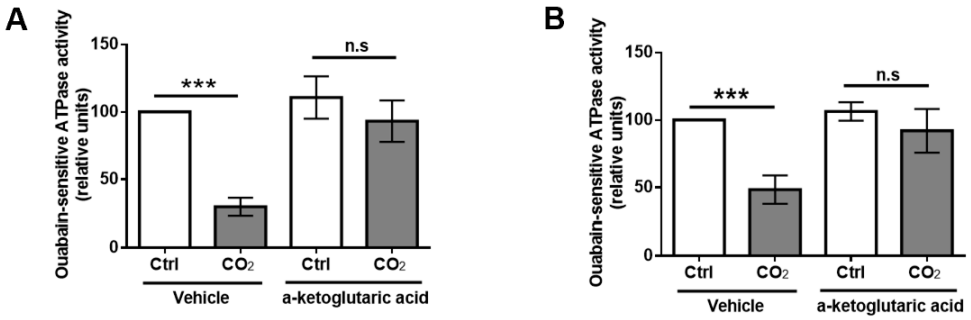

Figure 3.37 Treatment with α-ketoglutaric acid rescues Na,K-ATPase function after long-term hypercapnia treatment. A) Primary rat ATII and **(B)** A549 cells were exposed to normal (Ctrl, 40 mmHg; pH_e=7.4) or elevated CO_2 levels (CO_2, 120 mmHg; pH_e=7.4) for 12 h in the presence or absence of α-ketoglutaric acid (10 mM). Ouabain-sensitive activity of the Na,K-ATPase was measured in isolated membranes by using a colorimetric high-sensitivity ATPase assay kit. Graph bars represent the ouabain-sensitive ATPase activity. Data are expressed as mean ± SD, ***p<0.001 (n=5).

Consistent with the previously detected effects of α-ketoglutaric acid on Na,K-ATPase plasma membrane abundance, the function of the transporter was nearly completely rescued after the treatment in both hypercapnia-exposed primary ATII and A549 cells. Collectively, these results suggest that rescuing the mitochondrial function by α-ketoglutaric acid may decrease the hypercapnia-induced retention of the Na,K-ATPase β-subunit and increase plasma membrane abundance and function of the enzyme.

4. Discussion

Elevated levels of CO_2 are often observed in patients with acute and chronic lung diseases, as a consequence of epithelial barrier disruption and alveolar hypoventilation, often related to protective mechanical ventilation with low tidal volumes. It has been shown that hypercapnia, independently of acidosis, is associated with higher complication rates, more organ failure, worse outcomes and an increased risk of ICU mortality (87). Here we provide evidence that exposing murine PCLS and primary or cultured epithelial cells to hypercapnia disrupts the normal maturation of the Na,K-ATPase β-subunit in the ER and thus decreases its plasma membrane abundance. The decreased cell surface expression of the Na,K-ATPase, which is a key enzyme that is involved in establishing an osmotic Na^+ gradient in the alveolar epithelium and thus drives resolution of alveolar edema (27), is critical in patients with ARDS (4).

In addition to previously published data showing that hypercapnia impairs the Na,K-ATPase plasma membrane abundance by promoting its endocytosis from the cell surface (51,77,78), our current study suggests that CO_2 modifies the maturation of the β-subunit of the Na,K-ATPase in the ER. The short-term response to elevated CO_2 levels involves degradation of the Na,K-ATPase β-subunit in the ER, which is driven by MAN1B1 and EDEM1 via activation of the unfolded protein response receptor IRE1α. Activation of IRE1α is a result of depleted ER calcium stores due to an increased Ca^{2+} release by IP3R receptors. In contrast, long-term exposure to hypercapnia increases oxidation of the Na,K-ATPase β-subunit in the ER, thereby decreasing the assembly of the Na,K-ATPase-α:β complex and its delivery to the plasma membrane. We found that either blocking the Ca^{2+} release from the ER via IP3R receptors by 2-APB or reducing the carbonylation of ER proteins by α-ketoglutaric acid rescues the hypercapnia-induced downregulation of Na,K-ATPase cell surface abundance.

4.1 Hypercapnia decreases plasma membrane abundance and activity of the Na,K-ATPase and dynamically changes the amount of ER-resident Na,K-ATPase-β

Alveolar gas exchange strictly depends on the active clearance of excess lung alveolar fluid, which relies on the coordinated work of active, vectorial ion transport, thereby directing water reabsorption (24). Indeed, ENaC and the Na,K-ATPase are the central plasma membrane-localized proteins that establish vectorial Na^+ transport, and thus alveolar fluid clearance (27,28,55). A decreased expression and function of the above-mentioned transporters has a deleterious impact on the resolution of pulmonary edema in models of acute lung injury and in patients with ARDS (14,22).

A disruption of the alveolar-capillary barrier and protective mechanical ventilation with low tidal volumes, which is necessary in ARDS to prevent further deterioration of lung function, result in CO_2 retention, causes harmful effects including inhibition of alveolar fluid clearance (21,65,87). We and others have previously established that hypercapnia decreases the plasma membrane abundance of ENaC and the Na,K-ATPase by inducing a CO_2-specific pathway that involves phosphorylation of AMPK, ERK and JNK leading to subsequent retrieval of the transporters from the cell surface by endocytosis (51,77,78,98).

The Na,K-ATPase is a heterodimeric protein that consists of three subunits: a catalytic α-subunit, a regulatory β-subunit and an auxiliary γ-subunit, which need to be properly folded and assembled in the ER and Golgi before their delivery to the plasma membrane (29,45). Most previous studies have focused on the CO_2-induced endocytosis of the catalytic Na,K-ATPase α-subunit, while the influence of hypercapnia on the processes of folding, maturation and exocytosis of the β-subunit remained unknown. In the current work, we studied whether a elevated CO_2 levels mediate downregulation of Na,K-ATPase maturation in the ER and if such impairment of ER function may contribute to the decreased plasma membrane abundance and activity of the enzyme.

Our studies, using biotinylation, immunofluorescent confocal microscopy and measurement of the Na,K-ATPase activity, showed that elevated CO_2 levels significantly impaired the cell-surface expression and function of the enzyme upon both during the short- (up to 1 h) and long-term (up to 12 h) hypercapnia treatment of murine PCLS, primary rat ATII, and human A549 cells. Of note, we did not find any transcriptional repression of the Na,K-ATPase subunit. In contrast, despite a decrease in the plasma membrane abundance of the transporter, we observed an upregulation of Na,K-ATPase mRNA transcription after 12 h of CO_2 exposure. Previously published studies indicated that the hypercapnia-induced changes in gene expression are highly dynamic with marked differences between short- (up to 1 hour) and long-term responses (184,185). Indeed, various stimuli that impair alveolar fluid clearance, such as angiotensin II, ouabain, hyperoxia or elevated Ca^{2+} levels, have been shown to selectively upregulate transcription of the Na,K-ATPase α- or β-subunit, probably as an adaptive response (46,186).

Next, we examined the intracellular levels of the Na,K-ATPase and in particular the complex and the high mannose fractions of the Na,K-ATPase β-subunit. In contrast to the Na,K-ATPase α-subunit, hypercapnia dynamically changed the endogenous levels of the ER-resident high mannose fraction of the β-subunit. During the short-term treatment, CO_2 significantly decreased

the high mannose forms of the Na,K-ATPase β-subunit, while long-term exposure resulted in their retention. Furthermore, we found that the hypercapnia-induced changes in the regulation of the Na,K-ATPase β-subunit in the ER took place in a dose-dependent manner and partially independent from extracellular acidosis. Briva and colleagues reported that acute exposure to high CO_2 levels resulted in a transient (up to 10 min) decrease in intracellular pH, which was rapidly restored to the normal levels (69). However, it is possible that the ER environment is sensitive to such short-lasting changes in intracellular or extracellular pH. These speculations are supported by several reports suggesting that acidosis may activate the unfolded protein response pathways (119,141,187) and will require further experimental assessment in the settings of buffered and unbuffered hypercapnia.

It is well established that the Na,K-ATPase β-subunit is a glycoprotein that undergoes glycosylation during maturation in the ER (45,127). The formation of Na,K-ATPase-α:β complex relies on the β-subunit, which is crucial for the trafficking and correct membrane insertion of the NKA α-subunit (45,101). After showing different time-course responses to high CO_2 levels, we divided our further studies into short- and long-term hypercapnic regulation of the Na,K-ATPase β-subunit in the ER.

4.2 Short-term hypercapnia induces ERAD of the Na,K-ATPase β-subunit

We found that exposure of the alveolar epithelium to elevated CO_2 levels for up to 1 h resulted in decreased levels of the ER-resident Na,K-ATPase β-subunit of the high mannose type. Several potential mechanisms may explain this result. First, misfolded or unfolded proteins that fail to pass the ER quality system are degraded in a process termed ER-associated degradation (ERAD) in order to prevent unnecessary attempts to fold proteins that can not achieve a native structure (114). Second, the decreased amount of the Na,K-ATPase β-subunit in the ER may be explained by rapid translocation of properly folded molecules to the Golgi compartment for further maturation and delivery to the cell surface (106). However, since the plasma membrane levels of the transporter were reduced, we hypothesized that hypercapnia probably caused ERAD of the ER-resident Na,K-ATPase β-subunits. Prior studies have shown that the initial step of ERAD is to tag the substrates for degradation by trimming a mannose residue of the glycosylated peptide by the ER-specific mannosidase MAN1B1 (158,188) We used chemical and genetic approaches by either inhibiting the mannosidase activity with kifunensine or targeting MAN1B1 by a specific siRNA. Our experiments showed that both methods were sufficient to stabilize the levels of the ER-resident Na,K-ATPase β-subunit. To further investigate the mechanisms of hypercapnia-induced ERAD, cells were transfected with a

siRNA against EDEM1, a key element of ERAD that is involved in the formation of the degradation complex (176). Importantly, knockdown of the EDEM1 protein prevented the decrease in the ER-resident Na,K-ATPase β-subunit levels. Additionally, we observed that, in contrast to the lysosomal inhibition by chloroquine, decreasing the proteasomal activity by MG-132 prevented the hypercapnia-induced downregulation of the Na,K-ATPase β-subunit ER levels. These results suggest that the Na,K-ATPase subunits probably do not form aggregates (which are known to be degraded by lysosomes), but rather undergo deglycosylation, retrotranslocation and proteasomal degradation. Collectively, these experiments suggested that acutely elevated CO_2 levels may induce ERAD of the Na,K-ATPase β-subunit.

To the best of our knowledge, this is the first study that show that the Na,K-ATPase β-subunit is a substrate for ERAD under hypercapnic conditions. Our studies have also raised additional questions that need further exploration. It has been shown that the mannosidase activity of EDEM proteins depends on the folding state of the substrate (161), thus, it might be relevant to study the folding state of the degraded β-subunit molecules. Since the ERAD system is a complex structure, consisting of various peptides, it would also be interesting to investigate whether elevated levels of CO_2 affect the formation of the ERAD complex itself. It has previously been shown that a malfunction of ERAD results in increased amounts of misfolded proteins that has been associated with numerous pathological conditions such as Alzheimer's disease, Huntington's disease, Parkinson's disease, α_1-antitrypsin deficiency and cystic fibrosis (189,190). In contrast, acute noxae such as ischemia have been found to activate ERAD (166). Although it is evident that a decreased plasma membrane abundance of the Na,K-ATPase is associated with an impaired alveolar fluid clearance and is deleterious for ARDS patients, further work is warranted to establish whether acute hypercapnia-induced ERAD is an adaptive process aiming cellular maintenance or a maladaptive one.

4.3 Short-term hypercapnia activates IRE1α by decreasing ER calcium concentrations through activation of IP3R receptor-mediated calcium release

As mentioned earlier, the ER quality control tightly regulates protein folding by the coordinated action of three main receptors of the unfolded protein response pathway, IRE1α, PERK, and ATF6. Of these, IRE1α has been reported to actively degrade proteins via RNA-decay under stress conditions and to upregulate proteasomal and lysosomal pathways (134,158,167). Of note, IRE1α was found to be involved in lung conditions, e.g. by enhancing the influenza virus replication cycle (150,191). Therefore, the IRE1α signaling pathway is a potentially attractive therapeutic target in lung diseases.

We hypothesized that IRE1α may play a role in the hypercapnia-induced decrease of the ER-resident Na,K-ATPase β-subunit. Indeed, elevated CO_2 levels activated IRE1α rapidly in a time-dependent manner by its phosphorylation at S724. Furthermore, both genetic knock-down and treatment with a chemical inhibitor of IRE1α prevented the ERAD of the Na,K-ATPase β-subunit. Similarly, treatment with an ER stress inducer or with an IRE1α activator resulted in ERAD of the NKA-β confirming the role of IRE1α activity. These results are in line with previous studies, which found that IRE1α controls the degradation of misfolded receptors (167,192).

One of the downstream targets of IRE1α in the process of UPR is JNK (137). Interestingly, the JNK signaling pathway has been previously found to be involved in the CO_2-induced downregulation of ENaC and Na,K-ATPase (77,78,98). It has been shown that upon hypercapnia activation of JNK leads to reorganization of the actin cytoskeleton and enhanced interaction of Na,K-ATPase and LMO7b, which drives the endocytosis of NKA from the plasma membrane (78). In addition, IRE1α was found to be involved in remodeling of the cytoskeleton. It has been reported that, apart from the classical UPR response, IRE1α controls cytoskeleton remodeling by modulating filamin A signaling (193). Therefore, we hypothesized that JNK may be involved in the ERAD of the Na,K-ATPase β-subunit. However, although activation of JNK by hypercapnia was evident in our studies, inhibition of the kinase did not influence the ERAD of NKA-β.

Upon its activation, IRE1α possesses RNase activity that augments mRNA cleavage and its subsequent degradation, which leads to IRE1-dependent decay of mRNA (RIDD) (146). Recently, it has been shown that the Na,K-ATPase α-subunit may be a substrate of RIDD (177). However, our findings showed no differences in the mRNA expression of NKA after short-term exposure to CO_2, suggesting that ERAD of the Na,K-ATPase β-subunit is independent of the RIDD signaling pathway.

Another downstream protein of the RIDD-induced IRE1α activation is XBP1. The mRNA splicing of XBP1 by IRE1α leads to translation of active XBP1s, which has been found to be involved in protein degradation by activating genes involved in ERAD (146). Our study suggests that XBP1 is not involved in the ERAD of the Na,K-ATPase β-subunit, since neither inhibition of mRNA splicing activity nor depletion of XBP1 was sufficient to stabilize the Na,K-ATPase levels in the ER. On the other hand, treatment of cells with an ER stress inducer or an activator of IRE1α upregulated protein expression of XBP1s. However, XBP1s levels did

not correlate with IRE1α phosphorylation or the decrease of the ER-resident Na,K-ATPase β-subunit molecules. Taken together, these data suggest that the IRE1α/XBP1s axis does not play a role in the degradation of the Na,K-ATPase β-subunit upon short-term hypercapnic exposure of the alveolar epithelium.

Recently published data shed light on a potential connection between IRE1α and ERAD of the Na,K-ATPase β-subunit. It has been shown that unfolded proteins are IRE1α-activating ligands and IRE1α may bind these ligands directly (194,195). Thus, IRE1α might directly interact with the unfolded Na,K-ATPase β-subunit upon elevated CO_2 levels. Further studies focusing on the potential (direct) interaction between the Na,K-ATPase and IRE1α upon hypercapnic exposure are therefore warranted.

Changes is CO_2 concentrations have been shown to modify intracellular Ca^{2+} levels (51,76,100,196). Our data suggest that the hypercapnia-induced activation of IRE1α and subsequent ERAD of the Na,K-ATPase β-subunit were triggered by Ca^{2+}-dependent mechanisms. Interestingly, it has been found that depending on the cell type, Ca^{2+} levels, are elevated during both short- and long-term hypercapnia exposure, suggesting that several sources of intracellular Ca^{2+} increase may exist (51,76). In general, the response to the extracellular ligands or intracellular messengers may lead to a cytosolic increase in Ca^{2+}, either by Ca^{2+} influx through plasma membrane-localized channels or by Ca^{2+} efflux through internal stores via 1,4,5-triphosphate (IP3R) or ryanodine receptors (RyR) (117,179). Since it was found that RyR receptors are exclusively expressed in muscles and neurons, we focused on the IP3R receptors that are known to be expressed in epithelial cells (197). In order to maintain homeostatic conditions, the release of Ca^{2+} from intracellular ER stores may not lead to a decrease in the functional luminal ER Ca^{2+} concentration. To counteract a decrease in luminal ER Ca^{2+} concentrations, a “store-operated” Ca^{2+} entry mechanism is implied, in which STIM1/STIM2 proteins oligomerize and interact with ORAI1 at the plasma membrane and activate Ca^{2+} influx to the cell (197,198). Interestingly, the Ca^{2+} sensing mechanisms involved in the STIM1/ORAI1 interaction have been found to be engaged in response to hypoxia (199,200). Our studies revealed that the treatment with a Ca^{2+} chelator aggravates the degradation of the Na,K-ATPase β-subunit and enhances the phosphorylation of IRE1α. In addition, we found that the treatment with thapsigargin, which is known to increase the cytosolic Ca^{2+} concentration by inhibiting SERCA and activating IRE1α (201,202), induces the degradation of the Na,K-ATPase β-subunit ER fraction. Thus, we hypothesized that hypercapnia may deplete the Ca^{2+} stores of the ER and thus increases cytosolic concentrations

of the ion via the IP3R receptors of the ER. In line with this notion, the treatment of the alveolar epithelium with an IP3R inhibitor (2-APB) prevented the hypercapnia-induced ERAD and phosphorylation of IRE1α. These results are consistent with previously published reports, suggesting that the hypercapnia-induced Ca^{2+} elevation is due to the activation of IP3R receptors (100,196). Furthermore, it has been previously reported that the Na,K-ATPase through the scaffold protein, ankyrin may establish an interaction between the Na,K-ATPase α-subunit and the IP3R receptors in ER, suggesting direct Ca^{2+} sensing by the Na^+ pump (203,204). Of note, the dysfunction of SERCA or store-operated channels can also promote an imbalance in ER homeostasis. While we have now established that the IP3R receptors are involved in the hypercapnia-induced signaling cascade, the exact mechanisms of their activation by CO_2 remain unknown. Based on our findings, we postulate that the GPCR receptor coupling pathway may be involved in the detection of hypercapnia. Future studies will be conducted to address this hypothesis. Interestingly, recent reports suggested that a metabolic sensor, AMPK that we have previously implicated in the hypercapnia-induced downregulation of the Na,K-ATPase and ENaC (51,98), might be activated by IRE1α (205). However, we have not dissected any AMPK-mediated ERAD mechanisms, and thus, future studies will be essential to tease out whether AMPK affects the ERAD of the NKA β-subunit and whether there is also a link between AMPK and IRE1α activation upon hypercapnia.

One of the limitations of the current study is that no direct measurements of the ER Ca^{2+} levels were performed. A recent report suggested that there is a link between IRE1α and IP3R, as knock-down of IRE1α promotes apoptotic cell death by activating intracellular Ca^{2+} release through IP3R (201). Whether this mechanism is active during hypercapnia will need to be determined in the future. Although 2-APB is a selective inhibitor of IP3R (206), it may additionally inhibit transient receptor potential channels (TRP), which also requires further attention. Moreover, it will be important to evaluate the role of restoring ER Ca^{2+} stores by SERCA, as well as store operated Ca^{2+} entry, since hypercapnia may aggravate the ATP-dependent activity of these molecules.

4.4 Long-term hypercapnia promotes endoplasmic reticulum retention of the Na,K-ATPase β-subunit, decreases ER oxidation and activates the unfolded protein response

Next, we studied how long-term exposure to elevated CO_2 levels may affect the Na,K-ATPase β-subunit. We exposed alveolar epithelial cells to elevated CO_2 concentrations for up to 72 h and observed a a transient increase in the amount of the ER-resident high mannose glycosylated, forms of the Na,K-ATPase β-subunit with a maximum at 12 h. These findings were

accompanied by a significantly decreased plasma membrane abundance and function of the Na,K-ATPase. Subcellular fractionation by ultracentrifugation showed that levels of the Na,K-ATPase β-subunit in the ER were significantly increased, while Golgi-resident forms were decreased. Furthermore, we observed an increased co-localization of the Na,K-ATPase β-subunit with calnexin and BiP, suggesting that both unfolded and partially folded forms of the ER-resident Na,K-ATPase β-subunit were retained in the ER upon hypercapnic exposure. In addition, our results showed that hypercapnia disrupts the assembly of the Na,K-ATPase α:β complex.

Changes in the ER environment or modification of normal protein structure may result in protein misfolding and retention in the ER (119). For example, a mutation of the CFTR channel, which leads to deletion of three nucleotides that encode phenylalanine (Phe508) in the polypeptide chain results in ER retention of the channel (that, as a consequence, does not reach the plasma membrane) and manifestation of cystic fibrosis (207). As for the Na,K-ATPase, it has been reported that mutations in the Na,K-ATPase α:β interaction region (45), activation of oxidative stress and lipid peroxidation (56), removal of glycosylation sites (56) and overexpression of unassembled NKA β-subunits (208) result in ER retention of the enzyme subunits and their increased binding to ER-resident chaperones (56,208). Thus, we hypothesized that hypercapnia modifies the ER environment and prevents the maturation of the Na^+ pump.

As discussed above, protein folding in the ER requires ATP, high Ca^{2+} levels, chaperones, an oxidizing environment, and for glycoproteins, glycosylation enzymes (116,209). Recent evidence suggests that elevated CO_2 levels decrease ATP production by the inhibition of isocitrate dehydrogenase 2 (IDH2) in the tricarboxylic acid cycle (TCA) and thus impair mitochondrial function (93). In addition, hypercapnic acidosis was shown to modify the mitochondrial membrane potential, decrease ATP production, and induce mitochondrial dysfunction (210). Thus, we hypothesized that hypercapnia, the metabolic status of the cell and ER homeostasis were interrelated. In consistence with a previously published study (93), our current findings revealed that long-term hypercapnia decreases cellular ATP levels. It has been reported that low ATP may promote protein oxidation by activation of redox reactions (180,181). Our studies demonstrated that exposing alveolar epithelial cells to hypercapnia does not affect the oxidation pattern of total and cytosolic proteins. In contrast, we observed a marked increase in oxidation of ER proteins, including the Na,K-ATPase β-subunit. We measured protein oxidation by detection of carbonylation, which is the most common oxidative reaction

that is characterized by an irreversible addition of carbonyl groups to protein chains by various oxidative pathways (211,212). Indeed, detection of carbonylated proteins is the most commonly used marker of oxidative damage (213,214). Thus, increased protein oxidation in the ER might be a consequence of upregulation of carbonylation, which has been shown to be associated with protein misfolding in various disease conditions (121,215).

A possible cause of the increased oxidation of the Na,K-ATPase β-subunit may be a cellular response to transcriptional or translational errors (216), if elevated levels of CO_2 impaired these processes. Moreover, the NKA β-subunit may be more susceptible to oxidative stress than other NKA subunits due to glutathionylation of a cysteine in the middle of its transmembrane helix, which is not expressed in other Na,K-ATPase subunits (29,217). Further proteomic identification of carbonylated proteins and oxidation sites will need to be performed to assess these possibilities. Recently it has been shown that carbonylation of ER-resident chaperons may disrupt protein folding (121,122). Whether hypercapnia directly modifies proteins or causes dysfunction of chaperones remains unknown and will need to be addressed in future research.

Our current study demonstrated that short-term exposure to the elevated CO_2 levels results in activation of IRE1α, activation of the UPR and subsequent ERAD of the Na,K-ATPase β-subunit. On the other hand, we found that long-term hypercapnia interferes with ER protein folding by increasing protein oxidation and thus, activates ER stress pathways. After analyzing upstream and downstream targets of the UPR, we observed that long-term hypercapnia resulted in a time-dependent increase of eIF2α phosphorylation. Under non-stressful conditions, eIF2α plays a key role in mRNA translation initiation and recognition of the start codon (182,218). However, stress conditions such as hypoxia, viral infections, amino acid and glucose deprivation result in dimerization and subsequent autophosphorylation of four kinases, HRI, PKR, PERK and GCN2, thus resulting in activation of eIF2α (154,219-221). Our studies identified PERK, which is located in the ER and is active under ER stress conditions (222), as the kinase that is responsible for the eIF2α phosphorylation. These findings are in line with our hypothesis that long-term hypercapnia disturbs protein folding in the ER and activates the UPR.

Given that the activation of eIF2α by PERK and limitation of protein synthesis are integral parts of the cellular survival mechanisms (131,183), we hypothesized that CO_2 may induce the adaptive UPR. Therefore, we performed knock-down studies of PERK and eIF2α and found a significant increase in the amount of the ER-resident Na,K-ATPase β-subunits after CO_2 treatment, indicating the rescue of protein synthesis and ER overload. Moreover, in line with a

previously published study (93), after long-term hypercapnia treatment, we could not find any alterations in cellular viability or an upregulation of the key proteins involved in apoptotic UPR pathways, such as CHOP and ATF4 (148,155). These findings confirmed our hypothesis that elevated levels of CO_2 induce the adaptive UPR.

4.5 Endoplasmic reticulum protein oxidation and decreased Na,K-ATPase plasma membrane abundance are rescued by treatment with α-ketoglutaric acid

Prior studies have noted the importance of a sufficient mitochondrial function for ATP supply of the ER and thus, normal protein folding (114). It has been shown that treatment with α-ketoglutaric acid (α-KG), a TCA intermediate metabolite, increases ATP production and cell proliferation in CO_2 treated cells (93). Thus, we speculated that the long-term hypercapnia-induced changes in the ER and the subsequent retention of the Na,K-ATPase β-subunit may be consequences of a metabolic dysfunction and inhibition of the TCA cycle.

We evaluated this hypothesis by supplementing alveolar epithelial cells with α-KG during the exposure to hypercapnia. Our studies revealed that the hypercapnia-induced ER oxidation levels and eIF2α phosphorylation were significantly decreased after α-KG treatment. These effects were paralleled by a decreased amount of Na,K-ATPase β-subunit in the ER and increased cell surface abundance and function of the Na,K-ATPase. A possible explanation might be that the α-KG treatment rescued IDH2 activity and ATP production in the setting of sustained hypercapnia, thereby decreasing ER oxidation. However, recent reports suggested that the effects of α-KG are not limited to the TCA cycle, but are also relevant in several metabolic and cellular signaling pathways (223). Moreover, α-KG may function as an energy donor, a co-substrate for dioxygenases, an epigenetic regulator and regulates the activity of prolyl hydroxylases (223,224). These results were complemented by a report indicating that supplementation with α-KG extended the lifespan of *C. elegans* by inhibiting ATP synthase and TOR (225). Thus, although we were able to rescue the adverse hypercapnia-induced effects on the Na,K-ATPase β-subunit in the ER, the precise mechanism by which α-KG impacts the ER homeostasis will need to be further investigated.

4.6 Concluding remarks

Collectively, our study describes novel mechanisms by which hypercapnia regulates the Na,K-ATPase in the alveolar epithelium. We provide evidence that elevated CO_2 levels decrease plasma membrane abundance and function of the Na,K-ATPase by disturbing the maturation of its β-subunit in the ER through two different pathways depending on the duration of the

hypercapnic exposure. Upon short-term exposure, CO_2 causes a rapid degradation of the Na,K-ATPase β-subunit in the ER, whereas upon long-term exposure CO_2 results in the ER retention of oxidized NKA β-subunits and prevents the formation of the functional Na,K-ATPase α:β complex (Figure 4.1). These novel mechanisms of Na,K-ATPase downregulation may contribute to the hypercapnia-induced impairment of alveolar fluid clearance and thus, disruption of the alveolar-capillary barrier. Given that the resolution of alveolar edema is critical for survival of patients with ARDS, specific targeting of these new pathways may provide a novel therapeutic approach in the treatment of patients with hypercapnic respiratory failure.

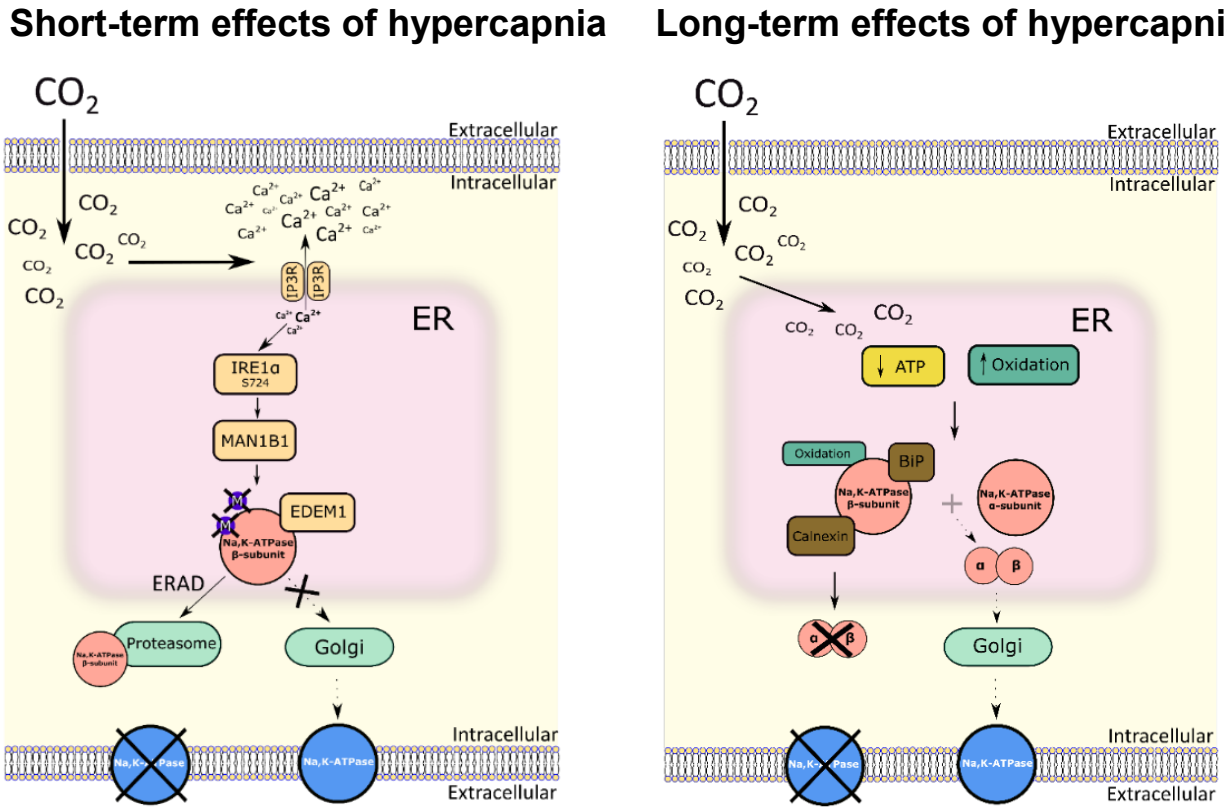

Figure 4.1 Proposed short- and long-term hypercapnic regulation of Na,K-ATPase maturation in the endoplasmic reticulum. (A) Exposure to short-term elevated CO_2 levels depletes the calcium stores of the endoplasmic reticulum by enhancing Ca^{2+} release by IP3R and increasing the intracellular calcium levels. The underlying signaling pathway involves the activation of IRE1α by its phosphorylation at S724 and the subsequent activation of the endoplasmic reticulum associated degradation (ERAD) of the enzyme involving MAN1B1 and EDEM1. A decrease in the high-mannose ER-resident Na,K-ATPase β-subunit forms aggravates the plasma membrane abundance of the transporter. **(B)** Long-term hypercapnia exposure results in the decrease of ATP production and increase in the protein oxidation in the ER and of the Na,K-ATPase β-subunit. Oxidized Na,K-ATPase β-subunits are retained in the ER with the assistance of calnexin and BiP, and cannot be assembled with the Na,K-ATPase α-subunits. An increase in the ER-resident Na,K-ATPase β-subunit prevents normal protein turnover and results in a decreased function of the enzyme at the plasma membrane.

List of tables

List of figures

References

1. Bellani, G., Laffey, J. G., Pham, T., Fan, E., Brochard, L., Esteban, A., Gattinoni, L., van Haren, F., Larsson, A., McAuley, D. F., Ranieri, M., Rubenfeld, G., Thompson, B. T., Wrigge, H., Slutsky, A. S., Pesenti, A., Investigators, L. S., and Group, E. T. (2016) Epidemiology, Patterns of Care, and Mortality for Patients With Acute Respiratory Distress Syndrome in Intensive Care Units in 50 Countries. *JAMA* **315**, 788-800
2. Thompson, B. T., Chambers, R. C., and Liu, K. D. (2017) Acute Respiratory Distress Syndrome. *N Engl J Med* **377**, 562-572
3. Ferguson, N. D., Fan, E., Camporota, L., Antonelli, M., Anzueto, A., Beale, R., Brochard, L., Brower, R., Esteban, A., Gattinoni, L., Rhodes, A., Slutsky, A. S., Vincent, J. L., Rubenfeld, G. D., Thompson, B. T., and Ranieri, V. M. (2012) The Berlin definition of ARDS: an expanded rationale, justification, and supplementary material. *Intensive Care Med* **38**, 1573-1582
4. Matthay, M. A., Zemans, R. L., Zimmerman, G. A., Arabi, Y. M., Beitler, J. R., Mercat, A., Herridge, M., Randolph, A. G., and Calfee, C. S. (2019) Acute respiratory distress syndrome. *Nat Rev Dis Primers* **5**, 18
5. Herold, S., Gabrielli, N. M., and Vadasz, I. (2013) Novel concepts of acute lung injury and alveolar-capillary barrier dysfunction. *Am J Physiol Lung Cell Mol Physiol* **305**, L665-681
6. Han, S., and Mallampalli, R. K. (2015) The acute respiratory distress syndrome: from mechanism to translation. *J Immunol* **194**, 855-860
7. Vadasz, I., and Sznajder, J. I. (2017) Gas Exchange Disturbances Regulate Alveolar Fluid Clearance during Acute Lung Injury. *Front Immunol* **8**, 757
8. Beitler, J. R., Malhotra, A., and Thompson, B. T. (2016) Ventilator-induced Lung Injury. *Clin Chest Med* **37**, 633-646
9. Spadaro, S., Park, M., Turrini, C., Tunstall, T., Thwaites, R., Mauri, T., Ragazzi, R., Ruggeri, P., Hansel, T. T., Caramori, G., and Volta, C. A. (2019) Biomarkers for Acute Respiratory Distress syndrome and prospects for personalised medicine. *J Inflamm (Lond)* **16**, 1
10. Calfee, C. S., Delucchi, K., Parsons, P. E., Thompson, B. T., Ware, L. B., Matthay, M. A., and Network, N. A. (2014) Subphenotypes in acute respiratory distress syndrome: latent class analysis of data from two randomised controlled trials. *Lancet Respir Med* **2**, 611-620

11. Famous, K. R., Delucchi, K., Ware, L. B., Kangelaris, K. N., Liu, K. D., Thompson, B. T., Calfee, C. S., and Network, A. (2017) Acute Respiratory Distress Syndrome Subphenotypes Respond Differently to Randomized Fluid Management Strategy. *Am J Respir Crit Care Med* **195**, 331-338
12. Calfee, C. S., Delucchi, K. L., Sinha, P., Matthay, M. A., Hackett, J., Shankar-Hari, M., McDowell, C., Laffey, J. G., O'Kane, C. M., McAuley, D. F., and Irish Critical Care Trials, G. (2018) Acute respiratory distress syndrome subphenotypes and differential response to simvastatin: secondary analysis of a randomised controlled trial. *Lancet Respir Med* **6**, 691-698
13. Mutlu, G. M., Dumasius, V., Burhop, J., McShane, P. J., Meng, F. J., Welch, L., Dumasius, A., Mohebahmadi, N., Thakuria, G., Hardiman, K., Matalon, S., Hollenberg, S., and Factor, P. (2004) Upregulation of alveolar epithelial active Na+ transport is dependent on beta2-adrenergic receptor signaling. *Circ Res* **94**, 1091-1100
14. Sznajder, J. I. (2001) Alveolar edema must be cleared for the acute respiratory distress syndrome patient to survive. *Am J Respir Crit Care Med* **163**, 1293-1294
15. Shyamsundar, M., McAuley, D. F., Ingram, R. J., Gibson, D. S., O'Kane, D., McKeown, S. T., Edwards, A., Taggart, C., Elborn, J. S., Calfee, C. S., Matthay, M. A., and O'Kane, C. M. (2014) Keratinocyte growth factor promotes epithelial survival and resolution in a human model of lung injury. *Am J Respir Crit Care Med* **189**, 1520-1529
16. Budinger, G. R., and Mutlu, G. M. (2014) beta2-agonists and acute respiratory distress syndrome. *Am J Respir Crit Care Med* **189**, 624-625
17. Guerin, C., Reignier, J., Richard, J. C., Beuret, P., Gacouin, A., Boulain, T., Mercier, E., Badet, M., Mercat, A., Baudin, O., Clavel, M., Chatellier, D., Jaber, S., Rosselli, S., Mancebo, J., Sirodot, M., Hilbert, G., Bengler, C., Richecoeur, J., Gainnier, M., Bayle, F., Bourdin, G., Leray, V., Girard, R., Baboi, L., Ayzac, L., and Group, P. S. (2013) Prone positioning in severe acute respiratory distress syndrome. *N Engl J Med* **368**, 2159-2168
18. National Heart, L., Blood Institute Acute Respiratory Distress Syndrome Clinical Trials, N., Wiedemann, H. P., Wheeler, A. P., Bernard, G. R., Thompson, B. T., Hayden, D., deBoisblanc, B., Connors, A. F., Jr., Hite, R. D., and Harabin, A. L. (2006) Comparison of two fluid-management strategies in acute lung injury. *N Engl J Med* **354**, 2564-2575
19. Guo, L., Xie, J., Huang, Y., Pan, C., Yang, Y., Qiu, H., and Liu, L. (2018) Higher PEEP improves outcomes in ARDS patients with clinically objective positive oxygenation response to PEEP: a systematic review and meta-analysis. *BMC Anesthesiol* **18**, 172

20. Acute Respiratory Distress Syndrome, N., Brower, R. G., Matthay, M. A., Morris, A., Schoenfeld, D., Thompson, B. T., and Wheeler, A. (2000) Ventilation with lower tidal volumes as compared with traditional tidal volumes for acute lung injury and the acute respiratory distress syndrome. *N Engl J Med* **342**, 1301-1308
21. Vadasz, I., Hubmayr, R. D., Nin, N., Sporn, P. H., and Sznajder, J. I. (2012) Hypercapnia: a nonpermissive environment for the lung. *Am J Respir Cell Mol Biol* **46**, 417-421
22. Bhattacharya, J., and Matthay, M. A. (2013) Regulation and repair of the alveolar-capillary barrier in acute lung injury. *Annu Rev Physiol* **75**, 593-615
23. Wang, Y., Tang, Z., Huang, H., Li, J., Wang, Z., Yu, Y., Zhang, C., Li, J., Dai, H., Wang, F., Cai, T., and Tang, N. (2018) Pulmonary alveolar type I cell population consists of two distinct subtypes that differ in cell fate. *Proc Natl Acad Sci U S A* **115**, 2407-2412
24. Huppert, L. A., and Matthay, M. A. (2017) Alveolar Fluid Clearance in Pathologically Relevant Conditions: In Vitro and In Vivo Models of Acute Respiratory Distress Syndrome. *Front Immunol* **8**, 371
25. Johnson, M. D., Widdicombe, J. H., Allen, L., Barbry, P., and Dobbs, L. G. (2002) Alveolar epithelial type I cells contain transport proteins and transport sodium, supporting an active role for type I cells in regulation of lung liquid homeostasis. *Proc Natl Acad Sci U S A* **99**, 1966-1971
26. Ware, L. B., and Matthay, M. A. (2005) Clinical practice. Acute pulmonary edema. *N Engl J Med* **353**, 2788-2796
27. Matthay, M. A., Folkesson, H. G., and Clerici, C. (2002) Lung epithelial fluid transport and the resolution of pulmonary edema. *Physiol Rev* **82**, 569-600
28. Matalon, S., Bartoszewski, R., and Collawn, J. F. (2015) Role of epithelial sodium channels in the regulation of lung fluid homeostasis. *Am J Physiol Lung Cell Mol Physiol* **309**, L1229-1238
29. Clausen, M. V., Hilbers, F., and Poulsen, H. (2017) The Structure and Function of the Na,K-ATPase Isoforms in Health and Disease. *Front Physiol* **8**, 371
30. Kaplan, J. H. (2002) Biochemistry of Na,K-ATPase. *Annu Rev Biochem* **71**, 511-535
31. Wieser, W., and Krumschnabel, G. (2001) Hierarchies of ATP-consuming processes: direct compared with indirect measurements, and comparative aspects. *Biochem J* **355**, 389-395

32. Tokhtaeva, E., Sun, H., Deiss-Yehiely, N., Wen, Y., Soni, P. N., Gabrielli, N. M., Marcus, E. A., Ridge, K. M., Sachs, G., Vazquez-Levin, M., Sznajder, J. I., Vagin, O., and Dada, L. A. (2016) The O-glycosylated ectodomain of FXYD5 impairs adhesion by disrupting cell-cell trans-dimerization of Na,K-ATPase beta1 subunits. *J Cell Sci* **129**, 2394-2406

33. Wujak, L. A., Blume, A., Baloglu, E., Wygrecka, M., Wygowski, J., Herold, S., Mayer, K., Vadasz, I., Besuch, P., Mairbaurl, H., Seeger, W., and Morty, R. E. (2016) FXYD1 negatively regulates Na(+)/K(+)-ATPase activity in lung alveolar epithelial cells. *Respir Physiol Neurobiol* **220**, 54-61

34. Vagin, O., Dada, L. A., Tokhtaeva, E., and Sachs, G. (2012) The Na-K-ATPase alpha(1)beta(1) heterodimer as a cell adhesion molecule in epithelia. *Am J Physiol Cell Physiol* **302**, C1271-1281

35. Lecuona, E., Trejo, H. E., and Sznajder, J. I. (2007) Regulation of Na,K-ATPase during acute lung injury. *J Bioenerg Biomembr* **39**, 391-395

36. Geering, K. (2008) Functional roles of Na,K-ATPase subunits. *Curr Opin Nephrol Hypertens* **17**, 526-532

37. Tokhtaeva, E., Sachs, G., Souda, P., Bassilian, S., Whitelegge, J. P., Shoshani, L., and Vagin, O. (2011) Epithelial junctions depend on intercellular trans-interactions between the Na,K-ATPase beta(1) subunits. *J Biol Chem* **286**, 25801-25812

38. Rajasekaran, S. A., Palmer, L. G., Quan, K., Harper, J. F., Ball, W. J., Jr., Bander, N. H., Peralta Soler, A., and Rajasekaran, A. K. (2001) Na,K-ATPase beta-subunit is required for epithelial polarization, suppression of invasion, and cell motility. *Mol Biol Cell* **12**, 279-295

39. Rajasekaran, S. A., Barwe, S. P., and Rajasekaran, A. K. (2005) Multiple functions of Na,K-ATPase in epithelial cells. *Semin Nephrol* **25**, 328-334

40. Cereijido, M., Contreras, R. G., Shoshani, L., and Larre, I. (2012) The Na+-K+-ATPase as self-adhesion molecule and hormone receptor. *Am J Physiol Cell Physiol* **302**, C473-481

41. Rajasekaran, S. A., Barwe, S. P., Gopal, J., Ryazantsev, S., Schneeberger, E. E., and Rajasekaran, A. K. (2007) Na-K-ATPase regulates tight junction permeability through occludin phosphorylation in pancreatic epithelial cells. *Am J Physiol Gastrointest Liver Physiol* **292**, G124-133

42. Tokhtaeva, E., Sachs, G., Sun, H., Dada, L. A., Sznajder, J. I., and Vagin, O. (2012) Identification of the amino acid region involved in the intercellular interaction between the beta1 subunits of Na+/K+ -ATPase. *J Cell Sci* **125**, 1605-1616

43. Vagin, O., Tokhtaeva, E., Yakubov, I., Shevchenko, E., and Sachs, G. (2008) Inverse correlation between the extent of N-glycan branching and intercellular adhesion in epithelia. Contribution of the Na,K-ATPase beta1 subunit. *J Biol Chem* **283**, 2192-2202

44. Flodby, P., Kim, Y. H., Beard, L. L., Gao, D., Ji, Y., Kage, H., Liebler, J. M., Minoo, P., Kim, K. J., Borok, Z., and Crandall, E. D. (2016) Knockout Mice Reveal a Major Role for Alveolar Epithelial Type I Cells in Alveolar Fluid Clearance. *Am J Respir Cell Mol Biol* **55**, 395-406

45. Tokhtaeva, E., Sachs, G., and Vagin, O. (2009) Assembly with the Na,K-ATPase alpha(1) subunit is required for export of beta(1) and beta(2) subunits from the endoplasmic reticulum. *Biochemistry* **48**, 11421-11431

46. Li, Z., and Langhans, S. A. (2015) Transcriptional regulators of Na,K-ATPase subunits. *Front Cell Dev Biol* **3**, 66

47. Vadasz, I., Raviv, S., and Sznajder, J. I. (2007) Alveolar epithelium and Na,K-ATPase in acute lung injury. *Intensive Care Med* **33**, 1243-1251

48. Lecuona, E., Sun, H., Vohwinkel, C., Ciechanover, A., and Sznajder, J. I. (2009) Ubiquitination participates in the lysosomal degradation of Na,K-ATPase in steady-state conditions. *Am J Respir Cell Mol Biol* **41**, 671-679

49. Gusarova, G. A., Dada, L. A., Kelly, A. M., Brodie, C., Witters, L. A., Chandel, N. S., and Sznajder, J. I. (2009) Alpha1-AMP-activated protein kinase regulates hypoxia-induced Na,K-ATPase endocytosis via direct phosphorylation of protein kinase C zeta. *Mol Cell Biol* **29**, 3455-3464

50. Dada, L. A., Chandel, N. S., Ridge, K. M., Pedemonte, C., Bertorello, A. M., and Sznajder, J. I. (2003) Hypoxia-induced endocytosis of Na,K-ATPase in alveolar epithelial cells is mediated by mitochondrial reactive oxygen species and PKC-zeta. *J Clin Invest* **111**, 1057-1064

51. Vadasz, I., Dada, L. A., Briva, A., Trejo, H. E., Welch, L. C., Chen, J., Toth, P. T., Lecuona, E., Witters, L. A., Schumacker, P. T., Chandel, N. S., Seeger, W., and Sznajder, J. I. (2008) AMP-activated protein kinase regulates CO2-induced alveolar epithelial dysfunction in rats and human cells by promoting Na,K-ATPase endocytosis. *J Clin Invest* **118**, 752-762

52. Helenius, I. T., Dada, L. A., and Sznajder, J. I. (2010) Role of ubiquitination in Na,K-ATPase regulation during lung injury. *Proc Am Thorac Soc* **7**, 65-70

53. Vadasz, I., Weiss, C. H., and Sznajder, J. I. (2012) Ubiquitination and proteolysis in acute lung injury. *Chest* **141**, 763-771

54. Magnani, N. D., Dada, L. A., and Sznajder, J. I. (2018) Ubiquitin-proteasome signaling in lung injury. *Transl Res* **198**, 29-39

55. Sznajder, J. I., Factor, P., and Ingbar, D. H. (2002) Invited review: lung edema clearance: role of Na(+)-K(+)-ATPase. *J Appl Physiol (1985)* **93**, 1860-1866

56. Tokhtaeva, E., Sachs, G., and Vagin, O. (2010) Diverse pathways for maturation of the Na,K-ATPase beta1 and beta2 subunits in the endoplasmic reticulum of Madin-Darby canine kidney cells. *J Biol Chem* **285**, 39289-39302

57. Selvakumar, P., Owens, T. A., David, J. M., Petrelli, N. J., Christensen, B. C., Lakshmikuttyamma, A., and Rajasekaran, A. K. (2014) Epigenetic silencing of Na,K-ATPase beta 1 subunit gene ATP1B1 by methylation in clear cell renal cell carcinoma. *Epigenetics* **9**, 579-586

58. Rajasekaran, S. A., Gopal, J., Willis, D., Espineda, C., Twiss, J. L., and Rajasekaran, A. K. (2004) Na,K-ATPase beta1-subunit increases the translation efficiency of the alpha1-subunit in MSV-MDCK cells. *Mol Biol Cell* **15**, 3224-3232

59. Hilbers, F., Kopec, W., Isaksen, T. J., Holm, T. H., Lykke-Hartmann, K., Nissen, P., Khandelia, H., and Poulsen, H. (2016) Tuning of the Na,K-ATPase by the beta subunit. *Sci Rep* **6**, 20442

60. Paula, S., Tabet, M. R., and Ball, W. J., Jr. (2005) Interactions between cardiac glycosides and sodium/potassium-ATPase: three-dimensional structure-activity relationship models for ligand binding to the E2-Pi form of the enzyme versus activity inhibition. *Biochemistry* **44**, 498-510

61. Vilchis-Nestor, C. A., Roldan, M. L., Leonardi, A., Navea, J. G., Padilla-Benavides, T., and Shoshani, L. (2019) Ouabain Enhances Cell-Cell Adhesion Mediated by beta1 Subunits of the Na(+),K(+)-ATPase in CHO Fibroblasts. *Int J Mol Sci* **20**

62. Larre, I., Lazaro, A., Contreras, R. G., Balda, M. S., Matter, K., Flores-Maldonado, C., Ponce, A., Flores-Benitez, D., Rincon-Heredia, R., Padilla-Benavides, T., Castillo, A., Shoshani, L., and Cereijido, M. (2010) Ouabain modulates epithelial cell tight junction. *Proc Natl Acad Sci U S A* **107**, 11387-11392

63. Nin, N., Angulo, M., and Briva, A. (2018) Effects of hypercapnia in acute respiratory distress syndrome. *Ann Transl Med* **6**, 37

64. Radermacher, P., Maggiore, S. M., and Mercat, A. (2017) Fifty Years of Research in ARDS. Gas Exchange in Acute Respiratory Distress Syndrome. *Am J Respir Crit Care Med* **196**, 964-984

65. Cummins, E. P., Strowitzki, M. J., and Taylor, C. T. (2019) Mechanisms and consequences of oxygen- and carbon dioxide-sensing in mammals. *Physiol Rev*

66. Shigemura, M., Lecuona, E., and Sznajder, J. I. (2017) Effects of hypercapnia on the lung. *J Physiol* **595**, 2431-2437

67. Putnam, R. W., Filosa, J. A., and Ritucci, N. A. (2004) Cellular mechanisms involved in CO(2) and acid signaling in chemosensitive neurons. *Am J Physiol Cell Physiol* **287**, C1493-1526

68. Chen, J., Lecuona, E., Briva, A., Welch, L. C., and Sznajder, J. I. (2008) Carbonic anhydrase II and alveolar fluid reabsorption during hypercapnia. *Am J Respir Cell Mol Biol* **38**, 32-37

69. Briva, A., Vadasz, I., Lecuona, E., Welch, L. C., Chen, J., Dada, L. A., Trejo, H. E., Dumasius, V., Azzam, Z. S., Myrianthefs, P. M., Batlle, D., Gruenbaum, Y., and Sznajder, J. I. (2007) High CO2 levels impair alveolar epithelial function independently of pH. *PLoS One* **2**, e1238

70. Endeward, V., Al-Samir, S., Itel, F., and Gros, G. (2014) How does carbon dioxide permeate cell membranes? A discussion of concepts, results and methods. *Front Physiol* **4**, 382

71. Boron, W. F., Endeward, V., Gros, G., Musa-Aziz, R., and Pohl, P. (2011) Intrinsic CO2 permeability of cell membranes and potential biological relevance of CO2 channels. *Chemphyschem* **12**, 1017-1019

72. Musa-Aziz, R., Chen, L. M., Pelletier, M. F., and Boron, W. F. (2009) Relative CO2/NH3 selectivities of AQP1, AQP4, AQP5, AmtB, and RhAG. *Proc Natl Acad Sci U S A* **106**, 5406-5411

73. Tresguerres, M., Buck, J., and Levin, L. R. (2010) Physiological carbon dioxide, bicarbonate, and pH sensing. *Pflugers Arch* **460**, 953-964

74. Cummins, E. P., Selfridge, A. C., Sporn, P. H., Sznajder, J. I., and Taylor, C. T. (2014) Carbon dioxide-sensing in organisms and its implications for human disease. *Cell Mol Life Sci* **71**, 831-845

75. Zhou, Y., Skelton, L. A., Xu, L., Chandler, M. P., Berthiaume, J. M., and Boron, W. F. (2016) Role of Receptor Protein Tyrosine Phosphatase gamma in Sensing Extracellular CO2 and HCO3. *J Am Soc Nephrol* **27**, 2616-2621

76. Shigemura, M., Lecuona, E., Angulo, M., Homma, T., Rodriguez, D. A., Gonzalez-Gonzalez, F. J., Welch, L. C., Amarelle, L., Kim, S. J., Kaminski, N., Budinger, G. R. S., Solway, J., and Sznajder, J. I. (2018) Hypercapnia increases airway smooth muscle contractility via caspase-7-mediated miR-133a-RhoA signaling. *Sci Transl Med* **10**

77. Vadasz, I., Dada, L. A., Briva, A., Helenius, I. T., Sharabi, K., Welch, L. C., Kelly, A. M., Grzesik, B. A., Budinger, G. R., Liu, J., Seeger, W., Beitel, G. J., Gruenbaum, Y., and Sznajder, J. I. (2012) Evolutionary conserved role of c-Jun-N-terminal kinase in CO2-induced epithelial dysfunction. *PLoS One* **7**, e46696

78. Dada, L. A., Trejo Bittar, H. E., Welch, L. C., Vagin, O., Deiss-Yehiely, N., Kelly, A. M., Baker, M. R., Capri, J., Cohn, W., Whitelegge, J. P., Vadasz, I., Gruenbaum, Y., and Sznajder, J. I. (2015) High CO2 Leads to Na,K-ATPase Endocytosis via c-Jun Amino-Terminal Kinase-Induced LMO7b Phosphorylation. *Mol Cell Biol* **35**, 3962-3973

79. Welch, L. C., Lecuona, E., Briva, A., Trejo, H. E., Dada, L. A., and Sznajder, J. I. (2010) Extracellular signal-regulated kinase (ERK) participates in the hypercapnia-induced Na,K-ATPase downregulation. *FEBS Lett* **584**, 3985-3989

80. Linthwaite, V. L., Janus, J. M., Brown, A. P., Wong-Pascua, D., O'Donoghue, A. C., Porter, A., Treumann, A., Hodgson, D. R. W., and Cann, M. J. (2018) The identification of carbon dioxide mediated protein post-translational modifications. *Nat Commun* **9**, 3092

81. Meigh, L., Greenhalgh, S. A., Rodgers, T. L., Cann, M. J., Roper, D. I., and Dale, N. (2013) CO(2)directly modulates connexin 26 by formation of carbamate bridges between subunits. *Elife* **2**, e01213

82. Contreras, M., Masterson, C., and Laffey, J. G. (2015) Permissive hypercapnia: what to remember. *Curr Opin Anaesthesiol* **28**, 26-37

83. Roberts, B. W., Mohr, N. M., Ablordeppey, E., Drewry, A. M., Ferguson, I. T., Trzeciak, S., Kollef, M. H., and Fuller, B. M. (2018) Association Between Partial Pressure of Arterial Carbon Dioxide and Survival to Hospital Discharge Among Patients Diagnosed With Sepsis in the Emergency Department. *Crit Care Med* **46**, e213-e220

84. Fuller, B. M., Mohr, N. M., Drewry, A. M., Ferguson, I. T., Trzeciak, S., Kollef, M. H., and Roberts, B. W. (2017) Partial pressure of arterial carbon dioxide and survival to hospital discharge among patients requiring acute mechanical ventilation: A cohort study. *J Crit Care* **41**, 29-35

85. Contreras, M., Ansari, B., Curley, G., Higgins, B. D., Hassett, P., O'Toole, D., and Laffey, J. G. (2012) Hypercapnic acidosis attenuates ventilation-induced lung injury by a nuclear factor-kappaB-dependent mechanism. *Crit Care Med* **40**, 2622-2630

86. Lu, Z., Casalino-Matsuda, S. M., Nair, A., Buchbinder, A., Budinger, G. R. S., Sporn, P. H. S., and Gates, K. L. (2018) A role for heat shock factor 1 in hypercapnia-induced inhibition of inflammatory cytokine expression. *FASEB J* **32**, 3614-3622

87. Nin, N., Muriel, A., Penuelas, O., Brochard, L., Lorente, J. A., Ferguson, N. D., Raymondos, K., Rios, F., Violi, D. A., Thille, A. W., Gonzalez, M., Villagomez, A. J., Hurtado, J., Davies, A. R., Du, B., Maggiore, S. M., Soto, L., D'Empaire, G., Matamis, D., Abroug, F., Moreno, R. P., Soares, M. A., Arabi, Y., Sandi, F., Jibaja, M., Amin, P., Koh, Y., Kuiper, M. A., Bulow, H. H., Zeggwagh, A. A., Anzueto, A., Sznajder, J. I., Esteban, A., and Group, V. (2017) Severe hypercapnia and outcome of mechanically ventilated patients with moderate or severe acute respiratory distress syndrome. *Intensive Care Med* **43**, 200-208

88. Casalino-Matsuda, S. M., Nair, A., Beitel, G. J., Gates, K. L., and Sporn, P. H. (2015) Hypercapnia Inhibits Autophagy and Bacterial Killing in Human Macrophages by Increasing Expression of Bcl-2 and Bcl-xL. *J Immunol* **194**, 5388-5396

89. Gates, K. L., Howell, H. A., Nair, A., Vohwinkel, C. U., Welch, L. C., Beitel, G. J., Hauser, A. R., Sznajder, J. I., and Sporn, P. H. (2013) Hypercapnia impairs lung neutrophil function and increases mortality in murine pseudomonas pneumonia. *Am J Respir Cell Mol Biol* **49**, 821-828

90. Wang, N., Gates, K. L., Trejo, H., Favoreto, S., Jr., Schleimer, R. P., Sznajder, J. I., Beitel, G. J., and Sporn, P. H. (2010) Elevated CO2 selectively inhibits interleukin-6 and tumor necrosis factor expression and decreases phagocytosis in the macrophage. *FASEB J* **24**, 2178-2190

91. Kikuchi, R., Tsuji, T., Watanabe, O., Yamaguchi, K., Furukawa, K., Nakamura, H., and Aoshiba, K. (2017) Hypercapnia Accelerates Adipogenesis: A Novel Role of High CO2 in Exacerbating Obesity. *Am J Respir Cell Mol Biol* **57**, 570-580

92. Casalino-Matsuda, S. M., Wang, N., Ruhoff, P. T., Matsuda, H., Nlend, M. C., Nair, A., Szleifer, I., Beitel, G. J., Sznajder, J. I., and Sporn, P. H. S. (2018) Hypercapnia Alters Expression of Immune Response, Nucleosome Assembly and Lipid Metabolism Genes in Differentiated Human Bronchial Epithelial Cells. *Sci Rep* **8**, 13508

93. Vohwinkel, C. U., Lecuona, E., Sun, H., Sommer, N., Vadasz, I., Chandel, N. S., and Sznajder, J. I. (2011) Elevated CO(2) levels cause mitochondrial dysfunction and impair cell proliferation. *J Biol Chem* **286**, 37067-37076

94. Tiruvoipati, R., Pilcher, D., Buscher, H., Botha, J., and Bailey, M. (2017) Effects of Hypercapnia and Hypercapnic Acidosis on Hospital Mortality in Mechanically Ventilated Patients. *Crit Care Med* **45**, e649-e656

95. Jaitovich, A., Angulo, M., Lecuona, E., Dada, L. A., Welch, L. C., Cheng, Y., Gusarova, G., Ceco, E., Liu, C., Shigemura, M., Barreiro, E., Patterson, C., Nader, G. A., and Sznajder, J. I. (2015) High CO2 levels cause skeletal muscle atrophy via AMP-activated kinase (AMPK), FoxO3a protein, and muscle-specific Ring finger protein 1 (MuRF1). *J Biol Chem* **290**, 9183-9194

96. Korponay, T. C., Balnis, J., Vincent, C. E., Singer, D. V., Chopra, A., Adam, A. P., Ginnan, R., Singer, H. A., and Jaitovich, A. (2019) High CO2 downregulates skeletal muscle protein anabolism via AMPKalpha2-mediated depressed ribosomal biogenesis. *Am J Respir Cell Mol Biol*

97. Yang, H., Xiang, P., Zhang, E., Guo, W., Shi, Y., Zhang, S., and Tong, Z. (2015) Is hypercapnia associated with poor prognosis in chronic obstructive pulmonary disease? A long-term follow-up cohort study. *BMJ Open* **5**, e008909

98. Gwozdzinska, P., Buchbinder, B. A., Mayer, K., Herold, S., Morty, R. E., Seeger, W., and Vadasz, I. (2017) Hypercapnia Impairs ENaC Cell Surface Stability by Promoting Phosphorylation, Polyubiquitination and Endocytosis of beta-ENaC in a Human Alveolar Epithelial Cell Line. *Front Immunol* **8**, 591

99. Lecuona, E., Sun, H., Chen, J., Trejo, H. E., Baker, M. A., and Sznajder, J. I. (2013) Protein kinase A-Ialpha regulates Na,K-ATPase endocytosis in alveolar epithelial cells exposed to high CO(2) concentrations. *Am J Respir Cell Mol Biol* **48**, 626-634

100. Turner, M. J., Saint-Criq, V., Patel, W., Ibrahim, S. H., Verdon, B., Ward, C., Garnett, J. P., Tarran, R., Cann, M. J., and Gray, M. A. (2016) Hypercapnia modulates cAMP signalling and cystic fibrosis transmembrane conductance regulator-dependent anion and fluid secretion in airway epithelia. *J Physiol* **594**, 1643-1661

101. Vagin, O., Kraut, J. A., and Sachs, G. (2009) Role of N-glycosylation in trafficking of apical membrane proteins in epithelia. *Am J Physiol Renal Physiol* **296**, F459-469

102. Brodsky, J. L., and Skach, W. R. (2011) Protein folding and quality control in the endoplasmic reticulum: Recent lessons from yeast and mammalian cell systems. *Curr Opin Cell Biol* **23**, 464-475

103. Hetz, C., Chevet, E., and Oakes, S. A. (2015) Proteostasis control by the unfolded protein response. *Nat Cell Biol* **17**, 829-838

104. Schwarz, D. S., and Blower, M. D. (2016) The endoplasmic reticulum: structure, function and response to cellular signaling. *Cell Mol Life Sci* **73**, 79-94

105. Alberts, B. (2015) *Molecular biology of the cell*, Sixth edition. ed., Garland Science, Taylor and Francis Group, New York, NY

106. Ellgaard, L., and Helenius, A. (2003) Quality control in the endoplasmic reticulum. *Nat Rev Mol Cell Biol* **4**, 181-191

107. Ellgaard, L., Sevier, C. S., and Bulleid, N. J. (2018) How Are Proteins Reduced in the Endoplasmic Reticulum? *Trends Biochem Sci* **43**, 32-43

108. Halperin, L., Jung, J., and Michalak, M. (2014) The many functions of the endoplasmic reticulum chaperones and folding enzymes. *IUBMB Life* **66**, 318-326

109. Aebi, M. (2013) N-linked protein glycosylation in the ER. *Biochim Biophys Acta* **1833**, 2430-2437

110. Gupta, G. S. (2012) Lectins in Quality Control: Calnexin and Calreticulin. in *Animal Lectins: Form, Function and Clinical Applications*. pp 29-56

111. Hebert, D. N., and Molinari, M. (2007) In and out of the ER: protein folding, quality control, degradation, and related human diseases. *Physiol Rev* **87**, 1377-1408

112. Wang, M., and Kaufman, R. J. (2016) Protein misfolding in the endoplasmic reticulum as a conduit to human disease. *Nature* **529**, 326-335

113. Tannous, A., Pisoni, G. B., Hebert, D. N., and Molinari, M. (2015) N-linked sugar-regulated protein folding and quality control in the ER. *Semin Cell Dev Biol* **41**, 79-89

114. Araki, K., and Nagata, K. (2011) Protein folding and quality control in the ER. *Cold Spring Harb Perspect Biol* **3**, a007526

115. Molinari, M., Calanca, V., Galli, C., Lucca, P., and Paganetti, P. (2003) Role of EDEM in the release of misfolded glycoproteins from the calnexin cycle. *Science* **299**, 1397-1400

116. Jager, R., Bertrand, M. J., Gorman, A. M., Vandenabeele, P., and Samali, A. (2012) The unfolded protein response at the crossroads of cellular life and death during endoplasmic reticulum stress. *Biol Cell* **104**, 259-270

117. Bagur, R., and Hajnoczky, G. (2017) Intracellular Ca(2+) Sensing: Its Role in Calcium Homeostasis and Signaling. *Mol Cell* **66**, 780-788

118. Krebs, J., Agellon, L. B., and Michalak, M. (2015) Ca(2+) homeostasis and endoplasmic reticulum (ER) stress: An integrated view of calcium signaling. *Biochem Biophys Res Commun* **460**, 114-121

119. Almanza, A., Carlesso, A., Chintha, C., Creedican, S., Doultsinos, D., Leuzzi, B., Luis, A., McCarthy, N., Montibeller, L., More, S., Papaioannou, A., Puschel, F., Sassano, M. L., Skoko, J., Agostinis, P., de Belleroche, J., Eriksson, L. A., Fulda, S., Gorman, A. M., Healy, S., Kozlov, A., Munoz-Pinedo, C., Rehm, M., Chevet, E., and Samali, A. (2019) Endoplasmic reticulum stress signalling - from basic mechanisms to clinical applications. *FEBS J* **286**, 241-278

120. Depaoli, M. R., Hay, J. C., Graier, W. F., and Malli, R. (2019) The enigmatic ATP supply of the endoplasmic reticulum. *Biol Rev Camb Philos Soc* **94**, 610-628

121. Dalle-Donne, I., Aldini, G., Carini, M., Colombo, R., Rossi, R., and Milzani, A. (2006) Protein carbonylation, cellular dysfunction, and disease progression. *J Cell Mol Med* **10**, 389-406

122. England, K., and Cotter, T. (2004) Identification of carbonylated proteins by MALDI-TOF mass spectroscopy reveals susceptibility of ER. *Biochem Biophys Res Commun* **320**, 123-130

123. Rabek, J. P., Boylston, W. H., 3rd, and Papaconstantinou, J. (2003) Carbonylation of ER chaperone proteins in aged mouse liver. *Biochem Biophys Res Commun* **305**, 566-572

124. Vishnu, N., Jadoon Khan, M., Karsten, F., Groschner, L. N., Waldeck-Weiermair, M., Rost, R., Hallstrom, S., Imamura, H., Graier, W. F., and Malli, R. (2014) ATP increases within the lumen of the endoplasmic reticulum upon intracellular Ca2+ release. *Mol Biol Cell* **25**, 368-379

125. Li, G., Mongillo, M., Chin, K. T., Harding, H., Ron, D., Marks, A. R., and Tabas, I. (2009) Role of ERO1-alpha-mediated stimulation of inositol 1,4,5-triphosphate receptor activity in endoplasmic reticulum stress-induced apoptosis. *J Cell Biol* **186**, 783-792

126. Vagin, O., Turdikulova, S., and Tokhtaeva, E. (2007) Polarized membrane distribution of potassium-dependent ion pumps in epithelial cells: different roles of the N-glycans of their beta subunits. *Cell Biochem Biophys* **47**, 376-391

127. Tokhtaeva, E., Munson, K., Sachs, G., and Vagin, O. (2010) N-glycan-dependent quality control of the Na,K-ATPase beta(2) subunit. *Biochemistry* **49**, 3116-3128

128. Samali, A., Fitzgerald, U., Deegan, S., and Gupta, S. (2010) Methods for monitoring endoplasmic reticulum stress and the unfolded protein response. *Int J Cell Biol* **2010**, 830307

129. Sano, R., and Reed, J. C. (2013) ER stress-induced cell death mechanisms. *Biochim Biophys Acta* **1833**, 3460-3470

130. Bergmann, T. J., Fregno, I., Fumagalli, F., Rinaldi, A., Bertoni, F., Boersema, P. J., Picotti, P., and Molinari, M. (2018) Chemical stresses fail to mimic the unfolded protein response resulting from luminal load with unfolded polypeptides. *J Biol Chem* **293**, 5600-5612

131. Han, J., Back, S. H., Hur, J., Lin, Y. H., Gildersleeve, R., Shan, J., Yuan, C. L., Krokowski, D., Wang, S., Hatzoglou, M., Kilberg, M. S., Sartor, M. A., and Kaufman, R. J. (2013) ER-stress-induced transcriptional regulation increases protein synthesis leading to cell death. *Nat Cell Biol* **15**, 481-490

132. Hetz, C., Chevet, E., and Harding, H. P. (2013) Targeting the unfolded protein response in disease. *Nat Rev Drug Discov* **12**, 703-719

133. Marciniak, S. J. (2017) Endoplasmic reticulum stress in lung disease. *Eur Respir Rev* **26**

134. Frakes, A. E., and Dillin, A. (2017) The UPR(ER): Sensor and Coordinator of Organismal Homeostasis. *Mol Cell* **66**, 761-771

135. Kim, S. R., Kim, D. I., Kang, M. R., Lee, K. S., Park, S. Y., Jeong, J. S., and Lee, Y. C. (2013) Endoplasmic reticulum stress influences bronchial asthma pathogenesis by modulating nuclear factor kappaB activation. *J Allergy Clin Immunol* **132**, 1397-1408

136. Korfei, M., Ruppert, C., Mahavadi, P., Henneke, I., Markart, P., Koch, M., Lang, G., Fink, L., Bohle, R. M., Seeger, W., Weaver, T. E., and Guenther, A. (2008) Epithelial endoplasmic reticulum stress and apoptosis in sporadic idiopathic pulmonary fibrosis. *Am J Respir Crit Care Med* **178**, 838-846

137. Adams, C. J., Kopp, M. C., Larburu, N., Nowak, P. R., and Ali, M. M. U. (2019) Structure and Molecular Mechanism of ER Stress Signaling by the Unfolded Protein Response Signal Activator IRE1. *Front Mol Biosci* **6**, 11

138. Tabas, I., and Ron, D. (2011) Integrating the mechanisms of apoptosis induced by endoplasmic reticulum stress. *Nat Cell Biol* **13**, 184-190

139. Bergmann, T. J., and Molinari, M. (2018) Three branches to rule them all? UPR signalling in response to chemically versus misfolded proteins-induced ER stress. *Biol Cell* **110**, 197-204

140. Raina, K., Noblin, D. J., Serebrenik, Y. V., Adams, A., Zhao, C., and Crews, C. M. (2014) Targeted protein destabilization reveals an estrogen-mediated ER stress response. *Nat Chem Biol* **10**, 957-962

141. Dong, L., Krewson, E. A., and Yang, L. V. (2017) Acidosis Activates Endoplasmic Reticulum Stress Pathways through GPR4 in Human Vascular Endothelial Cells. *Int J Mol Sci* **18**

142. Koumenis, C., Naczki, C., Koritzinsky, M., Rastani, S., Diehl, A., Sonenberg, N., Koromilas, A., and Wouters, B. G. (2002) Regulation of protein synthesis by hypoxia via activation of the endoplasmic reticulum kinase PERK and phosphorylation of the translation initiation factor eIF2alpha. *Mol Cell Biol* **22**, 7405-7416

143. Wang, S., and Kaufman, R. J. (2012) The impact of the unfolded protein response on human disease. *J Cell Biol* **197**, 857-867

144. Hiramatsu, N., Chiang, W. C., Kurt, T. D., Sigurdson, C. J., and Lin, J. H. (2015) Multiple Mechanisms of Unfolded Protein Response-Induced Cell Death. *Am J Pathol* **185**, 1800-1808

145. Prischi, F., Nowak, P. R., Carrara, M., and Ali, M. M. (2014) Phosphoregulation of Ire1 RNase splicing activity. *Nat Commun* **5**, 3554

146. Maurel, M., Chevet, E., Tavernier, J., and Gerlo, S. (2014) Getting RIDD of RNA: IRE1 in cell fate regulation. *Trends Biochem Sci* **39**, 245-254

147. Chen, Y., and Brandizzi, F. (2013) IRE1: ER stress sensor and cell fate executor. *Trends Cell Biol* **23**, 547-555

148. Iurlaro, R., and Munoz-Pinedo, C. (2016) Cell death induced by endoplasmic reticulum stress. *FEBS J* **283**, 2640-2652

149. Darling, N. J., and Cook, S. J. (2014) The role of MAPK signalling pathways in the response to endoplasmic reticulum stress. *Biochim Biophys Acta* **1843**, 2150-2163

150. Hassan, I. H., Zhang, M. S., Powers, L. S., Shao, J. Q., Baltrusaitis, J., Rutkowski, D. T., Legge, K., and Monick, M. M. (2012) Influenza A viral replication is blocked by inhibition of the inositol-requiring enzyme 1 (IRE1) stress pathway. *J Biol Chem* **287**, 4679-4689

151. Stahl, S., Burkhart, J. M., Hinte, F., Tirosh, B., Mohr, H., Zahedi, R. P., Sickmann, A., Ruzsics, Z., Budt, M., and Brune, W. (2013) Cytomegalovirus downregulates IRE1 to repress the unfolded protein response. *PLoS Pathog* **9**, e1003544

152. Muaddi, H., Majumder, M., Peidis, P., Papadakis, A. I., Holcik, M., Scheuner, D., Kaufman, R. J., Hatzoglou, M., and Koromilas, A. E. (2010) Phosphorylation of

eIF2alpha at serine 51 is an important determinant of cell survival and adaptation to glucose deficiency. *Mol Biol Cell* **21**, 3220-3231

153. James, C. C., and Smyth, J. W. (2018) Alternative mechanisms of translation initiation: An emerging dynamic regulator of the proteome in health and disease. *Life Sci* **212**, 138-144
154. Pakos-Zebrucka, K., Koryga, I., Mnich, K., Ljujic, M., Samali, A., and Gorman, A. M. (2016) The integrated stress response. *EMBO Rep* **17**, 1374-1395
155. Marciniak, S. J., Yun, C. Y., Oyadomari, S., Novoa, I., Zhang, Y., Jungreis, R., Nagata, K., Harding, H. P., and Ron, D. (2004) CHOP induces death by promoting protein synthesis and oxidation in the stressed endoplasmic reticulum. *Genes Dev* **18**, 3066-3077
156. Sala, A. J., Bott, L. C., and Morimoto, R. I. (2017) Shaping proteostasis at the cellular, tissue, and organismal level. *J Cell Biol* **216**, 1231-1241
157. Schubert, U., Anton, L. C., Gibbs, J., Norbury, C. C., Yewdell, J. W., and Bennink, J. R. (2000) Rapid degradation of a large fraction of newly synthesized proteins by proteasomes. *Nature* **404**, 770-774
158. Hwang, J., and Qi, L. (2018) Quality Control in the Endoplasmic Reticulum: Crosstalk between ERAD and UPR pathways. *Trends Biochem Sci* **43**, 593-605
159. Fregno, I., and Molinari, M. (2019) Proteasomal and lysosomal clearance of faulty secretory proteins: ER-associated degradation (ERAD) and ER-to-lysosome-associated degradation (ERLAD) pathways. *Crit Rev Biochem Mol Biol* **54**, 153-163
160. Stevenson, J., Huang, E. Y., and Olzmann, J. A. (2016) Endoplasmic Reticulum-Associated Degradation and Lipid Homeostasis. *Annu Rev Nutr* **36**, 511-542
161. Shenkman, M., Ron, E., Yehuda, R., Benyair, R., Khalaila, I., and Lederkremer, G. Z. (2018) Mannosidase activity of EDEM1 and EDEM2 depends on an unfolded state of their glycoprotein substrates. *Commun Biol* **1**, 172
162. Jeong, H., Sim, H. J., Song, E. K., Lee, H., Ha, S. C., Jun, Y., Park, T. J., and Lee, C. (2016) Crystal structure of SEL1L: Insight into the roles of SLR motifs in ERAD pathway. *Sci Rep* **6**, 20261
163. Hoseki, J., Ushioda, R., and Nagata, K. (2010) Mechanism and components of endoplasmic reticulum-associated degradation. *J Biochem* **147**, 19-25
164. Shen, Y., Ballar, P., Apostolou, A., Doong, H., and Fang, S. (2007) ER stress differentially regulates the stabilities of ERAD ubiquitin ligases and their substrates. *Biochem Biophys Res Commun* **352**, 919-924

165. Tsai, Y. C., and Weissman, A. M. (2010) The Unfolded Protein Response, Degradation from Endoplasmic Reticulum and Cancer. *Genes Cancer* **1**, 764-778

166. Belmont, P. J., Chen, W. J., San Pedro, M. N., Thuerauf, D. J., Gellings Lowe, N., Gude, N., Hilton, B., Wolkowicz, R., Sussman, M. A., and Glembotski, C. C. (2010) Roles for endoplasmic reticulum-associated degradation and the novel endoplasmic reticulum stress response gene Derlin-3 in the ischemic heart. *Circ Res* **106**, 307-316

167. Chiang, W. C., Messah, C., and Lin, J. H. (2012) IRE1 directs proteasomal and lysosomal degradation of misfolded rhodopsin. *Mol Biol Cell* **23**, 758-770

168. Sun, S., Shi, G., Sha, H., Ji, Y., Han, X., Shu, X., Ma, H., Inoue, T., Gao, B., Kim, H., Bu, P., Guber, R. D., Shen, X., Lee, A. H., Iwawaki, T., Paton, A. W., Paton, J. C., Fang, D., Tsai, B., Yates, J. R., 3rd, Wu, H., Kersten, S., Long, Q., Duhamel, G. E., Simpson, K. W., and Qi, L. (2015) IRE1alpha is an endogenous substrate of endoplasmic-reticulum-associated degradation. *Nat Cell Biol* **17**, 1546-1555

169. Niehof, M., Hildebrandt, T., Danov, O., Arndt, K., Koschmann, J., Dahlmann, F., Hansen, T., and Sewald, K. (2017) RNA isolation from precision-cut lung slices (PCLS) from different species. *BMC Res Notes* **10**, 121

170. Buchackert, Y., Rummel, S., Vohwinkel, C. U., Gabrielli, N. M., Grzesik, B. A., Mayer, K., Herold, S., Morty, R. E., Seeger, W., and Vadasz, I. (2012) Megalin mediates transepithelial albumin clearance from the alveolar space of intact rabbit lungs. *J Physiol* **590**, 5167-5181

171. Magnani, N. D., Dada, L. A., Queisser, M. A., Brazee, P. L., Welch, L. C., Anekalla, K. R., Zhou, G., Vagin, O., Misharin, A. V., Budinger, G. R. S., Iwai, K., Ciechanover, A. J., and Sznajder, J. I. (2017) HIF and HOIL-1L-mediated PKCzeta degradation stabilizes plasma membrane Na,K-ATPase to protect against hypoxia-induced lung injury. *Proc Natl Acad Sci U S A* **114**, E10178-E10186

172. Graham, J. M. (2002) Fractionation of Golgi, endoplasmic reticulum, and plasma membrane from cultured cells in a preformed continuous iodixanol gradient. *ScientificWorldJournal* **2**, 1435-1439

173. Williamson, C. D., Wong, D. S., Bozidis, P., Zhang, A., and Colberg-Poley, A. M. (2015) Isolation of Endoplasmic Reticulum, Mitochondria, and Mitochondria-Associated Membrane and Detergent Resistant Membrane Fractions from Transfected Cells and from Human Cytomegalovirus-Infected Primary Fibroblasts. *Curr Protoc Cell Biol* **68**, 3 27 21-33

174. Sporty, J. L., Horalkova, L., and Ehrhardt, C. (2008) In vitro cell culture models for the assessment of pulmonary drug disposition. *Expert Opin Drug Metab Toxicol* **4**, 333-345

175. Lazrak, A., Samanta, A., and Matalon, S. (2000) Biophysical properties and molecular characterization of amiloride-sensitive sodium channels in A549 cells. *Am J Physiol Lung Cell Mol Physiol* **278**, L848-857

176. Olivari, S., and Molinari, M. (2007) Glycoprotein folding and the role of EDEM1, EDEM2 and EDEM3 in degradation of folding-defective glycoproteins. *FEBS Lett* **581**, 3658-3664

177. Acosta-Alvear, D., Karagoz, G. E., Frohlich, F., Li, H., Walther, T. C., and Walter, P. (2018) The unfolded protein response and endoplasmic reticulum protein targeting machineries converge on the stress sensor IRE1. *Elife* **7**

178. Wiseman, R. L., Zhang, Y., Lee, K. P., Harding, H. P., Haynes, C. M., Price, J., Sicheri, F., and Ron, D. (2010) Flavonol activation defines an unanticipated ligand-binding site in the kinase-RNase domain of IRE1. *Mol Cell* **38**, 291-304

179. Santulli, G., Nakashima, R., Yuan, Q., and Marks, A. R. (2017) Intracellular calcium release channels: an update. *J Physiol* **595**, 3041-3051

180. Schutt, F., Aretz, S., Auffarth, G. U., and Kopitz, J. (2012) Moderately reduced ATP levels promote oxidative stress and debilitate autophagic and phagocytic capacities in human RPE cells. *Invest Ophthalmol Vis Sci* **53**, 5354-5361

181. Esposito, L. A., Melov, S., Panov, A., Cottrell, B. A., and Wallace, D. C. (1999) Mitochondrial disease in mouse results in increased oxidative stress. *Proc Natl Acad Sci U S A* **96**, 4820-4825

182. Wek, R. C. (2018) Role of eIF2alpha Kinases in Translational Control and Adaptation to Cellular Stress. *Cold Spring Harb Perspect Biol* **10**

183. Rajesh, K., Krishnamoorthy, J., Kazimierczak, U., Tenkerian, C., Papadakis, A. I., Wang, S., Huang, S., and Koromilas, A. E. (2015) Phosphorylation of the translation initiation factor eIF2alpha at serine 51 determines the cell fate decisions of Akt in response to oxidative stress. *Cell Death Dis* **6**, e1591

184. Azzam, Z. S., Sharabi, K., Guetta, J., Bank, E. M., and Gruenbaum, Y. (2010) The physiological and molecular effects of elevated CO2 levels. *Cell Cycle* **9**, 1528-1532

185. Sharabi, K., Hurwitz, A., Simon, A. J., Beitel, G. J., Morimoto, R. I., Rechavi, G., Sznajder, J. I., and Gruenbaum, Y. (2009) Elevated CO2 levels affect development, motility, and fertility and extend life span in Caenorhabditis elegans. *Proc Natl Acad Sci U S A* **106**, 4024-4029

186. Isenovic, E. R., Jacobs, D. B., Kedees, M. H., Sha, Q., Milivojevic, N., Kawakami, K., Gick, G., and Sowers, J. R. (2004) Angiotensin II regulation of the Na+ pump involves the phosphatidylinositol-3 kinase and p42/44 mitogen-activated protein kinase signaling pathways in vascular smooth muscle cells. *Endocrinology* **145**, 1151-1160

187. Aoyama, K., Burns, D. M., Suh, S. W., Garnier, P., Matsumori, Y., Shiina, H., and Swanson, R. A. (2005) Acidosis causes endoplasmic reticulum stress and caspase-12-mediated astrocyte death. *J Cereb Blood Flow Metab* **25**, 358-370

188. Brodsky, J. L., and Wojcikiewicz, R. J. (2009) Substrate-specific mediators of ER associated degradation (ERAD). *Curr Opin Cell Biol* **21**, 516-521

189. Guerriero, C. J., and Brodsky, J. L. (2012) The delicate balance between secreted protein folding and endoplasmic reticulum-associated degradation in human physiology. *Physiol Rev* **92**, 537-576

190. Qi, L., Tsai, B., and Arvan, P. (2017) New Insights into the Physiological Role of Endoplasmic Reticulum-Associated Degradation. *Trends Cell Biol* **27**, 430-440

191. Schmoldt, C., Vazquez-Armendariz, A. I., Shalashova, I., Selvakumar, B., Bremer, C. M., Peteranderl, C., Wasnick, R., Witte, B., Gattenlohner, S., Fink, L., Vadasz, I., Morty, R. E., Pleschka, S., Seeger, W., Gunther, A., and Herold, S. (2019) IRE1 Signaling As a Putative Therapeutic Target in Influenza Virus-induced Pneumonia. *Am J Respir Cell Mol Biol* **61**, 537-540

192. Chopra, S., Giovanelli, P., Alvarado-Vazquez, P. A., Alonso, S., Song, M., Sandoval, T. A., Chae, C. S., Tan, C., Fonseca, M. M., Gutierrez, S., Jimenez, L., Subbaramaiah, K., Iwawaki, T., Kingsley, P. J., Marnett, L. J., Kossenkov, A. V., Crespo, M. S., Dannenberg, A. J., Glimcher, L. H., Romero-Sandoval, E. A., and Cubillos-Ruiz, J. R. (2019) IRE1alpha-XBP1 signaling in leukocytes controls prostaglandin biosynthesis and pain. *Science* **365**

193. Urra, H., Henriquez, D. R., Canovas, J., Villarroel-Campos, D., Carreras-Sureda, A., Pulgar, E., Molina, E., Hazari, Y. M., Limia, C. M., Alvarez-Rojas, S., Figueroa, R., Vidal, R. L., Rodriguez, D. A., Rivera, C. A., Court, F. A., Couve, A., Qi, L., Chevet, E., Akai, R., Iwawaki, T., Concha, M. L., Glavic, A., Gonzalez-Billault, C., and Hetz, C. (2018) IRE1alpha governs cytoskeleton remodelling and cell migration through a direct interaction with filamin A. *Nat Cell Biol* **20**, 942-953

194. Kimata, Y., Ishiwata-Kimata, Y., Ito, T., Hirata, A., Suzuki, T., Oikawa, D., Takeuchi, M., and Kohno, K. (2007) Two regulatory steps of ER-stress sensor Ire1 involving its cluster formation and interaction with unfolded proteins. *J Cell Biol* **179**, 75-86

195. Gardner, B. M., and Walter, P. (2011) Unfolded proteins are Ire1-activating ligands that directly induce the unfolded protein response. *Science* **333**, 1891-1894

196. Cook, Z. C., Gray, M. A., and Cann, M. J. (2012) Elevated carbon dioxide blunts mammalian cAMP signaling dependent on inositol 1,4,5-triphosphate receptor-mediated Ca2+ release. *J Biol Chem* **287**, 26291-26301

197. Mekahli, D., Bultynck, G., Parys, J. B., De Smedt, H., and Missiaen, L. (2011) Endoplasmic-reticulum calcium depletion and disease. *Cold Spring Harb Perspect Biol* **3**

198. van Vliet, A. R., Giordano, F., Gerlo, S., Segura, I., Van Eygen, S., Molenberghs, G., Rocha, S., Houcine, A., Derua, R., Verfaillie, T., Vangindertael, J., De Keersmaecker, H., Waelkens, E., Tavernier, J., Hofkens, J., Annaert, W., Carmeliet, P., Samali, A., Mizuno, H., and Agostinis, P. (2017) The ER Stress Sensor PERK Coordinates ER-Plasma Membrane Contact Site Formation through Interaction with Filamin-A and F-Actin Remodeling. *Mol Cell* **65**, 885-899 e886

199. Gusarova, G. A., Trejo, H. E., Dada, L. A., Briva, A., Welch, L. C., Hamanaka, R. B., Mutlu, G. M., Chandel, N. S., Prakriya, M., and Sznajder, J. I. (2011) Hypoxia leads to Na,K-ATPase downregulation via Ca(2+) release-activated Ca(2+) channels and AMPK activation. *Mol Cell Biol* **31**, 3546-3556

200. Lahiri, S., Roy, A., Li, J., Mokashi, A., and Baby, S. M. (2003) Ca2+ responses to hypoxia are mediated by IP3-R on Ca2+ store depletion. *Adv Exp Med Biol* **536**, 25-32

201. Son, S. M., Byun, J., Roh, S. E., Kim, S. J., and Mook-Jung, I. (2014) Reduced IRE1alpha mediates apoptotic cell death by disrupting calcium homeostasis via the InsP3 receptor. *Cell Death Dis* **5**, e1188

202. Jones, K. T., and Sharpe, G. R. (1994) Thapsigargin raises intracellular free calcium levels in human keratinocytes and inhibits the coordinated expression of differentiation markers. *Exp Cell Res* **210**, 71-76

203. Tian, J., and Xie, Z. J. (2008) The Na-K-ATPase and calcium-signaling microdomains. *Physiology (Bethesda)* **23**, 205-211

204. Aizman, O., Uhlen, P., Lal, M., Brismar, H., and Aperia, A. (2001) Ouabain, a steroid hormone that signals with slow calcium oscillations. *Proc Natl Acad Sci U S A* **98**, 13420-13424

205. Meares, G. P., Hughes, K. J., Naatz, A., Papa, F. R., Urano, F., Hansen, P. A., Benveniste, E. N., and Corbett, J. A. (2011) IRE1-dependent activation of AMPK in response to nitric oxide. *Mol Cell Biol* **31**, 4286-4297

206. Saleem, H., Tovey, S. C., Molinski, T. F., and Taylor, C. W. (2014) Interactions of antagonists with subtypes of inositol 1,4,5-trisphosphate (IP3) receptor. *Br J Pharmacol* **171**, 3298-3312

207. Farinha, C. M., Matos, P., and Amaral, M. D. (2013) Control of cystic fibrosis transmembrane conductance regulator membrane trafficking: not just from the endoplasmic reticulum to the Golgi. *FEBS J* **280**, 4396-4406

208. Beggah, A., Mathews, P., Beguin, P., and Geering, K. (1996) Degradation and endoplasmic reticulum retention of unassembled alpha- and beta-subunits of Na,K-ATPase correlate with interaction of BiP. *J Biol Chem* **271**, 20895-20902

209. Braakman, I., and Hebert, D. N. (2013) Protein folding in the endoplasmic reticulum. *Cold Spring Harb Perspect Biol* **5**, a013201

210. Fergie, N., Todd, N., McClements, L., McAuley, D., O'Kane, C., and Krasnodembskaya, A. (2019) Hypercapnic acidosis induces mitochondrial dysfunction and impairs the ability of mesenchymal stem cells to promote distal lung epithelial repair. *FASEB J* **33**, 5585-5598

211. Marrocco, I., Altieri, F., and Peluso, I. (2017) Measurement and Clinical Significance of Biomarkers of Oxidative Stress in Humans. *Oxid Med Cell Longev* **2017**, 6501046

212. Wong, C. M., Marcocci, L., Liu, L., and Suzuki, Y. J. (2010) Cell signaling by protein carbonylation and decarbonylation. *Antioxid Redox Signal* **12**, 393-404

213. Levine, R. L., Wehr, N., Williams, J. A., Stadtman, E. R., and Shacter, E. (2000) Determination of carbonyl groups in oxidized proteins. *Methods Mol Biol* **99**, 15-24

214. Stadtman, E. R., and Berlett, B. S. (1997) Reactive oxygen-mediated protein oxidation in aging and disease. *Chem Res Toxicol* **10**, 485-494

215. Suzuki, Y. J., Carini, M., and Butterfield, D. A. (2010) Protein carbonylation. *Antioxid Redox Signal* **12**, 323-325

216. Dukan, S., Farewell, A., Ballesteros, M., Taddei, F., Radman, M., and Nystrom, T. (2000) Protein oxidation in response to increased transcriptional or translational errors. *Proc Natl Acad Sci U S A* **97**, 5746-5749

217. Rasmussen, H. H., Hamilton, E. J., Liu, C. C., and Figtree, G. A. (2010) Reversible oxidative modification: implications for cardiovascular physiology and pathophysiology. *Trends Cardiovasc Med* **20**, 85-90

218. Baird, T. D., and Wek, R. C. (2012) Eukaryotic initiation factor 2 phosphorylation and translational control in metabolism. *Adv Nutr* **3**, 307-321

219. Liu, L., Cash, T. P., Jones, R. G., Keith, B., Thompson, C. B., and Simon, M. C. (2006) Hypoxia-induced energy stress regulates mRNA translation and cell growth. *Mol Cell* **21**, 521-531

220. Liu, Y., Laszlo, C., Liu, Y., Liu, W., Chen, X., Evans, S. C., and Wu, S. (2010) Regulation of G(1) arrest and apoptosis in hypoxia by PERK and GCN2-mediated eIF2alpha phosphorylation. *Neoplasia* **12**, 61-68

221. Papadakis, A. I., Paraskeva, E., Peidis, P., Muaddi, H., Li, S., Raptis, L., Pantopoulos, K., Simos, G., and Koromilas, A. E. (2010) eIF2{alpha} Kinase PKR modulates the hypoxic response by Stat3-dependent transcriptional suppression of HIF-1{alpha}. *Cancer Res* **70**, 7820-7829

222. McQuiston, A., and Diehl, J. A. (2017) Recent insights into PERK-dependent signaling from the stressed endoplasmic reticulum. *F1000Res* **6**, 1897

223. Zdzisinska, B., Zurek, A., and Kandefer-Szerszen, M. (2017) Alpha-Ketoglutarate as a Molecule with Pleiotropic Activity: Well-Known and Novel Possibilities of Therapeutic Use. *Arch Immunol Ther Exp (Warsz)* **65**, 21-36

224. Liu, S., He, L., and Yao, K. (2018) The Antioxidative Function of Alpha-Ketoglutarate and Its Applications. *Biomed Res Int* **2018**, 3408467

225. Chin, R. M., Fu, X., Pai, M. Y., Vergnes, L., Hwang, H., Deng, G., Diep, S., Lomenick, B., Meli, V. S., Monsalve, G. C., Hu, E., Whelan, S. A., Wang, J. X., Jung, G., Solis, G. M., Fazlollahi, F., Kaweeteerawat, C., Quach, A., Nili, M., Krall, A. S., Godwin, H. A., Chang, H. R., Faull, K. F., Guo, F., Jiang, M., Trauger, S. A., Saghatelian, A., Braas, D., Christofk, H. R., Clarke, C. F., Teitell, M. A., Petrascheck, M., Reue, K., Jung, M. E., Frand, A. R., and Huang, J. (2014) The metabolite alpha-ketoglutarate extends lifespan by inhibiting ATP synthase and TOR. *Nature* **510**, 397-401

Acknowledgements

First of all, I would like to express my gratitude to Prof. Dr. Werner Seeger for giving me the opportunity to perform my PhD studies and his supervision, advice and support. I would like to express my gratitude to Prof. Dr. Martin Diener for his co-supervision of my doctoral thesis.

I would like to especially thank Dr. István Vadász for giving me the opportunity to start my PhD studies, his constant help, support and advice. I profoundly appreciate his open position to new approaches in research, his valuable comments and the time we spent during our scientific discussions. This attitude has helped me grow as a person and a scientist.

My big thanks go to all members of the Vadász Laboratory, especially Miri, Paulina and Andrés. Thank you, for having a wonderful time with you.

I would like to express my great thankfulness to Prof. Dr. Jacob I. Sznajder, who has given me the chance to start my path in research, for his mentorship, support, and advice.

I would like to thank the members of the laboratory of Prof. Dr. Jacob I. Sznajder at Northwestern University for their support, sharing of experiences and providing help in my research. My special thanks go to Dr. Laura A. Dada and Lynn Welch.

I feel very grateful to Dr. Olga Vagin for supporting me during my professional and private life.

My special thanks go to Dr. Rory E. Morty for giving me the opportunity to participate in the MBML program. I would like to thank the members of the MBML committee, Dr. Elie El Agha and Dr. Ivana Mižíková for organizing our interesting lectures, tutorials and retreats.

I am entirely thankful to all my friends for the constant support and for being at my side during these years.

I would like to thank my parents Lyudmila and Vitaliy. I am deeply thankful for your help, encouragement and constant support.

Finally, I would like to thank my wife Nina. Thank you very much for your enormous support, understanding and belief in me.